U.S. DEPARTMENT OF THE INTERIOR
U.S. GEOLOGICAL SURVEY

Estimated temperatures for geothermal drill holes at Medicine Lake Volcano, northeastern California, based on fluid inclusion and hydrothermal mineralogy studies

By Keith E. Bargar[1] and Terry E.C. Keith[2]

Open-File Report 97-716

[1]U.S. Geological Survey, M/S 910, 345 Middlefield Road, Menlo Park, California 94025
[2]U.S. Geological Survey, Alaska Volcano Observatory, Anchorage, Alaska 99508

CONTENTS

FIGURES

ATTACHMENT

TABLES

ABSTRACT

Medicine Lake volcano, a Pleistocene to Holocene Cascade shield volcano in the northeastern part of California, is one of the most promising geothermal energy prospects in the Pacific Northwest. Industry evaluation of the geothermal energy potential of the Medicine Lake area included completion of several exploration drill holes. At present, data (temperature, chemistry, etc.) obtained from the drill holes is proprietary. However, drill-core samples recovered from 12 holes have been made available for scientific investigations. Studies of hydrothermal alteration minerals contained in the drill core samples and fluid inclusions in a few mineral specimens provide reasonable estimates of late Pleistocene to present-day temperatures of fluids circulating through rocks penetrated by the drill holes.

More than 600 rhyolitic to basaltic drill-core specimens from the 12 drill holes (ranging in depth from about 340 to 1,370 m) were collected for this investigation. Volcanic glass and open spaces of fractures, vesicles, and between breccia fragments in core specimens from drill holes located both outside and within the caldera show the effects of hydrothermal alteration. The alteration is more pervasive and reflective of higher temperatures in the two intracaldera drill holes. Forty-five hydrothermal minerals were identified from these drill holes. Many clay minerals, zeolites, carbonates, silica minerals, sulfides, sulfates, iron oxides, and hydrated calcium silicate minerals undoubtedly formed at zeolite-facies temperatures (<~200°C). The presence of minor garnet, epidote, actinolite/tremolite, prehnite, and talc, from the intracaldera drill holes (ML 28-32 and ML 45-36) suggest previous higher (about 200° to 400°C) sub-greenschist- to greenschist-facies temperatures.

Homogenization temperatures (T_h) of fluid inclusions in hydrothermal quartz, calcite, and wairakite from drill hole ML 45-36 range between 178° and 373°C and confirm the higher temperatures suggested by alteration mineralogy of this drill hole. In the second studied intracaldera drill hole (ML 28-32), fluid-inclusion T_h measurements in hydrothermal quartz and calcite range between 125° and 225°C. However, the presence of several greenschist-facies hydrothermal minerals (garnet, epidote, prehnite, actinolite/tremolite, and talc) indicate that past temperatures have been substantially higher than suggested by the fluid-inclusion measurements of specimens from the lower part of the drill hole.

Minimum fluid-inclusion T_h measurements for hydrothermal mineral specimens at given depths in holes drilled in modern geothermal areas frequently coincide with present-day temperatures. T_h values of fluid inclusions in these minerals generally fall between a theoretical reference boiling-point curve and the present measured temperature at the sample depth. Minimum T_h values within the lower half of the ML 45-36 drill hole suggest that current temperatures near the bottom of this drill hole are approximately 200°C. Many of the ML 45-36 higher T_h values plot above the theoretical reference boiling-point curve drawn to the present ground surface. These liquid-rich fluid inclusions with high T_h measurements did not originate during boiling conditions. Instead, the high T_h values reflect pressures that were greater than at present. The fluid inclusions most likely formed during the late Pleistocene when the effective ground surface is estimated to have been at least 150 m higher than at the present time due to the presence of glacial ice.

Dozens of tiny (<0.5 to ~5 μm), mostly rod-shaped, bacteria-like moving particles were trapped inside a liquid-rich, primary fluid inclusion. The inclusion occurs within a hydrothermal quartz crystal that formed on a fracture in rhyolitic lava from 856-m depth in drill hole ML 45-36. The movement appears to be due to Brownian motion. If the particles are the remains of thermophilic microorganisms, the fluid-inclusion studies indicate that they must have been trapped at temperatures above 200°C.

INTRODUCTION

Medicine Lake volcano is a large (about 2,000 km^2) Pleistocene to Holocene volcano located in the Cascade Range of northeastern California about 50 km east-northeast of Mount Shasta (Figure 1) (Donnelly-Nolan, 1988; 1990). The accumulation

Figure 1 near here

of lava flows that comprise this low, broad, shield volcano probably began erupting about 1 million years ago (Donnelly-Nolan and others, 1990). At least 17 eruptions have occurred at Medicine Lake volcano during the past 12,000 years; composition of these lava flows ranges between basalt and rhyolite with only scarce dacite lavas (Donnelly-Nolan and others, 1990). The most recent volcanic activity (about 900 years ago), at Glass Mountain and Little Glass Mountain, occurs in the vicinity of the 7 x 12 km caldera (Figure 2) (Donnelly-Nolan and others, 1990).

Figure 2 near here

This recent volcanism makes Medicine Lake volcano and the Glass Mountain KGRA one of the most promising geothermal energy prospects in the Pacific Northwest. Industry evaluation of the geothermal energy potential of this area includes completion of several drill holes. Some general information on the petrology of eight flank drill holes is provided by Donnelly-Nolan (1990). A temperature of 105°C at 1.2 km depth and a geothermal gradient of 100°C/km between depths of 0.5 and 1.2 km are reported for the ML 88-12 drill hole (not shown in Figure 2) located about halfway between Mount Shasta and the Medicine Lake volcano (Blackwell and others, 1990). Measured geothermal gradients of 88°C km^{-1}, 227°C km^{-1}, and 548°C km^{-1} are given for 3 wells sited within the caldera of Medicine Lake volcano (Donnelly-Nolan and others, 1990).

At the present time, temperature, fluid composition, and other data from these drill holes is mostly proprietary; however, rhyolitic- to basaltic-core specimens from 12 drill holes were made available for study through the geothermal core storage facility at the Earth Science Environmental Research Institute in Salt Lake City, Utah. We collected more than 600 representative core specimens from the 12 drill holes, that range in depth from about 340 m to 1,370 m (see Figure 2 for locations of all but the ML 88-12 hole), in order to obtain information on hydrothermal alteration of the Medicine Lake volcanic rocks. Some volcanic glass, the open spaces of many fractures, vesicles, and areas between fragments of breccias in core specimens from all 12 drill holes show alteration effects caused by circulating hydrothermal fluids. This study of drill-hole samples from the Medicine Lake volcano area identified forty-five metamorphic minerals (Table 1) that formed by hydrothermal alteration at low to moderate temperatures. Table

Table 1 near here

1 shows the temperatures at which these minerals were found in well-studied geothermal areas throughout the world. Such metamorphic mineral assemblages are described as "very low grade metamorphism" by Frey and Kisch (1987), who used the term to refer to metamorphism that takes place in the temperature range of about 150° to 200° through 350° to 400°C. Mineral assemblages occurring in this temperature range include "zeolite-facies" minerals, which formed at (and below) the stated lower temperatures, and "subgreenschist-facies" and "greenschist-facies" minerals, which were produced at the higher temperatures (Liou and others, 1987). These facies terms are useful in conveying an impression of the degree to which a designated group of rocks have been metamorphosed.

In this report, we somewhat arbitratily simplified the temperature ranges of Frey and Kisch (1987) to indicate that zeolite-facies minerals mostly form at temperatures below 200°C and subgreenschist- to greenschist-facies minerals usually originate at temperatures between 200° and 400°C. These distinctions are merely intended to characterize the approximate temperature range at which the various minerals most likely formed. Many exceptions do occur. For example, the zeolite minerals analcime and wairakite have been reported at temperatures as high as 300°C (Kristmannsdóttir and Tómasson, 1978). Also, some subgreenschist to greenschist minerals such as chlorite have been found at temperatures below 100°C (Hulen and Nielson, 1986).

Temperature- and fluid-composition-data also were obtained from heating/freezing studies of fluid inclusions trapped inside appropriate hydrothermal mineral specimens from several depths in the two (ML 28-32 and ML 45-36) intracaldera drill holes (Figure 2). These studies provide valuable insight into the late Pleistocene to present-day geothermal regime of Medicine Lake volcano. Fluid inclusion studies of several geothermal drill holes in Japan indicate that at a given depth minimum homogenization temperature (T_h) values are generally the same or slightly warmer than the present measured temperatures (Taguchi and Hayashi, 1982; and Taguchi and others, 1984). These workers indicate that minimum T_h values can be used to estimate present-day temperatures where drill-hole temperature-data was not obtained or is unavailable for proprietary reasons.

ANALYTICAL METHODS

Mineral identifications were made by routine binocular microscope or petrographic microscope methods and X-ray diffraction (XRD) analyses (using a Norelco X-ray unit and Cu-Kα radiation). Semiquantitative chemical analyses were obtained for several minerals, using a Cambridge Stereoscan 250 scanning electron microscope equipped with an energy dispersive spectrometer (EDS), during scanning electron microscope studies of the paragenesis and morphology of the hydrothermal minerals. Quantitative chemical analyses of several minerals were obtained with a JEOL JXA-8900L electron probe microanalyzer using natural and synthetic mineral standards (Tables 2-14). Instrument conditions for analysis of the carbon-coated, polished thin-sections include a sample current of 7.5nA, beam diameter of 20 µm, count times of 20 seconds, and an accelerating voltage of 7.5 kV. Possible errors in the microprobe analyses might be as great as ±20% for concentrations <1% and as high as ±100% for concentrations <0.1% (L. Calk, personal commun., 1996). Total iron is reported as FeO or Fe_2O_3 whichever is appropriate for the analyzed mineral. Balance errors (<±7 is an acceptable analysis) for zeolite mineral analyses (Tables 2-8) are calculated according to a formula given in Passaglia (1970).

Doubly-polished thick sections of hydrothermal quartz, calcite, and wairakite, along with a few unpolished calcite cleavage chips, were utilized for fluid-inclusion analyses. Fluid-inclusion homogenization (T_h) and ice-melting (T_m) temperatures were obtained using a Linkam THM 600 heating/freezing stage and TMS 90 temperature control system. Successive calibration runs, using synthetic fluid inclusions (Bodnar and Sterner, 1984) and chemical compounds with known melting points recommended in Roedder (1984), suggest that the accuracy of the T_h measurements is within ±2.0°C and the T_m values are accurate to at least ±0.2°C. Salinities of the inclusion fluids were calculated, in weight % NaCl equivalent, using the equation given in Potter and others (1978).

HYDROTHERMAL MINERALOGY

Fractures and vesicles of drill core specimens from a few of the Medicine Lake volcano geothermal drill holes contain crystals of vapor-phase minerals (tridymite, plagioclase, and hematite?) and granophyric quartz. These minerals formed during cooling of the volcanic rocks prior to hydrothermal mineralization. Some orange to reddish staining and powdery to clayey deposits associated with the vapor-phase mineralization are amorphous to X-rays and appear to be early hydrothermal iron-oxide alteration. Hydrothermal alteration is most extensive in the two holes (ML 28-32 and ML 45-36) drilled within the caldera of Medicine Lake volcano (Figures 3d and f; Table 1).

Figure 3 near here

One or more hydrothermal minerals were identified in core samples from each of the flank drill holes but alteration appears to be much less prevalent outside the caldera rim. Forty-five hydrothermal alteration minerals identified from the 12 geothermal prospect drill holes include several clay minerals, zeolites, carbonates, silica minerals, sulfides, sulfates, and other oxide and silicate minerals (Table 1) (Bargar and Keith, 1993). The majority of these minerals most likely formed at temperatures <200°C and would be compatible with zeolite-facies metamorphism. However, some minerals from the lower parts of the two intracaldera drill holes contain minerals such as talc, garnet, epidote, actinolite/tremolite, and prehnite that undoubtedly formed at temperatures characteristic of sub-greenschist- to greenschist-facies metamorphism (about 200° to 400°C).

ZEOLITE MINERALS

The Medicine Lake volcano drill hole core samples contain eleven zeolite minerals; the number of zeolite specimens identified from a single drill hole varies from 0 to 6 (Table 1). The temperatures at which several zeolite minerals were found in active Icelandic geothermal areas (Kristmannsdóttir and Tómasson, 1978) provides a generally accepted guide (where temperature data are not available) for estimating the approximate temperatures at which these minerals most likely precipitated in other geothermal areas of the world. Chemical formulas for the zeolites (and other minerals) discussed below are from Fleischer and Mandarino (1991) except where noted.

Analcime. Analcime was only identified in vesicles of 3 specimens from the ML 86-23 (Figure 3j) drill hole in association with earlier smectite, and later calcite. Vesicles and fractures in these core samples also contain scolecite, levyne, stilbite/stellerite, thomsonite, phillipsite, gyrolite, apophyllite, and adularia. The analcime occurs as colorless, euhedral to subhedral crystals that range up to about 1 mm in size (Figure 4).

Figure 4 near here

Usually analcime forms clean trapezohedral crystals similar to the one shown in the lower right-hand corner of Figure 4. The majority of analcime crystals in Figure 4 display an unusual morphology that we previously have not observed elsewhere. Smaller tabular to prismatic crystals of another mineral (stilbite/stellerite also was identified in an XRD analysis of this specimen) subsequently filled some of the voids in the analcime crystals. Chemical analyses of the analcime crystals indicate that they are a pure analcime end member of the analcime ($NaAlSi_2O_6 \cdot H_2O$) — wairakite ($CaAl_2Si_4O_{12} \cdot 2H_2O$) solid solution series (Table 2, Figure 5). Analcime is sodium-rich whereas stilbite and

Table 2 near here

Figure 5 near here

stellerite contain significant calcium (Gottardi and Galli, 1985). Possibly, a change in the chemistry of the precipitating fluid interrupted formation of the analcime crystals resulting in deposition of later stilbite/stellerite crystals. Alternatively, the stilbite/stellerite? crystals may have formed following partial dissolution of the analcime. Hydrothermal mineralogy studies of Icelandic geothermal drill holes indicate that analcime can form at temperatures between 70° and 300°C (Kristmannsdóttir and Tómasson, 1978). Analcime in the 86-23 drill hole is associated with low-temperature zeolites and other minerals (Figure 3j) that typically are found at temperatures less than 200°C in modern geothermal areas (Table 1).

Wairakite. Wairakite also typically forms euhedral to subhedral, colorless, trapezohedral crystals (Figure 6). In the ML 28-32 drill hole, wairakite occurs as vein

Figure 6 near here

fillings in three narrow zones of very altered rock at depths of about 1,097 to 1,101 m, 1,328.2 m, and 1,365 to 1,369 m (Figure 3d). In the ML 45-36 drill hole (Figure 3f), wairakite was identified in 5 scattered core samples. Chemical analyses of wairakite from both drill holes (Table 2) show that the mineral is nearly a pure wairakite solid-solution end member (Figure 5).

Wairakite also has been identified at temperatures as high as 300°C in Icelandic geothermal areas (Kristmannsdóttir and Tómasson, 1978). In these Icelandic studies, wairakite was reported at temperatures as low as ~180°C (Table 1). Formation temperatures for wairakite and associated hydrothermal minerals in shallower zones of the Medicine Lake volcano drill holes was probably slightly below 200°C; alteration mineralogy of the deeper zones is consistent with temperatures well above 200°C.

Chabazite. Chabazite ($CaAl_2Si_4O_{12}\cdot 6H_2O$) coats intersecting fractures in drill holes OWML5 and ML 52-4 (Table 1) in association with earlier calcite, smectite, and, in two specimens, stilbite/stellerite. The colorless, pseudocubic rhombohedral, chabazite crystals range in size up to 0.5 mm and mostly are twinned (Figure 7). A chemical

Figure 7 near here

analysis of one chabazite crystal from 776 m depth in the OWML5 drill hole contains (in weight percent oxide) 55.65% SiO_2, 16.33% Al_2O_3, 0.08% Fe_2O_3, 0.14% MgO, 8.15% CaO, 0.75% Na2O, 0.32% K_2O, 0.01% MnO, 0.36% SrO, and 0.00% BaO (total = 81.79%). Accordingly, the formula for the chabazite specimen would be $Ca_{1.40}Sr_{0.36}K_{0.32}Na_{0.23}Mg_{0.03}(Al_{3.07}Fe_{0.01}Si_{8.89}O_{24})\cdot 12H_2O$.

Chabazite is a characteristic hydrothermal mineral in low-temperature (<75°C) alteration zones of Icelandic geothermal areas (Kristmannsdóttir and Tómasson, 1978). Chabazite deposits in geothermal drill holes of the Oregon Cascade Range also occur at similar low temperatures (Bargar and Oscarson, 1997). Chabazite in drill core samples from the Medicine Lake volcano area probably also formed at similar low temperatures.

Heulandite group minerals. Heulandite group minerals (clinoptilolite—$(Na,K,Ca)_{2\text{-}3}Al_3(Al,Si)_2Si_{13}O_{36}\cdot 12H_2O$ and heulandite—$(Na,Ca)_{2\text{-}3}Al_3(Al,Si)_2Si_{13}O_{36}\cdot 12H_2O$) were identified in 5 of the studied drill holes (Table 1; Figures 3a,d, f, g, and i). These minerals occur as tiny, colorless, tabular, euhedral to subhedral crystals (sometimes twinned) (Figure 8) that fill vesicles and fractures of lava flows, line open spaces between

Figure 8 near here

fragments of breccias, and replace glass in lithic tuffs and pumice fragments. Associated hydrothermal minerals include stilbite/stellerite, mordenite, smectite, calcite, siderite, iron oxide, pyrite, gypsum, and chalcedony.

Electron microprobe analyses of two specimens (Table 3) indicate that both

Table 3 near here

heulandite and clinoptilolite (Figure 9) are present in the Medicine Lake drill holes.

Figure 9 near here

In addition to potassium, the clinoptilolite specimen contains significant barium (Table 3) which usually is absent or a very minor constituent in other analyzed heulandite group minerals from the Cascade Mountains of Oregon (Oscarson and Bargar, 1996).

Heulandite group minerals typically are found in Icelandic geothermal areas at low to moderate temperatures (about 60° to 170°C) (Kristmannsdóttir and Tómasson, 1978). However, heulandite and clinoptilolite occur at measured temperatures as low as 30°C in one Oregon Cascade Mountains geothermal drill hole (Bargar, 1990).

Laumontite. Laumontite ($CaAl_2Si_4O_{12}\cdot 4H_2O$) forms over a wide temperature range (43° to 230°C) in modern geothermal areas (Kristmannsdóttir and Tómasson, 1978; McCulloh and others, 1981). Laumontite is a common zeolite mineral in outcrops and geothermal drill holes in the Oregon Cascade Mountains, but it only occurs in three of the Medicine Lake drill holes (Table 1). The white, euhedral, prismatic, laumontite crystals (Figure 10) occur in fractures, vesicles, and open spaces between fragments in breccias.

Figure 10 near here

Associated minerals commonly include calcite, chlorite, mixed-layer chlorite-smectite, and epidote; less commonly, laumontite occurs in specimens that also contain pyrite, iron oxide, wairakite, mixed-layer illite-smectite, chalcedony, quartz, prehnite, anhydrite, and actinolite/tremolite. Closely associated hydrothermal minerals and fluid-inclusion data suggest that laumontite in the two intracaldera drill holes probably formed near the high end of the temperature range given in Table 1. Conversely, laumontite in the flank drill hole could have precipitated at somewhat lower temperatures. Electron microprobe analyses of laumontite from the two intracaldera drill holes (Table 4 and Figure 11) are

Table 4 near here

Figure 11 near here

Ca-rich with only minor amounts of other exchangeable cations.

Levyne. A single specimen from the ML 86-23 drill hole contains vesicle fillings of frosted, blocky levyne [$(Ca,Na_2,K_2)Al_2Si_4O_{12}\cdot 6H_2O$] (Table 1). Other hydrothermal minerals identified in vesicles of the sample include smectite, analcime, calcite, phillipsite, scolecite, stilbite/stellerite, thomsonite, and gyrolite (Figure 3j). Electron microprobe analyses of the levyne specimen show that calcium is the dominant cation with some sodium and a trace of potassium (Table 5). Many published chemical analyses

Table 5 near here

of levyne (Gottardi and Galli, 1985; Tschernich, 1992) are similar in composition to the ML 86-23 sample but there can be a considerable variation in cation content of the mineral as shown in Figure 12. In Icelandic geothermal areas, levyne occurs at

Figure 12 near here

temperatures less than 70°C (Kristmannsdóttir and Tómasson, 1978).

Mordenite. Four of the Medicine Lake geothermal drill holes contain colorless or white, cottony mattes or radiating sprays of acicular to fibrous mordenite [$(Ca,Na_2,K_2)Al_2Si_{10}O_{24}\cdot 7H_2O$] (Figure 13). Qualitative chemical analyses of the

Figure 13 near here

mordenite by EDS during scanning electron microscope studies indicates that the dominant constituents are Ca, Al, and Si; traces of K and Na were observed in a few analyses. The mordenite occurs as a late deposit in vesicles, fractures or between breccia fragments in association with numerous other hydrothermal minerals (Figures 3d, f, g, and i). Mordenite in Icelandic geothermal areas occurs over a wide temperature range (~75° to 230°C) (Kristmannsdóttir and Tómasson, 1978).

Phillipsite. A single specimen of phillipsite [$(K,Na,Ca)_{1\text{-}2}(Si,Al)_8O_{16}\cdot 6H_2O$] was identified from each of two wells (ML 18-34 and ML 86-23) (Figures 3b and j). The colorless to white, euhedral, pseudo-orthorhombic crystals (Figure 14) fill vesicles in the

Figure 14 near here

two lava flows. Vesicles containing phillipsite in drill hole ML 18-34 also contain calcite and smectite; vesicles in the ML 86-23 lava flow are filled by one or more of the following minerals: phillipsite, calcite, smectite, scolecite, levyne, stilbite/stellerite, analcime, thomsonite, or gyrolite. In Icelandic geothermal areas, phillipsite occurs at low temperatures (60° to 85°C) (Kristmannsdóttir and Tómasson, 1978); however it has been reported at temperatures as low as 37°C in a drill hole at Surtsey volcano (Jakobsson and Moore, 1986).

The composition of phillipsite can vary considerably from formulas (such as the one given above) provided in textbooks (Gottardi and Galli, 1985; Tschernich, 1992). Electron microprobe data (Table 6) for one specimen analyzed for this report is compared

Table 6 near here

with analyses of phillipsite from a geothermal drill hole in Oregon (OR phillipsite) (Oscarson and Bargar, 1996) and other phillipsites (Gottardi and Galli, 1985; Tschernich, 1992) (Figure 15). The figure shows a wide variation in compositions for phillipsite;

Figure 15 near here

however, the composition of phillipsite from the Oregon and Medicine Lake volcano geothermal drill holes is quite close.

Scolecite. White, acicular to fibrous scolecite (Figure 16) fills vesicles along with

Figure 16 near here

dark green smectite in two drill core specimens from the ML 86-23 drill hole (Figure 3j). Composition of this scolecite (Table 7 and Figure 17) differs somewhat from the normal

Table 7 near here

Figure 17 near here

stoichiometric formula ($CaAl_2Si_3O_{10}\cdot 3H_2O$) for scolecite in that the analyzed sample contains between 1.23 and 1.76 atoms of sodium (Table 6). Gottardi and Galli (1985) indicate that scolecite can contain as much as 1.4 atoms of sodium. Mesolite/scolecite was reported at temperatures of about 65° to 100°C in geothermal areas of Iceland (Kristmannsdóttir and Tómasson, 1978).

Stilbite/stellerite. Three of the Medicine Lake volcano geothermal drill holes contain core specimens with vesicles or fractures that are lined by colorless to white, euhedral, stilbite/stellerite ($NaCa_2Al_5Si_{13}O_{36}\cdot 14H_2O/CaAl_2Si_7O_{18}\cdot 7H_2O$) crystals (Table 1). The two solid-solution series minerals are combined here because they are distinguishable with confidence only by single-crystal XRD analysis (R.C. Erd, written communication, 1992) which was not attempted for this report. Calcite, smectite, heulandite, and chabazite are frequently found in close association with the stilbite/stellerite; other minerals identified in the same samples are shown in figures 3a, g, and j. Scanning electron microscope studies only show the presence of Ca, Al, and Si in the rectangular, flat-topped crystals (Figure 18) that are characteristic of both stilbite

Figure 18 near here

and stellerite (Tschernich, 1992). Stilbite from Iceland geothermal drill holes occurs over a temperature range of 70°C to about 170°C (Kristmannsdóttir and Tómasson, 1978).

Thomsonite. Vesicles in two very altered lava flow specimens from the ML 86-23 drill hole contain hemispherical clusters of colorless to white, bladed to fibrous crystals that consist of thomsonite ($NaCa_2Al_5Si_5O_{20}\cdot 6H_2O$), gyrolite, and apophyllite in XRD. The specimens also contain smectite, calcite, scolecite, levyne, stilbite/stellerite, analcime, and phillipsite (Figure 3j). Electron microprobe analyses (Table 8) show that

Table 8 near here

the ML 86-23 thomsonite has a little more calcium than sodium as is common for many thomsonites while others may contain substantial sodium or strontium (Figure 19). The

Figure 19 near here

temperature range for thomsonite in Icelandic geothermal drill holes is about 65° to 110°C (Kristmannsdóttir and Tómasson, 1978).

CARBONATE MINERALS

The distribution of carbonate minerals (aragonite, calcite, dolomite, kutnohorite, rhodochrosite, and siderite) in the Medicine Lake volcano geothermal drill holes is shown in Table 1 and Figure 3 (a-k). Most of the identified carbonate minerals are found in other geothermal areas at temperatures below 100°C (Table 1). Minerals, such as dolomite or calcite, can form over a wide temperature range (<100° to 350°C for calcite) and, by themselves, are not helpful in estimating the temperatures at which they formed. However, some temperature data was obtained from fluid inclusions in calcite (discussed in a later section).

Aragonite. Aragonite ($CaCO_3$) was only identified (by XRD) from a single lava flow specimen obtained from 469.1 m depth in the ML 28-32 drill hole; colorless acicular crystals of aragonite line a shallow dipping fracture along with smectite and calcite. In geothermal drill holes at Newberry volcano, aragonite was found at measured temperatures <~80°C (Bargar and Keith, in press).

Rhodochrosite. Bladed, buff-colored, rhodochrosite ($MnCO_3$) crystals fill a few cavities along with smectite, quartz, calcite, and mordenite in a single drill-core sample

collected from 428.2 m depth in the ML 45-36 hole. In the Newberry volcano drill holes, rhodochrosite occurs at measured temperatures between ~30°C and ~130°C (Bargar and Keith, in press).

Kutnohorite. Two of the collected specimens from the ML 27-27 drill hole contain fracture or breccia-cavity fillings composed of powdery yellow or colorless, massive kutnohorite [$Ca(Mn,Mg,Fe)(CO_3)$] in addition to calcite, ±smectite, and illite. Yellow, orange or tan carbonate deposits, consisting in part of kutnohorite, also occur as fillings in fractures or vesicles (along with calcite, ±siderite, and smectite) in five samples from the ML 28-32 drill hole. On two of the fractures with narrow openings, the kutnohorite formed tiny (~1 mm), flattened, circular deposits with concentric growth(?) rings similar to those shown in Figure 22 below. Measured temperatures in one Newberry volcano drill hole at which kutnohorite occurred range from <10° to ~70°C (Bargar and Keith, in press).

Dolomite. Traces of dolomite [$CaMg(CO_3)_2$] were found as fracture fillings or between breccia fragments in three of the Medicine Lake volcano drill holes (OWML5, ML 28-32, and ML 62-21). Colorless to white dolomite coating breccia fragments at 748.6 m depth in the ML 28-32 drill hole consists of intergrown, tiny, rhombic crystals (Figure 20). Other

Figure 20 near here

colorless to white dolomite deposits are massive and include one or more associated minerals (smectite, iron oxide, calcite, quartz, chalcedony, or cristobalite).

Measured temperatures at the depths in a drill hole at Newberry volcano where ankerite/dolomite was found ranges from <10° to ~150°C (Bargar and Keith, in press). Dolomite from drill core Y-4 in Yellowstone National Park occurs at a temperature of 190°C (T.E.C. Keith, unpub data, 1991). Dolomite and ankerite from drill holes in the Salton Sea geothermal area are reported as ranging from less than 100°C to over 200°C (Muffler and White, 1969) or even as high as ~250°C (McDowell and Paces, 1985).

Siderite. Pale yellow to dark caramel-colored siderite ($FeCO_3$) was identified in vesicle and fracture fillings of a few core specimens from three flank drill holes (OWML5, ML 18-32, and ML 52-4). However, numerous core samples in the upper 1,000 m of the ML 28-32 intracaldera drill hole contain siderite open-space fillings. Morphology of the siderite varies substantially. Some siderite occurs as individual rhombic crystals or stacked crystal clusters (Figure 21a, b). More commonly, siderite has

Figure 21 near here

a botryoidal appearance with spherical to hemispherical clusters of crystals (Figure 21c, d). In fractures with narrow openings between the top and bottom surfaces, siderite deposits have a flattened, disc-shaped habit (Figure 21e) often with concentric growth rings (Figure 21f) marked by multiple colors of siderite rings (Figure 22). In the

Figure 22 near here

Newberry volcano geothermal drill holes, the measured temperatures at which siderite was found ranged from <10°C to ~160°C (Bargar and Keith, in press).

Calcite. All of the Medicine Lake geothermal drill holes, except ML 68-16, contain calcite ($CaCO_3$) as a significant component (Table 1). Open spaces within vesicles and fractures, and between breccia fragments frequently contain white massive or colorless crystalline calcite deposits. Crystal morphology of the calcite is variable and ranges from thin-bladed crystal clusters to individual rhombic and scalenohedral crystals (Figure 23a, b). Electron microprobe analysis of one calcite specimen from 1,361.5 m

Figures 23a &b near here

depth in the ML 28-32 drill hole shows the presence of minor Mn and Fe in addition to Ca. The most intense XRD peak for calcite typically ranges from about 3.02Å to 3.05Å. Some of the Medicine Lake volcano calcite deposits have their most intense X-ray reflection between 2.99Å and 3.01Å, which indicates that the mineral contains some manganese (Krieger, 1930; Bargar and Beeson, 1984).

SHEET-SILICATE MINERALS

Except for drill hole ML 68-16, one or more sheet silicate minerals were identified in all of the studied Medicine Lake volcano geothermal drill holes (Table 1; Figure 3). Kaolinite, halloysite, smectite, mixed-layer illite-smectite, illite, mixed-layer chlorite-smectite, chlorite, talc, apophyllite, and prehnite are all classified as sheet silicates (Deer, Howie, and Zussman, 1966). Most of these minerals occur in the two intracaldera drill holes (ML 28-32 and ML 45-36) while the other drill holes contain between one and three of the sheet-silicate minerals (Table 1).

Kaolinite. White kaolinite [$Al_2Si_2O_5(OH)_4$] coats fractures along with one or more other hydrothermal minerals (smectite, calcite, pyrrhotite, quartz, and hematite) in five of the ML 28-32 specimens collected between depths of 730 m and 985.7 m (Figure 3d). Kaolinite has been reported at temperatures as high as 170°C in drill core from Yellowstone National Park (Bargar and Beeson, 1985).

Halloysite. A single specimen of halloysite (a kaolinite-serpentine group mineral with the same chemical formula as kaolinite) occurs as a brown fracture filling at 534.3 m depth in the ML 52-4 drill hole. The scarcity of kaolinite and halloysite might indicate that acidic conditions have occurred infrequently in the Medicine Lake volcano geothermal system. Measured temperatures at the depths where these two kaolinite-serpentine group minerals were identified in Newberry volcano drill holes were less than 50°C (Bargar and Keith, in press).

Smectite. Smectite group minerals [primarily saponite? $(Ca/2,Na)_{0.3}(Mg,Fe)_3(Si,Al)_4O_{10}(OH)_2{\cdot}4H_2O$] are the most abundant clay minerals in all but one (ML 68-16) of the Medicine Lake volcano drill holes (Table 1). Black, red, orange, yellow, white, and green (predominant color) smectite coats open spaces of vesicles and fractures, fills voids between breccia fragments, and replaces glass in tuffaceous core samples. Smectite morphology varies from closely spaced sheet-like or platy crystals to open-textured (honeycomb-like), randomly-oriented, sheet-like crystals (Figure 24 a & b). Detailed

Figure 24a & b near here

XRD studies of smectite show (001) basal reflections that range from~12Å to 15Å; the basal spacing expands to ~17Å following exposure to ethylene glycol vapors at 60°C for 1 hour. The range of unglycolated (001) basal reflections suggests that there is some variation in the exchangeable cations (Grim, 1968) which may indicate the occurrence of more than one smectite-group mineral. Electron microprobe analyses (Table 9) show

Table 9 near here

substantial differences in iron and alumina content between smectite (saponite?) specimens from two of the drill holes. Smectite occurs in most geothermal areas at temperatures <200°C (Table 1).

Mixed-layer illite-smectite. Brown, light green, or dark green clay, identified as mixed-layer illite-smectite, occurs in fractures or between breccia fragments in a few core samples from three of the drill holes (Table 1). Low, broad, asymmetrical XRD

reflections for most of the samples show a $(001)_I/(001)_S$ spacing of ~11Å that contracts to ~9.6Å (smectite peak not seen) after exposure to ethylene glycol for 1 hour at 60°C. For three of the specimens, the ~11Å XRD reflection splits into two peaks at ~9.6Å and ~12.7Å following glycolation. The mineral is tentatively identified as an alevardite ordered mixed-layer illite-smectite (Hower, 1981). About 75 percent of the layers in these clay specimens consists of illite which corresponds to a formation temperature of ~110°C Horton (1985).

Illite. Illite $\{(K,H_3O)(Al,Mg,Fe)_2(Si,Al)_4O_{10}[(OH)_2,H_2O]\}$ was identified only in the two Medicine Lake volcano drill holes located within the caldera (Table 1). It occurs as white or green clay from altered glass, altered potassium feldspar crystals, and open-space fillings of vesicles, fractures, and spaces between breccia fragments. Frequent associated alteration minerals include chlorite, quartz, and calcite; chalcedony, hematite, magnetite, pyrite, pyrrhotite, wairakite, mordenite, garnet, actinolite/tremolite, and epidote occur in the same core samples as illite. In XRD analyses of illite, the basal (001) peak is a low, broad ~10Å reflection that does not shift following glycollation. Some illite is massive with closely packed sheet-like crystals deposited one on top of another. More frequently, the sheet-like crystals formed are randomly oriented with open spaces between the sheets (Figure 25). Chemical analyses of one illite specimen (Table 10)

Figure 25 near here

Table 10 near here

appears to be close to an analysis of hydromuscovite given in Deer, Howie, and Zussman (1966). Measured temperatures at depths where illite occurs in a geothermal hole drilled within Newberry caldera ranged between ~150° and 265°C (Bargar and Keith, in press).

Mixed-layer chlorite-smectite. Mixed-layer chlorite-smectite was identified only in the two intracaldera drill holes (Table 1). The green clay mineral coats fractures and vesicles between 1,052.9 and 1,108.5 m depth in the ML 28-32 drill hole, and from 1,053.1 to 1,202.4 m depth in the ML 45-36 drill hole. In both drill holes the chlorite-smectite appears to be an early hydrothermal deposit. Associated (later?) hydrothermal minerals include calcite, laumontite, chlorite, pyrite, hematite, quartz, wairakite, laumontite, chalcedony, epidote, actinolite/tremolite, and prehnite. Mixed-layer chlorite-smectite was found in drill holes at Newberry volcano at depths where the measured temperatures ranged from 110° to 160°C (Bargar and Keith, in press). Geothermal drill holes in Iceland and other areas contain mixed-layer chlorite-smectite at temperatures ranging between <100° and 240°C (Table 1). The Medicine Lake volcano mixed-layer chlorite-smectite deposits appear to be well crystallized and have sharp (001) and (002) XRD reflections at about 14.6Å and 7.3Å that show slight expansion to about 15.3Å and 7.4Å following exposure to ethylene glycol vapors at 60°C for one hour.

Chlorite. In the deeper parts of three of the Medicine Lake volcano drill holes (ML 28-32, ML 45-36. and ML 88-12), chlorite $\{(Mg,Al,Fe)_{12}[(Si,Al)_8O_{20}](OH)_{16}\}$ is the dominant sheet-silicate mineral (Table 1). Occasionally, chlorite replaces primary mafic minerals in the groundmass of the volcanic deposits; however, chlorite most commonly occurs as a filling in open spaces of breccias, fractures, and vesicles. Associated minerals in these open-space deposits include calcite, smectite, hematite, illite, mixed-layer illite-smectite, laumontite, quartz, pyrite, wairakite, chalcedony, magnetite, actinolite/tremolite, talc, garnet, epidote, and pyrrhotite.

Green chlorite is easily distinguished from green smectite by XRD analysis; chlorite has 14Å and 7Å reflections that do not expand after exposure to ethylene glycol vapors for 1 hour at 60°C whereas smectite and mixed-layer chlorite-smectite show marked displacement of the (001) and (002) XRD peaks following glycolation. The character of the XRD reflections range from very sharp peaks to low, broad peaks. Sharp

XRD peaks for chlorite are correlated with well-crystallized deposits consisting of hexagonal platelets or books of platelets (Figure 26a). Chlorite that is not as well

Figure 26 near here

crystallized (Figure 26b) will have broader XRD reflections.

Two electron-microprobe analyses of chlorite from the ML 45-36 drill hole (Table 10) would plot in the pycnochlorite field of a Si vs Fe/Fe+Mg diagram (Hey, 1954, p. 280). This is also true for chlorite from geothermal drill holes at Newberry volcano where the measured temperatures range from 120° to 265°C (Bargar and Keith, in press). In Iceland and other geothermal areas chlorite occurs over a wide temperature range (<100° to 350°C) (Table 1).

Apophyllite. A single drill core specimen from 1,042.4 m depth in the ML 86-23 drill hole contains vesicle and fracture fillings of dark green smectite, and later hemispheric clusters of white to colorless, bladed, and acicular crystals of scolecite, thomsonite, and gyrolite. In addition, some colorless, prismatic crystals were identified by XRD as apophyllite [$KFCa_4(Si_8O_{20})_8H_2O$] which is an uncommon phyllosilicate or sheet-silicate mineral; apophyllite usually is associated with zeolites and a few other hydrothermal minerals in open spaces of mafic volcanic rocks (Deer, Howie, and Zussman, 1966). Apophyllite also was identified in geothermal drill hole core samples from Hawaii, at a depth where the measured temperature was 70°C (Bargar, Keith, and Trusdell, 1995), and Newberry volcano (measured temperature at sample depth was ~50°C.) (Bargar and Keith, in press).

Most of the chemical analyses of apophyllite from the Medicine Lake volcano drill hole specimen (Table 11, analyses 3-8) appear to be consistent with the reported

Table 11 near here

chemical composition of apophyllite. However, analyses 1 and 2 in Table 11 suggest that Al substitutes for Si, and possibly, Na for K. These two analyses are also quite high in Ca and very low in K compared with the remaining analyses in Table 11.

Prehnite. Prehnite [$Ca_2Al_2Si_3O_{10}(OH)_2$] is also classified as a sheet-silicate mineral (Deer, Howie, and Zussman, 1966). Three drill core specimens from near the bottom of the ML 45-36 drill hole (Figure 3f) contain vesicle and fracture fillings of individual or radiating masses of colorless, blocky, prehnite crystals (Figure 27).

Figure 27 near here

Associated minerals include chlorite, quartz, chalcedony, epidote, actinolite/tremolite, anhydrite, wairakite, laumontite, and calcite. Chemical analyses of prehnite from two of the drill core specimens (Table 12) suggest some substitution of Fe for Al; analysis 1 for

Table 12 near here

sample ML 45-36 3820 contains substantial (anomalous?) Mg which is usually very low in prehnite (Deer, Howie, and Zussman, 1966). Temperatures at depths where prehnite has been reported from geothermal drill holes in Iceland and other areas of the world range from about 210° to 350°C (Table 1).

Talc. A single XRD analysis of a green clay, fracture-filling-specimen, obtained from 1,316.7 m depth in the ML 28-32 drill hole, has reflections for talc [$Mg_3Si_4O_{10}(OH)_2$], another sheet-silicate mineral. Fractures and vesicles in the analyzed sample also contain iron oxide, chlorite, calcite, and epidote. Talc has been reported occasionally from modern geothermal areas of the world at temperatures of about 290° to 320°C (Table 1).

SILICA MINERALS

Core samples from seven of the Medicine Lake volcano drill holes contain silica minerals (Table 1) that span the range of crystallinity from noncrystalline opal to poorly-crystallized cristobalite (XRD reflection at 4.11Å) to better ordered cristobalite (XRD peak at 4.04Å) to chalcedony—a cryptocrystalline variety of quartz—to well-crystallized quartz. Keith, White, and Beeson (1978) discuss the solubilities of these silica minerals at various temperatures as well as indications that the less well-crystallized silica phases can be converted to better-crystallized silica minerals through solid-state recrystallization as in the conversion from opal to cristobalite or from poorly ordered cristobalite to well-ordered cristobalite. Solution and redeposition are thought to be required in converting chalcedony to quartz and in the formation of chalcedony from cristobalite (Murata and Larson, 1975).

Opal. Amorphous opal ($SiO_2 \cdot nH_2O$) was only identified in fracture fillings of three samples from the upper part of the ML 45-36 drill hole (Figure 3f). The three opal specimens mostly consist of colorless to white, botryoidal deposits. Traces of smectite, the only associated mineral, were found on fractures from two specimens. Opal coating the fracture at 87.2 m depth is only partly botryoidal; it also has an unusual wormy, columnar, or tube-like (some broken tubes have a hollow core) morphology (Figure 28).

Figure 28 near here

The tubes appear to consist of coalesced opal spheres such as can be seen in the lower right corner and near the center of Figure 28. Opal is a fairly common hydrothermal deposit in modern geothermal areas where temperatures are <100°C (Table 1).

Cristobalite. Cristobalite (SiO_2) was identified in core samples obtained from five of the studied drill holes (Table 1). XRD analyses of colorless to white botryoidal silica (Figure 29) fracture fillings show the presence of both chalcedony and poorly

Figure 29 near here

crystalline cristobalite. Comparison of Figures 28 and 29 appears to show some degree of crystallinity in cristobalite/chalcedony that is absent in the amorphous opal. Other hydrothermal minerals lining these fractures include smectite, calcite, siderite, quartz, iron oxide, marcasite, pyrite, mordenite, heulandite, and stilbite/stellerite. Well-crystallized cristobalite was detected in only two XRD analyses. Cristobalite is a fairly common hydrothermal mineral in many geothermal areas where it was found at temperatures of <100° to 210°C (Table 1).

Chalcedony. Chalcedony (SiO_2) occurs only in core specimens from the same five drill holes that contained cristobalite (Table 1). Vesicles, fractures, and spaces between breccia fragments are partly filled by colorless, white, gray, or bluish botryoidal, powdery, or massive chalcedony. Other hydrothermal minerals in these open-space deposits include smectite, calcite, siderite, quartz, dolomite, pyrrhotite, marcasite, pyrite, hematite, chlorite, illite, epidote, magnetite, mordenite, heulandite, prehnite, and anhydrite. Chalcedony generally forms at temperatures below 100°C but it does occur in geothermal drill holes at measured temperatures as high as 240°C (Table 1).

Quartz. Core specimens from four of the five drill holes that contain cristobalite and chalcedony also contain colorless quartz (SiO_2) crystals; two drill holes containing quartz do not have cristobalite or chalcedony (Table 1). In these six drill holes, quartz crystals occur in association with most of the other hydrothermal minerals listed in Table 1. The quartz formed in open spaces of the various rock units as subhedral, dipyramidal (Figure 30) to euhedral prismatic crystals (Figures 25 and 26). Quartz has been reported

Figure 30 near here

from most studied geothermal areas at measured temperatures ranging from about 100°C to more than 300°C.

SULFIDE MINERALS

Marcasite. Tabular marcasite (FeS_2) crystals (Figure 31) were identified on

Figure 31 near here

fractures in five core specimens from two of the studied drill holes (Table 1). Associated minerals include siderite, heulandite, smectite, chalcedony, cristobalite, quartz, pyrite, natrojarosite and gypsum. Marcasite is metastable with respect to pyrite at low temperature (Craig and Scott, 1974) and is converted to pyrite at temperatures greater than 160°C in the Salton Sea geothermal system (McKibben, 1979). Marcasite occurs at temperatures of about 80° to 170°C in drill cores from Yellowstone National Park (Bargar and Beeson, 1984), at temperatures slightly less than 140°C at Steamboat Springs, Nevada (Sigvaldson and White, 1962), and at about 74° to 98°C in one Newberry volcano core hole (Bargar and Keith, in press).

Pyrrhotite. Tabular, bronze, hexagonal, slightly to strongly magnetic, pyrrhotite ($Fe_{1-x}S$) crystals (Figure 32) line fractures, cavities, and open spaces between breccia

Figure 32 near here

fragments, and are disseminated in several core specimens from two zones in the ML 28-32 drill hole; disseminated pyrrhotite was also identified, along with illite, chalcedony, and pyrite, in a single core specimen from the ML 45-36 drill hole. Hydrothermal minerals identified from the shallow pyrrhotite zone of drill hole ML 28-32 (Figure 3d) include: quartz, siderite, smectite, pyrite, chalcedony, heulandite, mordenite, calcite, kaolinite/serpentine, iron oxide, and mixed-layer illite-smectite. A deeper pyrrhotite-bearing zone in this drill hole contains, chlorite, epidote, wairakite, and illite. Browne and Ellis (1970) and Steiner (1977) reported pyrrhotite in drill cores from New Zealand geothermal areas at temperatures ranging from 152° to 268°C. Pyrrhotite in drill cores from Yellowstone National Park occur at temperatures measured during drilling of 130° to 152°C (Bargar and Beeson, 1981). At Newberry volcano, the measured temperatures at the depths where drill-hole specimens containing pyrrhotite occurred ranged between about 97° and 265°C (Bargar and Keith, in press).

Pyrite. Tiny (~2μm to 2 mm), cubic (occasionally pyritohedron), pyrite (FeS_2) crystals (Figure 33a) are present in core specimens from five of the Medicine Lake

Figure 33 near here

volcano drill holes (Table 1). One lithic tuff specimen from the ML 28-32 hole contains small nodular clusters of pyrite crystals (Figure 33b); this framboidal pyrite has been attributed to colloidal deposition or to the action of microorganisms (Deer, Howie, and Zussman, 1966). More commonly, pyrite in drill core samples from the five holes is deposited as subhedral to euhedral crystals either in open spaces of fractures, vesicles, lithophysal cavities, and breccias or is disseminated throughout the specimens. Some pyrite crystals or crystal clusters have a surrounding yellowish, orangish, or reddish halo suggesting minor oxidation has occurred. In addition, colorless gypsum needles had formed on the pyrite deposits in several of the collected core specimens. Other hydrothermal minerals identified in the same core specimens as pyrite include: smectite, natrojarosite, quartz, marcasite, calcite, cristobalite, heulandite, chlorite, mixed-layer

illite-smectite, illite, chalcedony, pyrrhotite, mixed-layer chlorite-smectite, actinolite/tremolite, epidote, anhydrite, laumontite, mordenite, iron oxide, rhodochrosite, siderite, kutnohorite, wairakite, and magnetite. Pyrite can form over a wide range of temperatures; studies of many geothermal areas indicate that pyrite can form at temperatures <100°C to >350°C (Table 1).

SULFATE MINERALS

The sulfate minerals (anhydrite, gypsum, and natrojarosite) identified in a few core specimens from three of the Medicine Lake volcano drill holes (Table 1) appear to have formed due to oxidation of pyrite or marcasite.

Anhydrite. One core specimen from the ML 28-32 and three specimens from the ML 45-36 drill holes contain colorless, blocky to tabular, anhydrite ($CaSO_4$) crystals that were deposited in vesicles and fractures (Table 1). Other hydrothermal minerals in these open-space fillings include mixed-layer illite-smectite, pyrite, calcite, chlorite, chalcedony, quartz, epidote, prehnite, actinolite/tremolite, and laumontite. Anhydrite can form over a wide temperature range (60° to 300°C) (Table 1). Associated hydrothermal minerals suggest that anhydrite very likely formed near the high end of this temperature range.

Gypsum. Gypsum ($CaSO_4 \cdot 2H_2O$) was identified in only two of the drill holes (Table 1) where it formed in open spaces of the rocks along with closely associated oxidized pyrite or marcasite. Other hydrothermal minerals in these specimens include natrojarosite, smectite, siderite, heulandite, chalcedony, and cristobalite. Some of the white to colorless, fibrous to acicular, gypsum crystals or sprays of crystals formed on the outer cored surface of the samples which indicates that the mineral precipitated after the core was brought to the surface. Gypsum precipitates at fairly low temperatures (<70°C) (Holland and Malinin, 1979).

Natrojarosite. Yellowish, powdery, open-space fillings in eight core specimens from the ML 28-32 and ML 36-28 drill holes (Table 1) were identified as natrojarosite [$NaFe_3(SO_4)_2(OH)_6$] in XRD analyses. Scanning electron microscope studies show that the powdery material consists of clusters of tiny, tabular, natrojarosite crystals (Figure 34). Natrojarosite generally forms in near-surface hydrothermal acid-sulfate or fumarolic

Figure 34 near here

conditions (Hemley and others, 1969). The natrojarosite is closely associated with oxidized pyrite or marcasite; smectite, gypsum, siderite, and calcite also are present in some specimens. Probably the natrojarosite formed from acid-sulfate conditions due to oxidation of pyrite. Natrojarosite in one geothermal drill hole at Newberry volcano occurs at a depth where the measured temperature is about 50°C (Bargar and Keith, in press).

OTHER MINERALS

Iron oxide. Both matrix and open spaces of many core specimens from eight of the drill holes (Table 1) contain brownish, reddish, black, orangish, or yellowish iron-oxide staining. XRD analyses of most of the specimens indicate that the iron oxide is amorphous to X-rays (limonite?) [$FeO(OH) \cdot nH_2O$]; hematite (Fe_2O_3) was identified from a few XRD analyses. Most iron oxide occurs as an early hydrothermal (or late vapor phase, see Figure 35) deposit that coats vapor-phase minerals (tridymite and K-feldspar);

Figure 35 near here

granophyric quartz; and open spaces of fractures, vesicles, or areas between breccia fragments. A few chalcedony deposits are stained red. Some sulfides have orangish to yellowish halos (plus gypsum or natrojarosite) which suggests oxidation of the sulfide minerals. Iron-oxide deposits usually are earthy, powdery, or clayey; however, black, metallic, specular hematite is associated with vapor-phase minerals in two specimens. Groundmass magnetite in several red-stained core specimens is altered to hematite. Most other hydrothermal minerals in core samples from the eight drill holes occur in association with the iron oxide. Hematite has been reported from drill holes in many geothermal areas at depths where measured temperatures ranged from <100° to 250°C (Table 1).

Magnetite. Fracture and vug fillings of magnetite (Fe_3O_4) or disseminated magnetite occurs in a few core specimens from the ML 28-32 drill hole. The morphology of these deposits varies from massive to crystalline; in one specimen, the massive deposits are botryoidal. The magnetite has partly altered to reddish hematite. XRD analyses also show the presence of chlorite, epidote, garnet, wairakite, quartz, chalcedony, calcite, and illite in the same specimens. Many of the associated minerals indicate that at least some of the magnetite probably formed at temperatures above 200°C.

Gyrolite. Two core specimens from the ML 86-23 drill hole contain white or colorless, bladed, gyrolite [$NaCa_{16}(Si_{23}Al)O_{60}(OH)_5 \cdot 15H_2O$] crystals. XRD analyses indicate that smectite, calcite, scolecite, levyne, stilbite/stellerite, analcime, thomsonite, phillipsite, and apophyllite also occur in these vesicles. Gyrolite appears to be a rare hydrothermal mineral. Gyrolite was deposited in core from one Newberry volcano drill hole where the measured temperature was <50°C (Bargar and Keith, in press). One core specimen from a drill hole in Yellowstone National Park contains gyrolite at a depth where the measured temperature was abut 125°C (Bargar, Beeson, and Keith, 1981). Gyrolite also has been identified in Icelandic geothermal drill holes at temperatures above 200°C (Kristmannsdóttir and Tómasson, 1978).

Adularia. Euhedral adularia ($KAlSi_3O_8$) crystals (Figure 36) were identified by

Figure 36 near here

XRD and SEM analyses of one core specimen from each of two drill holes (ML 86-23 and ML 28-32) (Table 1). Other hydrothermal minerals in these samples include: smectite, calcite, stilbite/stellerite, mordenite, heulandite, analcime, quartz, chalcedony, pyrite, and pyrrhotite. Adularia has been reported at temperatures between 150° and >300°C in modern geothermal areas (Table 1).

Actinolite/tremolite. Light green or white, fibrous, actinolite/tremolite [$Ca_2(Mg,Fe)_5Si_8O_{22}(OH)_2$] crystals (Figure 37a and b) were identified in vesicles and

Figure 37 near here

fractures near the bottom of the two intracaldera drill holes (Table 1). Associated hydrothermal minerals include: calcite, chlorite, mixed-layer chlorite-smectite, illite, chalcedony, epidote, pyrite, quartz, prehnite, anhydrite, and laumontite. The light green to white color of the clusters of fibrous crystals suggests that both tremolite and actinolite may be present. EDS semiquantitative analysis of two specimens shows Ca>Mg>Fe in the white one and Ca>Fe>Mg in the light green sample; minor Al in these analyses may result from substitution of Al for Si. Actinolite/tremolite occurs at temperatures between 260° and 400°C in drill holes of many modern geothermal areas (Table 1).

Epidote. Euhedral, yellow-green, epidote [$Ca_2(Fe,Al)_3(SiO_4)_3(OH)$] crystals (Figure 38) line vugs and fractures of lava flows, and spaces between fragments of

Figure 38 near here

breccias near the bottoms of the two intracaldera (ML 28-32 and ML 45-36) drill holes (Table 1). Hydrothermal minerals associated with epidote include prehnite and actinolite/tremolite (Figure 37), chlorite, illite, talc?, anhydrite, laumontite, mixed-layer chlorite-smectite, calcite, quartz, iron oxide, chalcedony, pyrite, pyrrhotite, magnetite, garnet, and wairakite. Electron microprobe analyses (Table 13) of several epidote

Table 13 near here

specimens from the two drill holes suggest some Fe—Al substitution with Fe enrichment and Al depletion of epidote crystals from the ML 28-32 drill hole. Epidote forms at temperatures between 220° and 350°C in many studied geothermal areas (Table 1).

Garnet. Fractures and vugs in seven core specimens obtained from 1,321.0 to 1,328.9 m depth in the ML 28-32 drill hole contain yellow-orange garnet [$Ca_3Fe_2(SiO_4)_3$] crystals (Figure 39). Hydrothermal magnetite was identified in these

Figure 39 near here

same specimens; other minerals lining these fractures and vugs include: epidote, calcite, chlorite, hematite, quartz, illite, wairakite, and chalcedony. Electron microprobe analyses of garnet crystals from one core specimen show that Ca and Fe are the dominant cations (Table 14) indicating that the mineral is an andradite garnet. Such garnets in drill-hole

Table 14 near here

samples from other geothermal areas were found at temperatures between 250° and >300°C (Table 1).

FLUID-INCLUSION DATA

Fluid-inclusion data were only obtained for quartz, calcite, and wairakite from the two geothermal drill holes (ML 28-32 and ML 45-36) that were completed within the caldera of Medicine Lake volcano. Hydrothermal quartz crystals occur in open spaces of six drill holes, calcite was found in all but 1 drill hole, and wairakite was identified only in the two intracaldera holes (Table 1). Calcite and wairakite are colorless to white soft minerals for which leakage of fluid from the inclusions potentially could result in erroneous fluid-inclusion data; on the other hand, quartz is a colorless hard mineral which generally is not believed to leak and is regarded as a very good mineral for fluid inclusion analyses (Roedder, 1984). Most fluid inclusions appear to have formed along healed fractures and are classified as being of secondary origin. Some inclusions may be classified as pseudosecondary because it appears that additional mineral growth occurred on exterior crystal faces which sealed off the fractured zones leaving rims almost free of fluid inclusions. A few inclusions are very large compared with the size of the host crystal and appear to be isolated from other fluid inclusions; these inclusions are classified as primary in this report. Quartz specimens first were frozen and gradually thawed to the temperature (T_m) at which the last piece of ice melts which provides an estimate of the salinity of the fluid trapped within the inclusions. These specimens were then heated to the homogenization temperature (T_h)—temperature at which the liquid and vapor phases in individual fluid inclusions merged to a single phase by expansion or contraction of the liquid upon heating. The order of heating and freezing was reversed for the soft calcite and wairakite minerals because of the possibility that fluid inclusions in these minerals might decrepitate during freezing.

ML 28-32. Homogenization temperatures (T_h) were obtained for 94 liquid-rich, secondary and pseudosecondary(?), fluid inclusions in quartz specimens from three

depths in the ML 28-32 drill hole; the T_h values range between 125° and 223°C (Table 15; Figure 40). Only 24 melting-point temperature (T_m) measurements were obtained

Table 15 near here

Figure 40 near here

for these fluid inclusions. Some of the analyzed specimens were too murky to determine the temperature at which the last piece of ice melted. The vapor bubble for several fluid inclusions disappeared during freezing and did not reappear until +2.6° to +4.1°C. These positive T_m values indicate metastability and the fluid inclusions cannot be used for salinity calculations (Roedder, 1984). Other T_m values range between -0.5° and -1.2°C corresponding to 0.9 to 2.1 weight percent NaCl equivalent. T_m data were not obtained for two calcite cleavage chips; T_h values for 44 fluid inclusions in the calcite specimens range between 139° and 225°C.

ML 45-36. Homogenization temperatures were obtained for 215 liquid-rich, secondary, pseudosecondary, and primary fluid inclusions in quartz crystals that line open spaces in drill core from five depths in the ML 45-36 drill hole (Table 15). Three vapor-rich pseudosecondary fluid inclusions from one specimen also were analyzed; these inclusions homogenized to the vapor state but the precise T_h values were not observed. T_h measurements for quartz specimens from this drill hole range between 145° and 373°C (Figure 41). T_m values of 120 fluid inclusions are mostly 0.0° and -0.1°C corresponding

Figure 41 near here

to a salinity of 0.0 to 0.2 weight percent NaCl equivalent. Nine fluid inclusions in one quartz specimen have a T_m value of -1.7°C which corresponds to a salinity of 2.9 weight percent NaCl equivalent.

Thirty T_m values were obtained for secondary liquid-rich fluid inclusions in one of two calcite specimens analyzed from this drill hole. T_m measurements for 22 fluid inclusions in one crystal from this specimen were 0.0°C (salinity = 0.0 weight percent NaCl equivalent). Eight fluid inclusions in a separate calcite crystal from the same specimen had T_m values of -1.1°C corresponding to a salinity of 1.9 weight percent NaCl equivalent. T_h values for 71 analyzed fluid inclusions in the two calcite specimens ranged from 178°C to 285°C. Forty one liquid-rich fluid inclusions in a wairakite specimen mostly leaked during heating. No T_m values were measured for the wairakite fluid inclusions, and only four T_h values between 186° and 263°C were recorded.

Reliability of the fluid-inclusion measurements in calcite and wairakite crystals may be suspect; however, the measured T_h and T_m values of these inclusions fall within the range of data for the quartz specimens from this drill hole (Figure 41 and Table 15). Several T_h measurements for liquid-rich fluid inclusions in quartz crystals from this drill hole are higher than a theoretical reference boiling-point curve—reflecting the maximum temperature attainable in a hot-water geothermal system at a given depth in a drill hole—drawn to the present ground surface (Figure 41). These fluid inclusions must have formed at some time in the past because present-day fluid inclusions forming at temperatures even slightly higher than the theoretical reference boiling-point curve would be expected to be vapor-rich. It is likely that these high T_h fluid inclusions formed at a time when the origin of the theoretical reference-boiling-point curve was at a much higher elevation owing to the presence of glacial ice (discussed in Bargar and Fournier, 1988a). Some effects of a late-Pleistocene glaciation at Medicine Lake volcano are discussed by Anderson (1941) and Donnelly-Nolan and Nolan (1986). These workers indicate that the estimated thickness of the glacial ice within the caldera of this volcano

must have been on the order of 150 m. If the boiling-point curve in Figure 41 were raised by 150 m, the majority of the high T_h fluid inclusions would plot below the adjusted theoretical reference boiling-point curve and would be liquid-rich inclusions (same as the observed fluid inclusions).

BACTERIA-LIKE PARTICLES

Scanning electron microscope studies of the Medicine Lake drill cores show tiny spherical, rod-shaped, or filamentous bacteria-like particles that appear to have lived on heulandite and mordenite in a few of the examined core specimens from the ML 28-32 drill hole (Figure 42 a and b) and on euhedral quartz crystals ML 45-36 (Figure 43 a and

Figure 42 near here

Figure 43 near here

b) drill hole. No controls to detect contamination by surface microorganisms were employed during drilling of the Medicine Lake holes or during subsequent handling of the core samples. Therefore, it cannot be determined if the bacteria-like particles actually were present in these rocks before the geothermal holes were drilled. Without the existence of appropriate controls during the drilling and handling of the core specimens, it would be imprudent to suggest that the particles are not the result of contamination.

A 2-mm-long, colorless, euhedral, quartz crystal from a fracture in a rhyolitic lava flow from 856-m depth in drill hole ML 45-36 contains dozens of similar bacteria-like moving particles that were trapped within a 200μm x 130μm, liquid-rich, primary fluid inclusion (Figure 44) (Bargar, 1992). The moving particles, ranging in size from <0.5μm

Figure 44 near here

(undefined shapes) to ~3μm to 5 μm (rodlike) (Figure 45), were first noticed during

Figure 45 near here

initial heating of the fluid inclusion. The submicron-sized particles move very rapidly at ambient temperature while the larger, rod-shaped particles move very sluggishly and are difficult to distinguish among the shadows near the vapor bubble and the outer margins of the fluid inclusion. At about 62°C, a large number of moving particles became apparent near the lower surface of the vapor bubble. Each particle moved in a constant circular mode perpendicular to the length of the vapor bubble; the combined movement of all of the particles defines a cylindrical current (see Attachment 1 video tape). Individual particles appear to bounce off the boundary between water and the vapor bubble, become caught in the continuous current, and then return to the water-vapor interface. The thermal-induced current has a greater velocity at the lower end (right side of Figure 44 photograph). Towards the upper end (near center of fluid inclusion) of the short tubular-shaped convective cell, the current velocity appears to gradually decrease, and the particles eventually drift off into the large interior area of the fluid inclusion. Some particles disappear behind the vapor bubble, but they most likely reenter the convective cell because the number of particles within the cell appears to remain nearly constant. As the temperature is reduced, movement of the larger rod-shaped particles decreases until at room temperature only a very slow Brownian-like motion is observed.

Salinity of the water in the fluid inclusion is very low with a T_m value of 0.0°C. No T_h measurement was obtained because heating was discontinued at ~130°C in order to insure preservation of the very large fluid inclusion. Fifty-five other liquid-rich,

secondary or pseudosecondary(?) fluid inclusions in quartz crystals from the same fracture have T_h values between 197° and 373°C (average of 244°C); T_m values for 33 of these fluid inclusions is 0.0° or -0.1°C (salinity =0.0 to 0.2 weight percent NaCl equivalent) (Table 15).

Similar moving particles were found in liquid-rich, secondary fluid inclusions in quartz crystals from depths of 753.8 (T_h of 253° to 278°C; T_m of 0.0°C), 841.6 (T_h of 233° to 265°C; T_m of 0.0° and -1.7°C), and 855.0 m (T_h of 260° and 289°C; T_m of 0.0°C) in the ML 45-36 drill hole. Bacteria-like moving particles were trapped within fluid inclusions in hydrothermal quartz crystals that formed on fractures of a 150-ka rhyolite lava flow penetrated by a U.S. Geological Survey research drill hole in Lower Geyser Basin, Yellowstone National Park, Wyoming (Bargar, Fournier, and Theodore, 1985) (T_h of 190° to 280°C; T_m of 0.0°C). In addition to this report of moving particles in fluid inclusions, bacteria-like particles in fluid inclusions also have been observed by the first author during fluid-inclusion studies of drill hole specimens from other geothermal areas. Rod-shaped moving particles are present within several liquid-rich fluid inclusions (T_h of 249° to 286°C; T_m of 0.0°C) in hydrothermal quartz crystals from 1,133-m depth in drill core from the Geysers geothermal area of northern California (Bargar, Fournier, and Theodore, 1985). A few liquid-rich fluid inclusions (T_m of -0.9°C; T_h of 215° and 241°C) in hydrothermal quartz crystals from the Miravalles geothermal area, Costa Rica, contain as many as 3 irregular or rodlike, micrometer-size moving particles (Bargar and Fournier, 1988b). A hydrothermal quartz crystal in one drill-hole sample from the Long Valley, California, geothermal area has 2 liquid-rich fluid inclusions (T_h of 191° and 209°C; T_m of -0.3°C) that contain one and two rodlike moving particles, respectively (Bargar, 1995). Also, tiny threadlike and rodlike moving particles were observed in liquid-rich fluid inclusions (T_h of 250° and 258°C; T_m of 0.0°C) from a fossil geothermal area near Mount Hood, Oregon (Bargar, Keith, and Beeson, 1993).

SUMMARY AND CONCLUSIONS

This study of core samples from 12 geothermal prospect drill holes in the Medicine Lake volcano area identified forty-five minerals that we believe must have formed by hydrothermal alteration at low to moderate temperatures of zeolite-facies to greenschist-facies metamorphism. The facies terms are used for characterizing the degree to which rocks in different areas of the volcano have been metamorphosed. The identified mineral assemblages (zeolites, carbonates, sheet-silicates, silica minerals, sulfides, sulfates, and other minerals) from the drill holes sited outside the caldera of Medicine Lake volcano (Table 1, Figures 3a-c, e, and g-k) are generally characteristic of conditions attributed to zeolite-facies metamorphism. The minerals identified from the upper parts of the two intracaldera drill holes (Table 1, Figures 3d and f) also appear to reflect the same low-temperature (<200°C) conditions. It is only near the bottoms of the ML 28-32 and ML 45-36 intracaldera drill holes that several of the identified minerals (garnet, epidote, actinolite/tremolite, prehnite, and talc) undoubtedly formed under higher-temperature (200° to 400°C) subgreenschist- to greenschist-facies conditions.

No fluid inclusions were found in minerals (calcite) from the drill holes located outside the Medicine Lake caldera. Studies of fluid inclusions within quartz and calcite deposits from the ML 28-32 drill hole produced homogenization temperatures (T_h) that are mostly characteristic of zeolite-facies metamorphism (Table 15, Figure 40). It is only the presence of the metamorphic minerals garnet, epidote, actinolite/tremolite, and talc (Table 1, Figure 3d) that indicates the existence of past higher temperatures in this drill hole. However, in the ML 45-36 drill hole the T_h values for calcite and quartz fluid inclusions predominantly fall in the 200° to 300°C range (Table 15, Figure 41) characteristic of subgreenschist- to greenschist-facies conditions. The presence of

epidote, actinolite/tremolite, and prehnite (Table 1, Figure 3f) provides additional support for higher-temperature metamorphism. Minimum T_h measurements for fluid inclusions in the lower half of the ML 45-36 drill hole suggest that present-day temperatures at some depths may be near 200°C.

One aspect of the fluid-inclusion studies of the ML 45-36 drill core samples provides support for late Pleistocene glaciation in the Medicine Lake volcano area. T_h measurements of numerous liquid-rich fluid inclusions from several depths in the ML 45-36 drill hole plot above a theoretical reference boiling point curve drawn to the present ground surface (Figure 41). If the temperatures at which the fluid inclusions formed exceed this boiling point curve they should be mostly vapor-rich or at least include coexisting vapor-rich fluid inclusions. For liquid-rich fluid inclusions to form at the measured T_h values, they must have formed under very different conditions than occur at the present time. Anderson (1941) and Donnelly-Nolan and Nolan (1986) discussed evidence for a glacial cover about 150 thick in the Medicine Lake volcano area. An additional ground cover of 150 m of glacial ice would require that pore-fluid pressures in the underlying rock be increased in proportion to the weight of the overlying column of ice. Accordingly, a theoretical reference boiling-point curve, reflecting the maximum temperature attainable in a hot-water geothermal system at a given depth, would be elevated and temperatures within that thermal upflow system would be increased. The thickness of ice required to elevate the boiling-point curve sufficient to account for the observed fluid inclusion T_h values is nearly coincident with the estimated glacial thickness from the surface geology studies.

During fluid-inclusion studies, dozens of tiny (~ 3 to 4 μm) rod-shaped moving particles (see Attachment 1 video tape) were observed within fluid inclusions in quartz from 4 depths (753.8, 841.6, 854.4, and 856.2 m) in the ML 45-36 drill hole. Many other particles were too small to discern their shape. The particles apparently were trapped over a period of time because they are contained within primary, pseudosecondary, and secondary liquid-rich fluid inclusions.

At the present time, the possibility that the moving particles within these fluid inclusions might be bacteria is highly speculative. The size and shapes of the particles are consistent with that of bacteria, however, attempts to determine by Raman (R. C. Burruss, written commun., 1990) and infrared spectroscopy methods if organic material might be present within one of the Yellowstone particle-bearing fluid inclusions were inconclusive. Nonetheless, an inorganic origin for the particles is difficult to envision from a chemical viewpoint. First, a high degree of supersaturation would be required for the simultaneous nucleation of large numbers of particles, and thereafter some special circumstance would have to prevail that prevented growth of large crystals at the expense of the smaller particles. The fluid inclusions mostly have very low salinities which would tend to negate any supersaturation hypothesis. Also, moving particles were trapped in relatively few fluid inclusions; the vast majority of nearby contemporary inclusions do not contain the moving particles. Thus, it seems highly probable that the moving particles (whatever their origin—organic or inorganic) were carried by the fluids from which the quartz crystals precipitated. These particle-bearing fluids flowed through fractures, and subsequently, were trapped within fluid inclusions of the precipitating quartz crystals.

If the moving particles within fluid inclusions in quartz crystals from Medicine Lake volcano, Yellowstone National Park, and elsewhere eventually are proven to be bacteria, they somehow must have become adapted to survival at temperatures above 200°C. The upper temperature limit for life to exist is not presently known but is believed to be between 110°C (hottest temperature at which bacteria have been conclusively identified) and about 200° or 250°C (Brock, 1985). On the other hand, thermophilic bacteria are reported to have been collected from a 350°C "black smoker" hot spring on the East Pacific Rise and grown in the laboratory at 250°C and elevated

pressures (Baross and Deming, 1983). The results from this study were disputed (Trent, Chastain, and Yayanos, 1984); however, Baross, Deming, and Becker (1984) provided additional amino acid analyses and other data in support of their contention that extreme thermophilic microorganisms do exist.

ACKNOWLEDGMENTS

We thank the Energy and Geoscience Institute of the University of Utah in Salt Lake City for allowing us to obtain the necessary samples for this study. We also thank J. M. Donnelly-Nolan, R. H. Mariner, and Steve McKnight for applying their muscles to moving the tons(?) of drill core that ultimately were examined. While moving the hundreds of boxes of drill core off and back on the storage shelves, general discussions with these colleagues provided us with good background information on the geology and geothermal exploration of Medicine Lake volcano. R. L. Oscarson provided the scanning electron microscope photographs used in the report. We are very grateful to Lasertec U.S.A., Inc., of San Jose, California for allowing us to use their laser scanning microscope to photograph and videotape moving particles in one fluid inclusion from the Medicine Lake volcano drill core. Reviews of the manuscript by J. M. Donnelly-Nolan and J. B. Lowenstern improved the report.

REFERENCES CITED

Anderson, C. A., 1941, Volcanoes of the Medicine Lake Highland, California: University of California Publications Bulletin of the Department of Geological Sciences, v. 25, no. 7, p. 347-422.

Aumento, F., and Liguori, P. E., 1986, Conceptual reservoir models through geoscientific investigations: Geothermics, v. 15, p. 799-806.

Bargar, K. E., 1990, Hydrothermal alteration in geothermal drill hole CTGH-1, High Cascade Range, Oregon: Oregon Geology, v. 52, no. 4, p. 75-81.

_____, 1992, Video-tape of bacteria-like moving particles in fluid inclusions from Medicine Lake volcano, northern California (abs.): EOS, Transactions, American Geophysical Union, v. 73, no. 43, p. 640.

_____, 1995, Some fluid-inclusion measurements for geothermal drill holes in California, Nevada, El Salvador, and Russia: U.S. Geological Survey Open-File Report 95-826, 14 p.

Bargar, K. E., and Beeson, M. H., 1981, Hydrothermal alteration in research drill hole Y-2, Lower Geyser Basin, Yellowstone National Park, Wyoming: American Mineralogist, v. 66, p. 473-490.

_____1984, Hydrothermal alteration in research drill hole Y-6, Upper Firehole River, Yellowstone National Park, Wyoming: U.S. Geological Survey Professional Paper 1054-B, 24 p.

_____, 1985, Hydrothermal alteration in research drill hole Y-3, Lower Geyser Basin, Yellowstone National Park, Wyoming: U.S. Geological Survey Professional Paper 1054-C, 23 p.

Bargar, K. E., Beeson, M. H., and Keith, T. E. C., 1981, Zeolites in Yellowstone National Park: The Mineralogical Record, v. 12, p. 29-38.

Bargar, K. E., and Fournier, R. O., 1988a, Effects of glacial ice on subsurface temperatures of hydrothermal systems in Yellowstone National Park, Wyoming: Fluid-inclusion evidence: Geology, v. 16, p. 1,077-1,080.

_____, 1988b, Fluid-inclusion evidence for previous higher temperatures in the Miravalles geothermal field, Costa Rica: Geothermics, v. 17, no. 5/6, p. 681-693.

Bargar, K. E., Fournier, R. O., and Theodore, T. G., 1985, Particles in fluid inclusions from Yellowstone National Park—bacteria?: Geology, v. 13, p. 483-486.

Bargar, K. E., and Keith, T. E. C., 1993, Hydrothermal alteration in cores from geothermal drill holes at Medicine Lake volcano, northeastern California (abs.): EOS, Transactions, American Geophysical Union, v. 74, no. 43, p. 688.

_____, in press, Hydrothermal mineralogy of core from geothermal drill holes at Newberry volcano, Oregon: U.S. Geological Survey Bulletin, 290 p.

Bargar, K. E., Keith, T. E. C., and Beeson, M. H., 1993, Hydrothermal alteration in the Mount Hood area, Oregon: U.S. Geological Survey Bulletin 2054, 70 p.

Bargar, K. E., Keith, T. E. C., and Trusdell, F. A., 1995, Fluid-inclusion evidence for past temperature fluctuations in the Kilauea East Rift Zone geothermal area, Hawaii: Geothermics, v. 24, no. 5/6, p. 639-659.

Bargar, K. E., and Oscarson, R. L., 1997, Zeolites and selected other hydrothermal minerals in the Cascade Mountains of northern Oregon: U.S. Geological Survey Open-File Report 97-100, 64 p.

Baross, J. A., and Deming, J. W., 1983, Growth of 'black smoker' bacteria at temperatures of at least 250°C: Nature, v. 303, p. 423-426.

Baross, J. A., Deming, J. W., and Becker, R. R., 1984, Evidence for microbial growth in high-pressure, high-temperature environments: *in* Klug, M. J., and Reddy, C. A., ed., Current Perspectives in Microbial Ecology: American Society for Microbiology, Washington D.C., p. 186-195.

Blackwell, D. D., Steele, J. L., Frohme, M. K., Murphey, C. F., Priest, G. R., and Black, G. L., 1990, Heat flow in the Oregon Cascade Range and its correlation with regional gravity, Curie point depths, and geology: Journal of Geophysical Research, v. 95, no. B12, p. 19,475-19,493.

Bodnar, R. J., and Sterner, S. M., 1984, Synthetic fluid inclusions in natural quartz I; compositional types synthesized and applications to experimental geochemistry: Geochimica et Cosmochimica Acta, v. 48, p. 2,659-2,668.

Brock, T. D., 1985, Life at high temperatures: Science, v. 230, p. 132-138.

Browne, P. R. L., and Ellis, A. J., 1970, The Ohaki-Broadlands hydrothermal area, New Zealand, mineralogy and related geochemistry: American Journal of Science, v. 269, p. 97-131.

Cavarretta, G., Gianelli, G., and Puxeddu, M., 1982, Formation of authigenic minerals and their use as indicators of the physicochemical parameters of the fluid in the Larderello—Travale geothermal field: Economic Geology, v. 77, p. 1,071-1,084.

Craig, J. R., and Scott, S. D., 1974, Sulfide phase equilibria, *in* P H. Ribbe, ed., Sulfide Mineralogy: Mineralogical Society of America Short Course Notes, v. 1, p. CS1-CS110.

Deer, W. A., Howie, R. A., and Zussman, J., 1966, An introduction to the rock-forming minerals: London, Longman, 528 p.

Donnelly-Nolan, J. M., 1988, A magmatic model of Medicine Lake volcano, California: Journal of Geophysical Research, v. 93, no. B5, p. 4,412-4,420.

_____1990, Geology of Medicine Lake volcano, northern California Cascade Range: Geothermal Resources Council Transactions, v. 14, pt. II, p. 1,395-1,396.

Donnelly-Nolan, J. M., Champion, D. E., Miller, C. D., Grove, T. L., and Trimble, D. A., 1990, Post-11,000-year volcanism at Medicine Lake volcano, Cascade Range, northern California: Journal of Geophysical Research, v. 95, no. B12, p. 19,693-19,704.

Donnelly-Nolan, J. M., and Nolan, K. M., 1986, Catastrophic flooding and eruption of ash-flow tuff at Medicine Lake volcano, California: Geology, v. 14, p. 875-878.

Elder, J., 1981, Geothermal Systems: London, Academic Press, 508 p.

Elders, W. A., Hoagland, J. R., McDowell, S. D., and Cobo, J. M., 1979, Hydrothermal mineral zones in the geothermal reservoir of Cerro Prieto: Geothermics, v. 8, p. 201-209.

Fleischer, Michael, and Mandarino, J. A., 1991, Glossary of mineral species: Tucson, The Mineralogical Record Inc., 256 p.

Frey, Martin, and Kisch, H. J., 1987, Scope of subject, *in* Frey, Martin, ed., Low temperature metamorphism: New York, Chapman and Hall, p. 1-8.
Fridleifsson, G. O., 1991, Hydrothermal systems and associated alteration in Iceland: Geological Survey of Japan Report 277, p. 83-90.
Grim, R. E., 1968, Clay mineralogy: San Francisco, McGraw-Hill Book Co. 596 p.
Gottardi, Glauco, and Galli, Ermanno, 1985, Natural Zeolites: Berlin, Springer-Verlag, 409 p.
Hemley, J. J., Hostetler, P. B., Gude, A. J., and Mountjoy, W. T., 1969, Some stability relations of alunite: Economic Geology, v. 64, p. 599-612.
Hey, M. H., 1954, A new review of the chlorites: Mineralogical Magazine, v. 30, p. 277-292.
Holland, H. D., and Malinin, S. D., 1979, The solubility and occurrence of non-ore minerals, *in* Barnes, H. L., ed., Geochemistry of Hydrothermal Ore Deposits, New York, John Wiley, p. 461-508.
Honda, S., and Muffler, L. J. P., 1970, Hydrothermal alteration in core from research drill hole Y-1, Upper Geyser Basin, Yellowstone National Park, Wyoming: American Mineralogist, v. 55, p. 1,714-1,737.
Horton, D. G., 1985, Mixed-layer illite/smectite as a paleotemperature indicator in the Amethyst vein system, Creed district, Colorado, USA: Contributions to Mineralogy and Petrology, v. 91, p. 171-179.
Hower, J., 1981, X-ray diffraction identification of mixed-layer clay minerals: *in* Longstaffe, F. J., ed., Short Course in Clays and the Research Geologist, Short Course Handbook 7, Toronto, Mineralogical Association of Canada, p. 39-59.
Hulen, J. B., and Nielson, D. L., 1986, Hydrothermal alteration in the Baca Geothermal System, Redondo Dome, Valles Caldera, NM: Journal of Geophysical Research, v. 91, p. 1,867-1,886.
Jakobsson, S. P., and Moore, J. G., 1986, Hydrothermal minerals and alteration rates at Surtsey Volcano, Iceland: Geological Society of America Bulletin, v. 97, p. 648-659.
Keith, T. E. C., White, D. E., and Beeson, M. H., 1978, Hydrothermal alteration and self-sealing in Y-7 and Y-8 drill holes in northern part of Upper Geyser Basin, Yellowstone National Park, Wyoming: U.S. Geological Survey Professional Paper 1054-A, 26 p.
Krieger, P., 1930, Notes on an X-ray diffraction study of the series calcite-rhodochrosite: American Mineralogist, v. 15, p. 23-29.
Kristmannsdóttir, Hrefna, 1979, Alteration of basaltic rocks by hydrothermal activity at 100-300°C: *in* Mortland, M. M., and Farmer, V. C., eds., International Clay Conference 1978, Amsterdam, Elsevier, p. 359-367.
Kristmannsdóttir, Hrefna, and Tómasson, Jens, 1978, Zeolite zones in geothermal areas of Iceland, *in* Sand, L. B., and Mumpton, F. A., eds., Natural Zeolites, Occurrence, Properties, Use: New York, Pergamon, p. 277-284.
Leach, T. M., Wood, C. P., and Reyes, A. G., 1983, Geology and hydrothermal alteration of the Tongonan geothermal field, Leyte, Republic of the Philippines (abs.): Fourth International Symposium on Water-Rock Interaction, Misasa, Japan, 29 August-3 September, 1983, p. 275-278.
Liou, J. G., Maruyama, Shigenori, and Cho, Moonsup, 1987, Very low-grade metamorphism of volcanic and volcaniclastic rocks-mineral assemblages and mineral facies, *in* Frey, Martin, ed., Low temperature metamorphism: New York, Chapman and Hall, p. 59-113.
McCulloh, T. H., Frizzell, V. A., Jr., Stewart, R. J., and Barnes, Ivan, 1981, Precipitation of laumontite with quartz thenardite, and gypsum at Sespe Hot Springs, Western Transverse Ranges, California: Clays and Clay Minerals, v. 29, no. 5, p. 353-364.
McDowell, S. D., and Paces, J. B., 1985, Carbonate alteration minerals in the Salton Sea geothermal system, California, USA: Mineralogical Magazine, v. 49, p. 469-479.

McKibben, M. A., 1979, Ore minerals in the Salton Sea Geothermal system, Imperial Valley, California, U.S.A.: Riverside, University of California, M.S. thesis, 90 p.
Muffler, L. J. P., and White, D. E., 1969, Active metamorphism of Upper Cenozoic sediments in the Salton Sea geothermal field and the Salton Trough, southeastern California: Geological Society of America Bulletin, v. 80, p. 157-182.
Murata, K. J., and Larson, R. R., 1975, Diagenesis of Miocene siliceous shales, Temblor Range, California: U.S. Geological Survey Journal of Research, v. 3, p. 553-566.
Oscarson, R. L., and Bargar, K. E., 1996, Electron microprobe analyses of zeolite minerals from Neogene volcanic rocks in the Breitenbush-Austin Hot Springs area, Oregon: U.S. Geological Survey Open-File Report 96-41, 61 p.
Passaglia, Elio, 1970, The crystal chemistry of chabazites: American Mineralogist, v. 55, p. 1,278-1,301.
Potter, R. W., II, Clynne, M. A., and Brown, D. L., 1978, Freezing point depression of aqueous sodium chloride solutions: Economic Geology, v. 73, p. 284-285.
Roedder, Edwin, 1984, Fluid inclusions, *in* Ribbe, P. H., ed., Reviews in Mineralogy, v. 12: Washington, D. C., Mineralogical Society of America, 644 p.
Sigvaldson, G. E., and White, D. E., 1962, Hydrothermal alteration in drill holes GS-5 and GS-7, Steamboat Springs, Nevada: U.S. Geological Survey Professional Paper 450-D, p. D113-D117.
Steiner, A., 1977, The Wairaki geothermal area, North Island, New Zealand, its subsurface geology and hydrothermal rock alteration: New Zealand Geological Survey Bulletin 90, 136 p.
Taguchi, S., and Hyashi, M., 1982, Application of the fluid inclusion thermometer to some geothermal fields in Japan: Geothermal Resources Council Transactions, v. 6, p. 59-62.
Taguchi, S., Hayashi, M., Mimura, T., Kinoshita, Y., Gokou, K., and Abe, I., 1984, Fluid inclusion temperature of hydrothermal minerals from the Kirishima geothermal area, Kyushu, Japan: Journal of the Japan Geothermal Energy Association, v. 21, no. 2, p. 119-129.
Tómasson, Jens, and Kristmannsdóttir, Hrefna, 1972, High-temperature alteration minerals and thermal brines, Reykjanes, Iceland: Contributions to Mineralogy and Petrology, v. 36, p. 123-137.
Trent, J. D., Chastain, R. A., and Yayanos, A. A., 1984, Possible artifactual basis for apparent bacterial growth at 250°C: Nature, v. 307, p. 737-740.
Tschernich, R. W., 1992, Zeolites of the World: Phoenix, Geoscience Press, Inc. 563 p.
White, D. E., Hutchinson, R. A., and Keith, T. E. C., 1988, The geology and remarkable thermal activity of Norris Geyser Basin, Yellowstone National Park, Wyoming: U.S. Geological Survey Professional Paper 1456, 84 p.

1. Location map of Medicine Lake volcano, northern California in relation to other volcanoes of the Cascade Mountain Range (shaded areas).

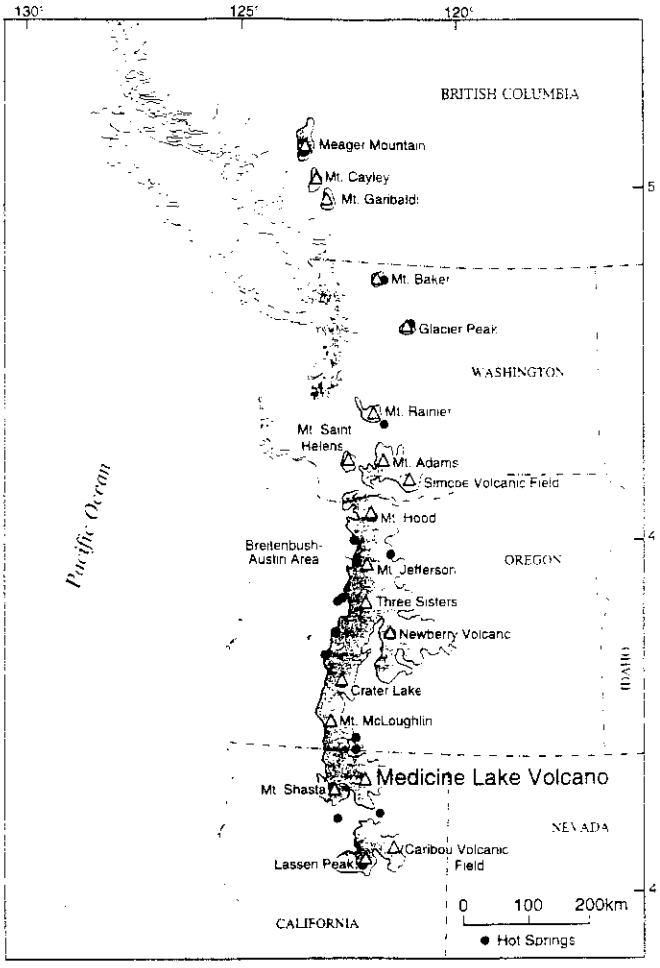

2. Topographic map of Medicine Lake volcano, northern California showing the location of 11 of the 12 geothermal prospect drill holes included in this study. Drill hole ML 88-12 is located about 10 kilometers west of the ML 52-4 drill hole. The rim of the caldera lies within the closed 7,000 foot contour lines.

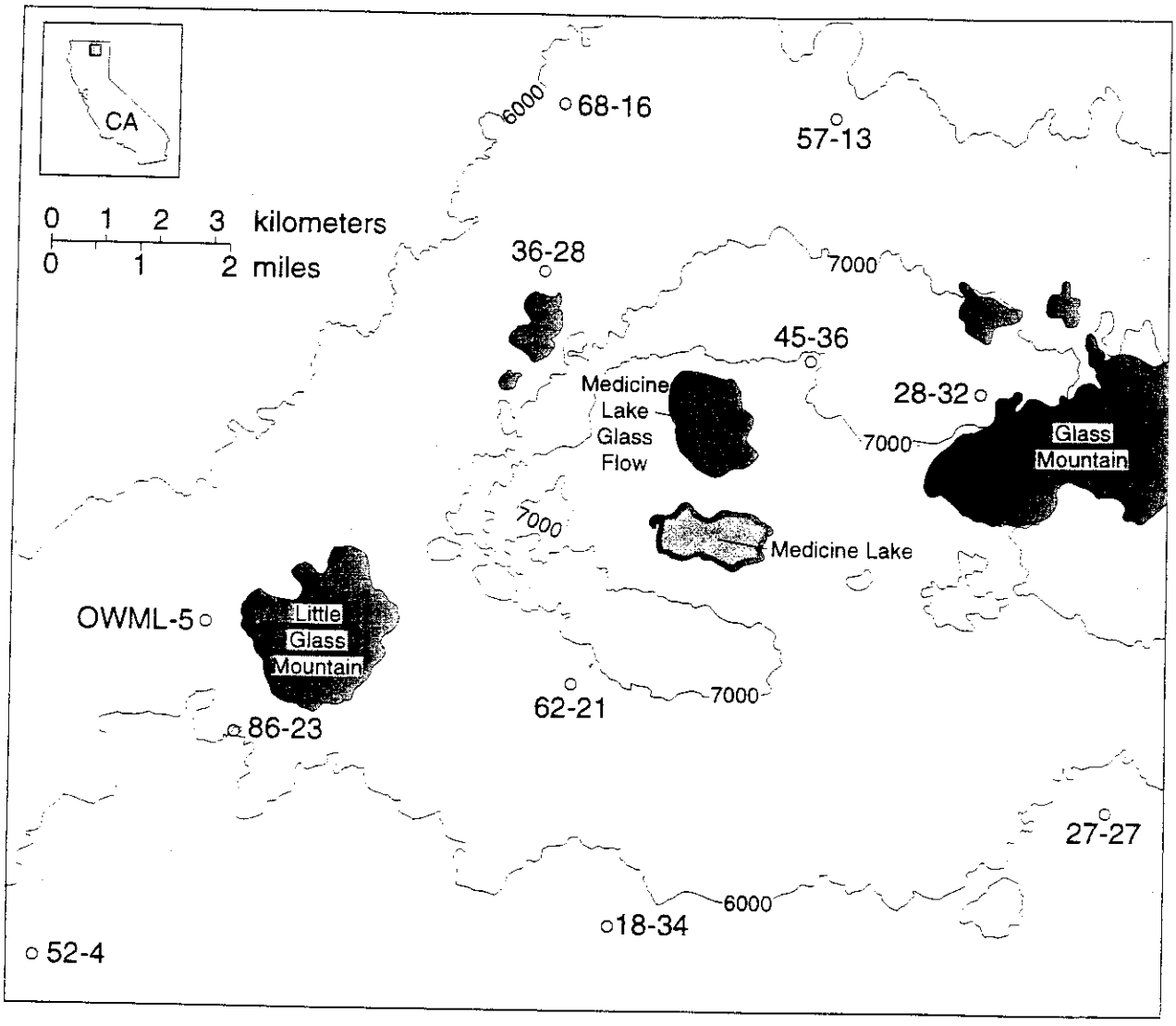

3a. Diagram showing the distribution of hydrothermal alteration minerals with depth in geothermal drill hole OWML5 (Figure 2). Tick marks at the extreme right side of the figures 3a to 3k show the depth at which the studied samples were collected from each drill hole.

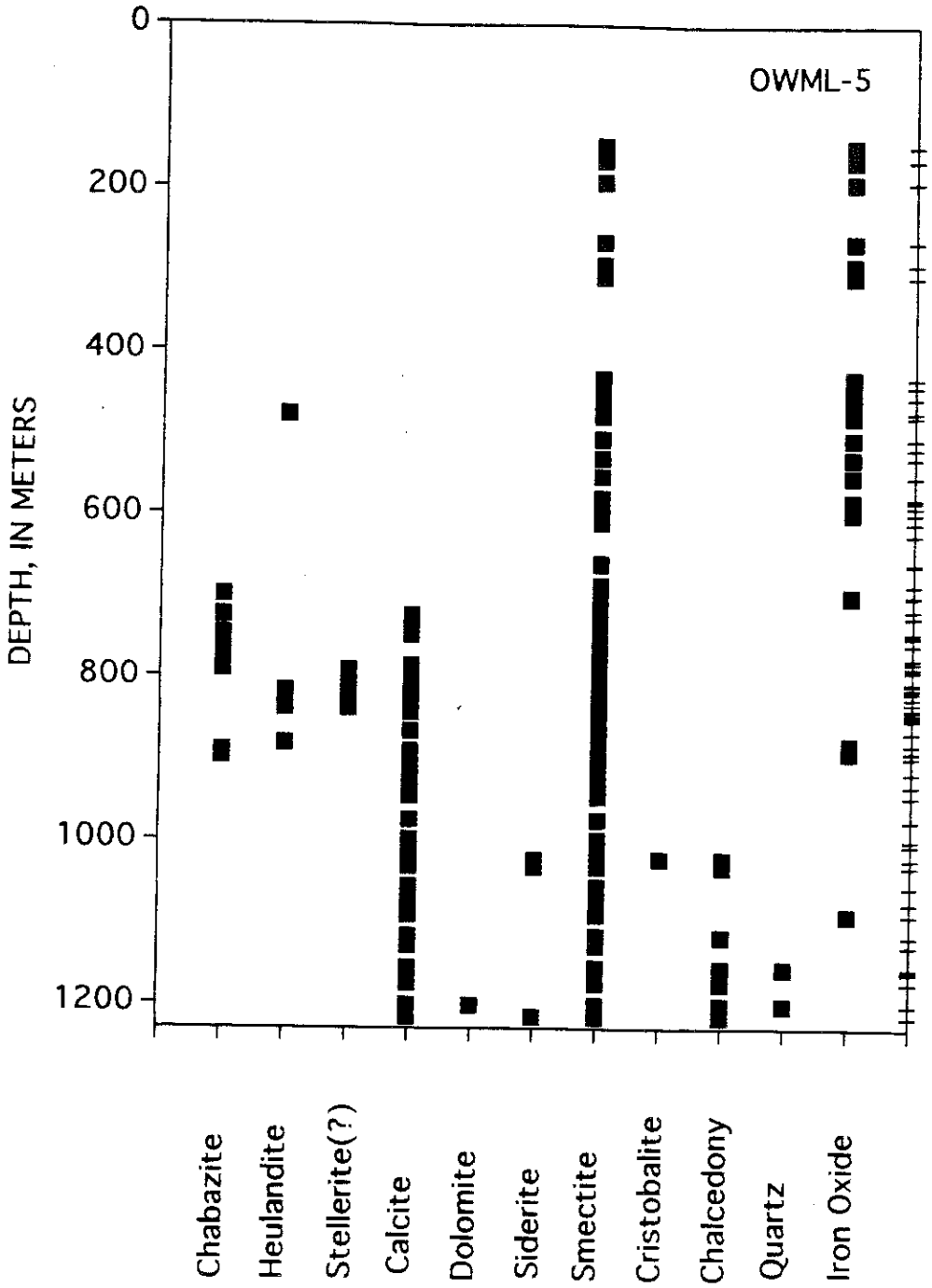

3b. Diagram showing the distribution of hydrothermal alteration minerals with depth in geothermal drill hole ML 18-34.

Done

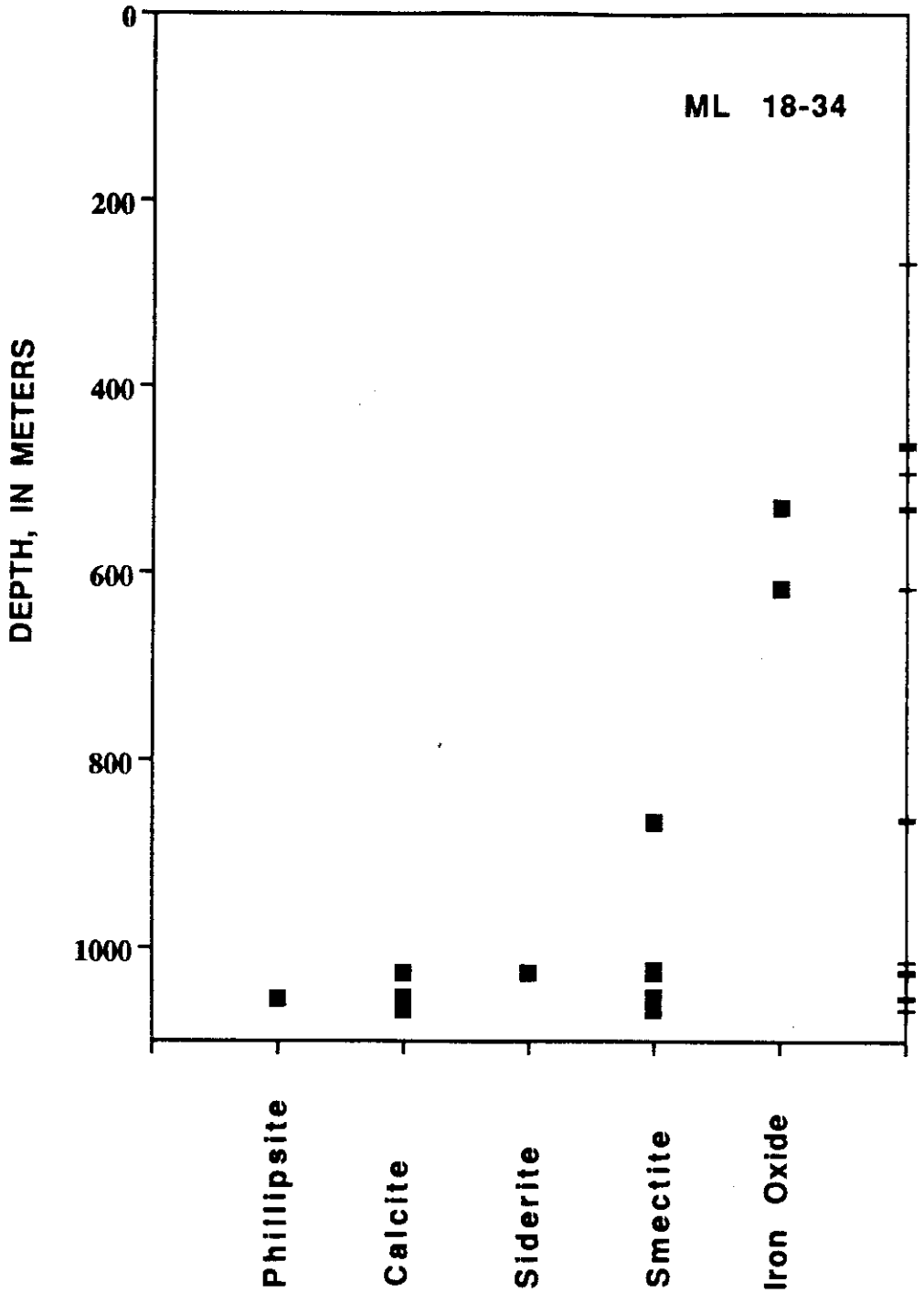

3c. Diagram showing the distribution of hydrothermal alteration minerals with depth in geothermal drill hole ML 27-27.

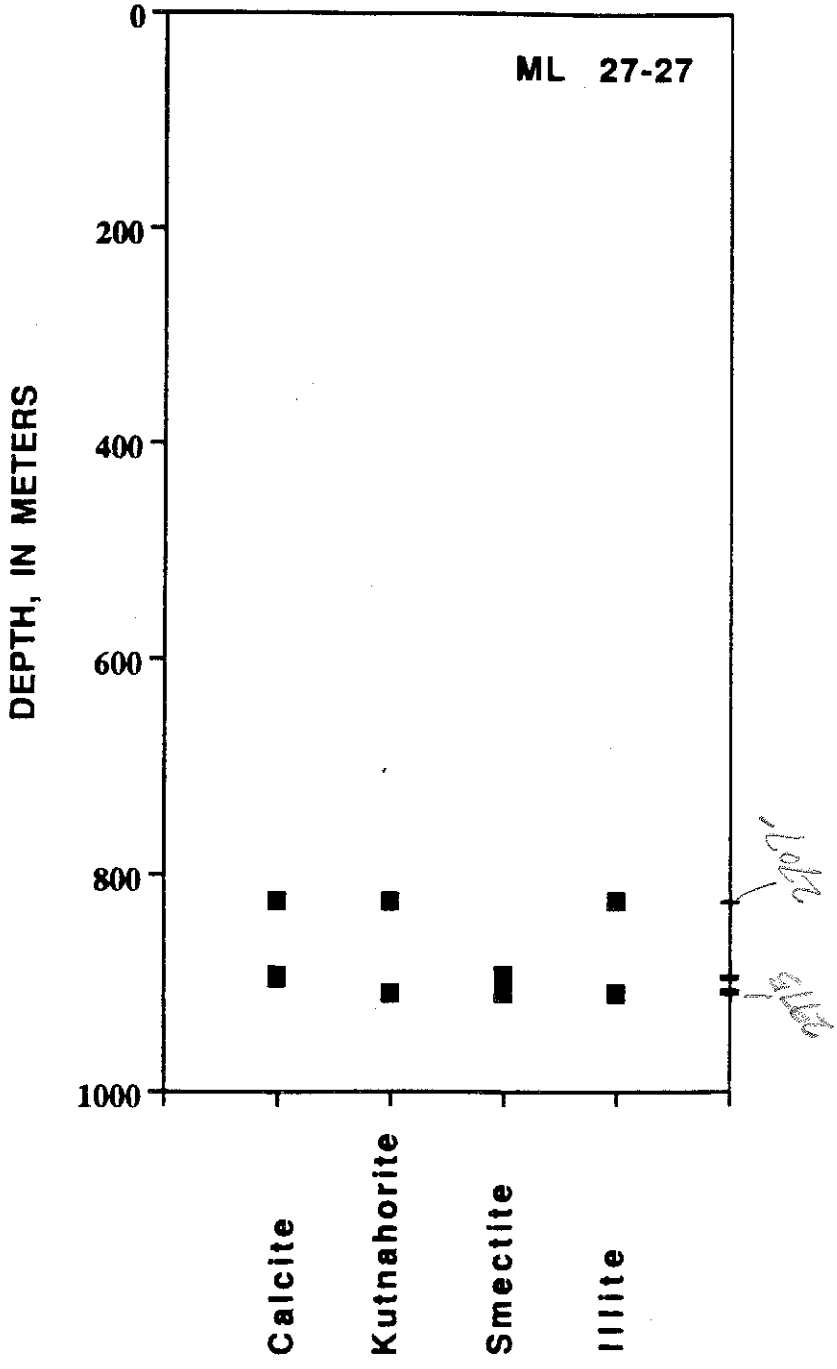

3d. Diagram showing the distribution of hydrothermal alteration minerals with depth in geothermal drill hole ML 28-32.

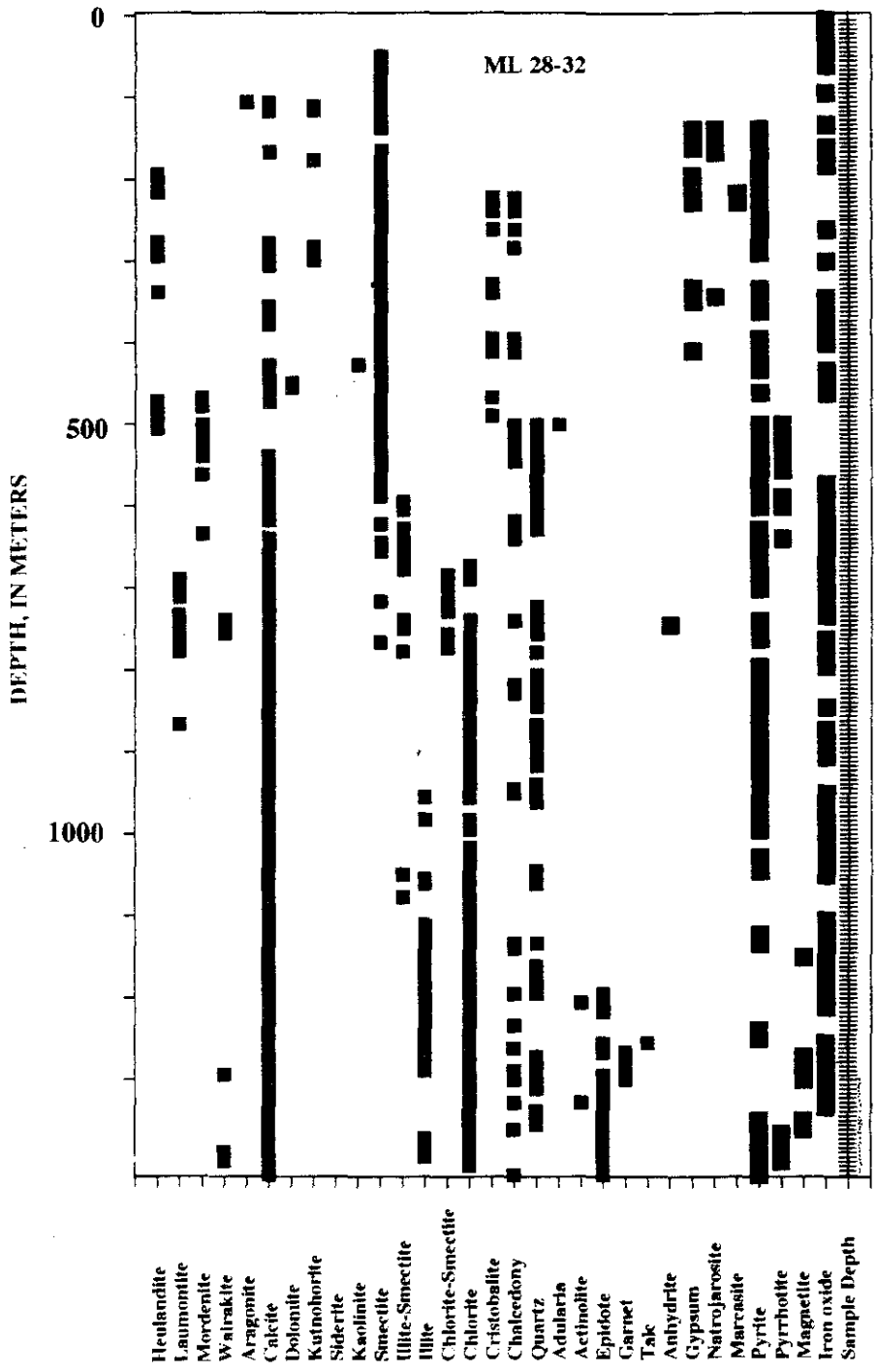

3e. Diagram showing the distribution of hydrothermal alteration minerals with depth in geothermal drill hole ML 36-28.

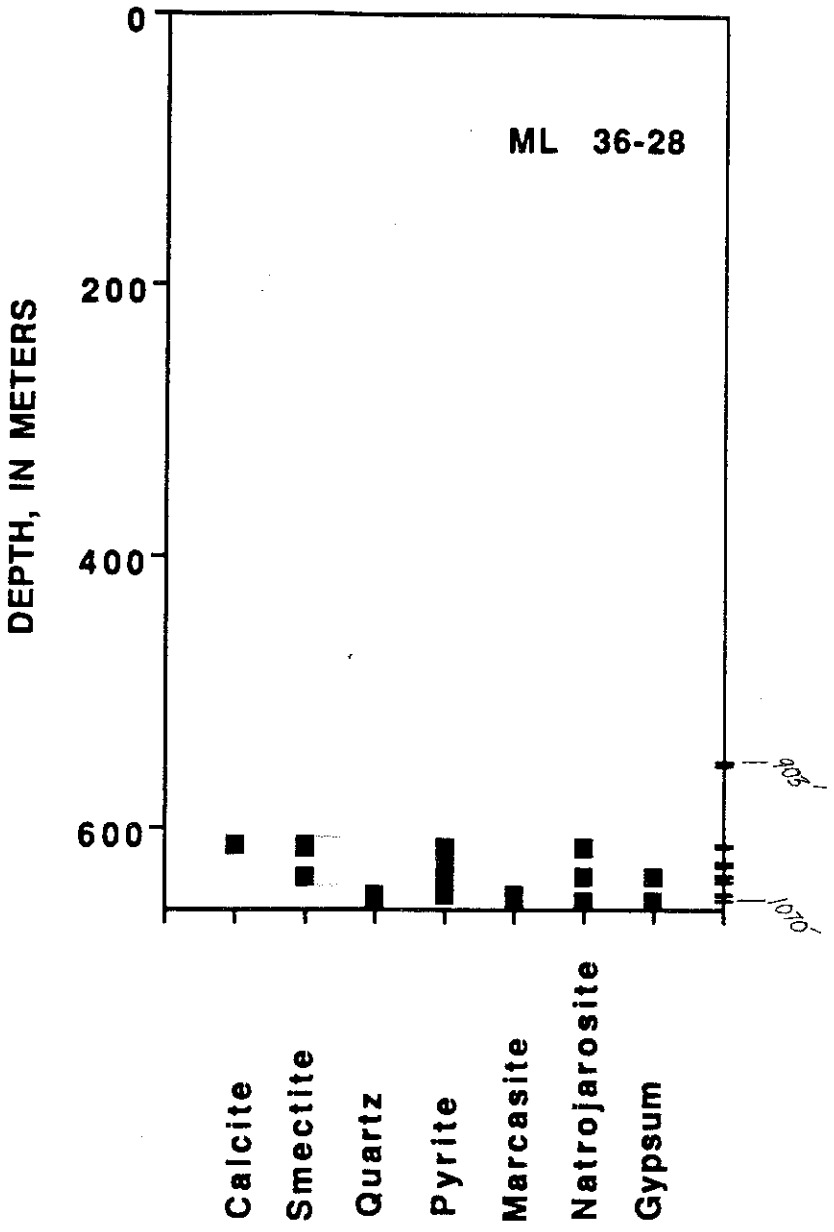

3f. Diagram showing the distribution of hydrothermal alteration minerals with depth in geothermal drill hole ML 45-36.

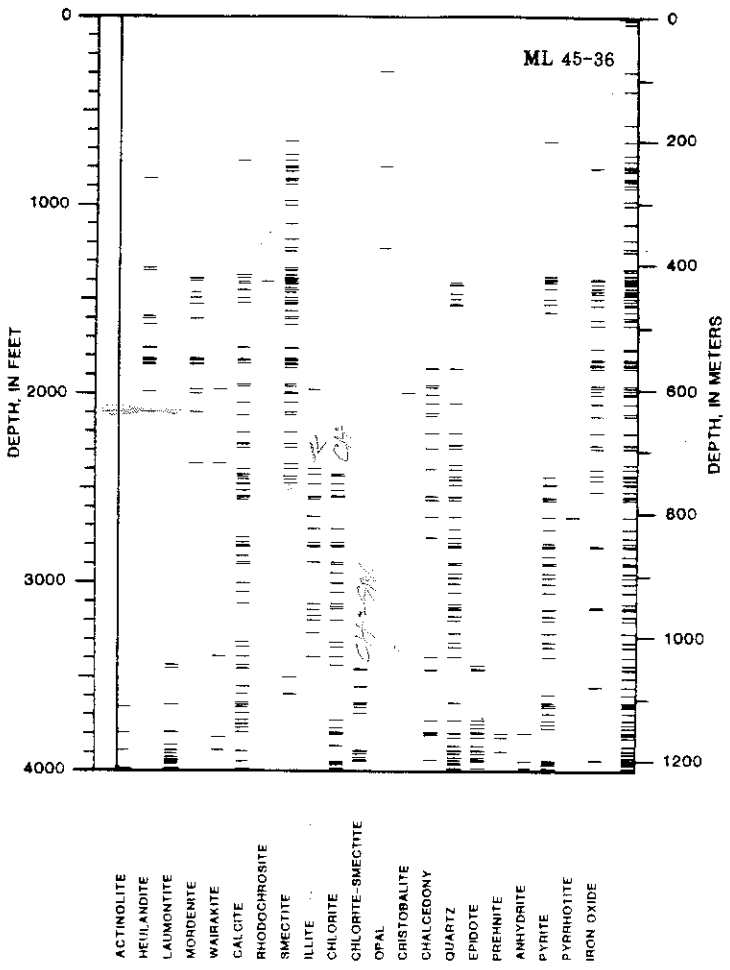

3g. Diagram showing the distribution of hydrothermal alteration minerals with depth in geothermal drill hole ML 52-4.

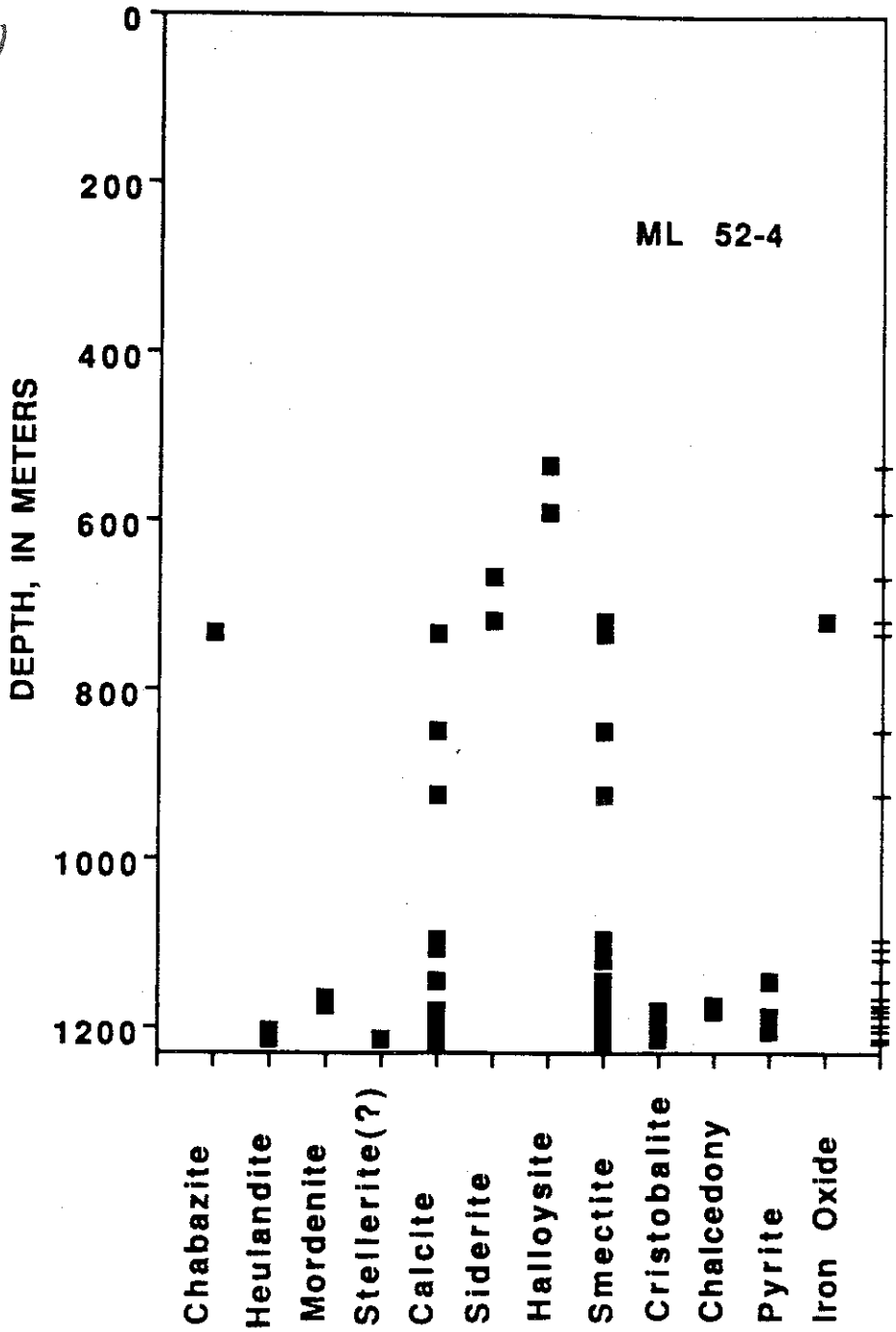

3h. Diagram showing the distribution of hydrothermal alteration minerals with depth in geothermal drill hole ML 57-13.

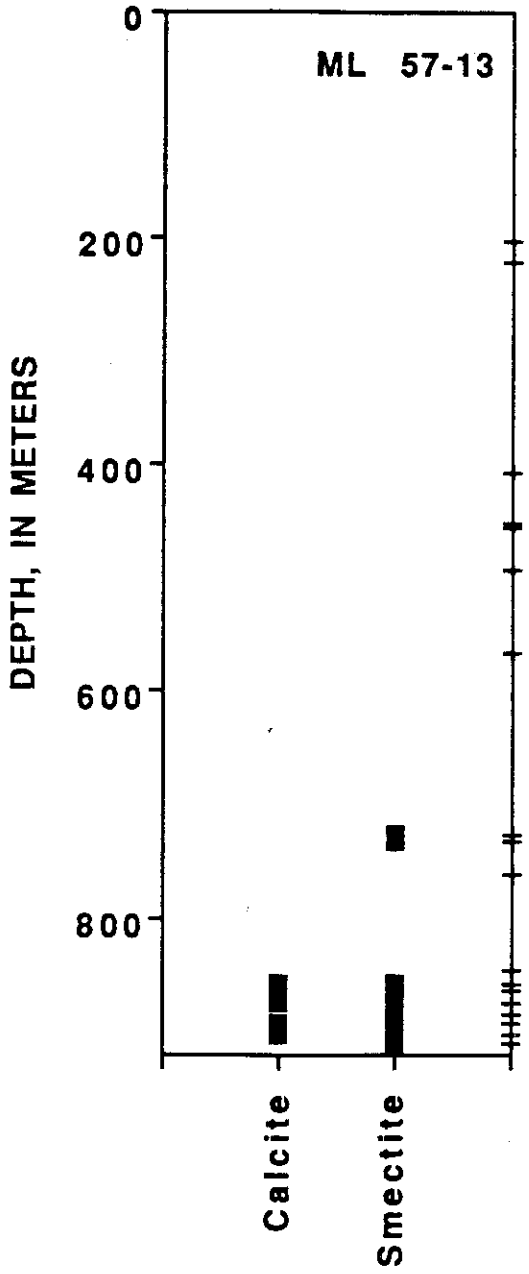

Done

3i. Diagram showing the distribution of hydrothermal alteration minerals with depth in geothermal drill hole ML 62-21.

done

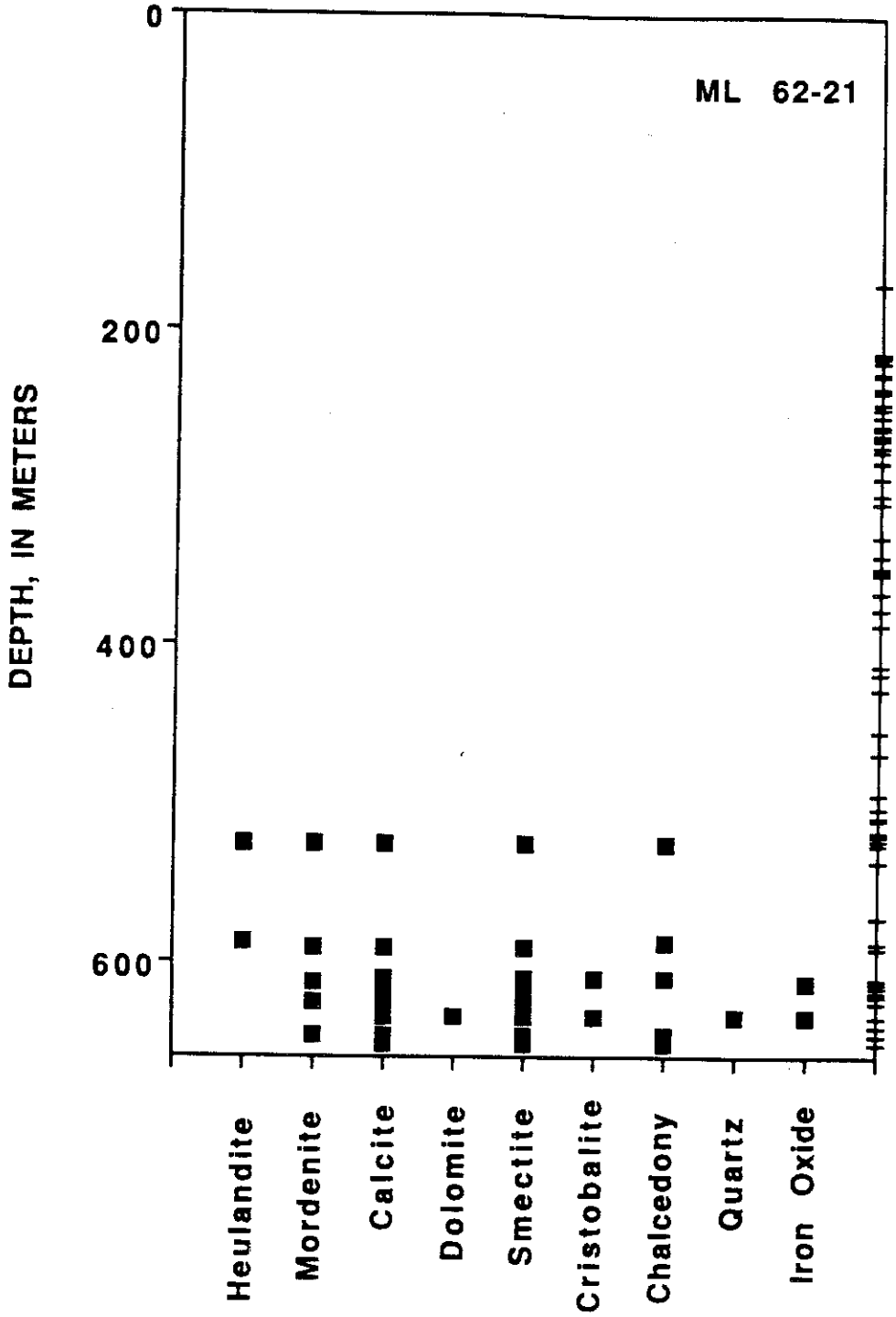

3j. Diagram showing the distribution of hydrothermal alteration minerals with depth in geothermal drill hole ML 86-23.

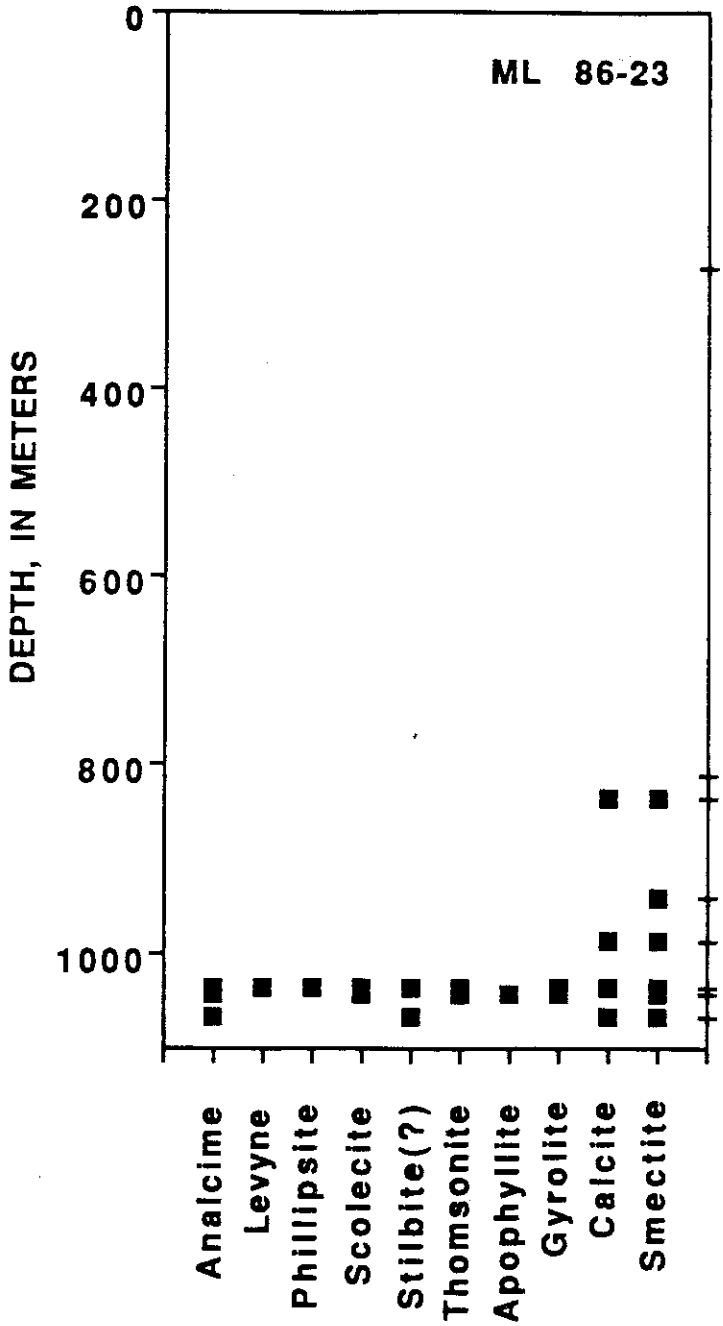

3k. Diagram showing the distribution of hydrothermal alteration minerals with depth in geothermal drill hole ML 88-12.

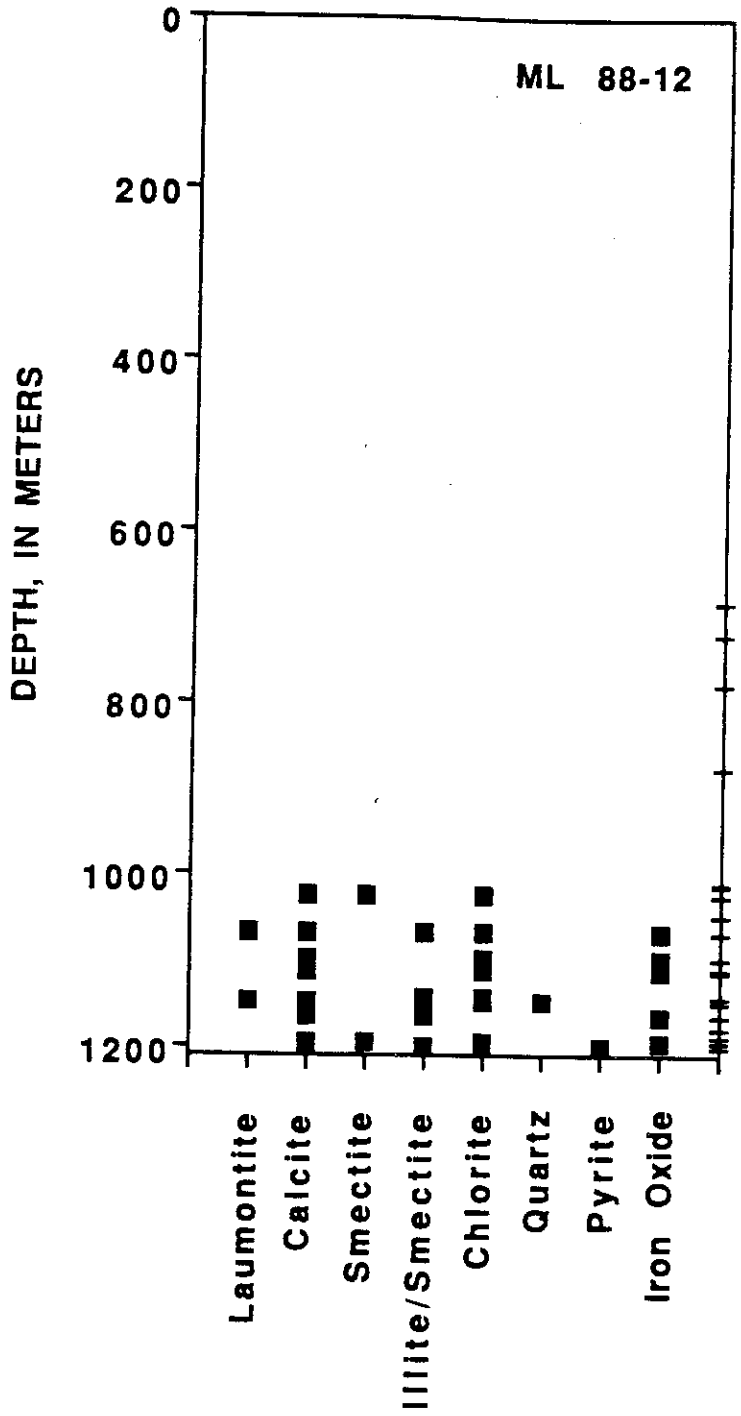

4. Scanning electron micrograph showing subhedral, trapezohedral analcime crystals that fill a vesicle in core from 1,066.8 m depth in the ML 86-23 drill hole. Clusters of tabular stilbite/stellerite crystals appear to be deposited later than the analcime.

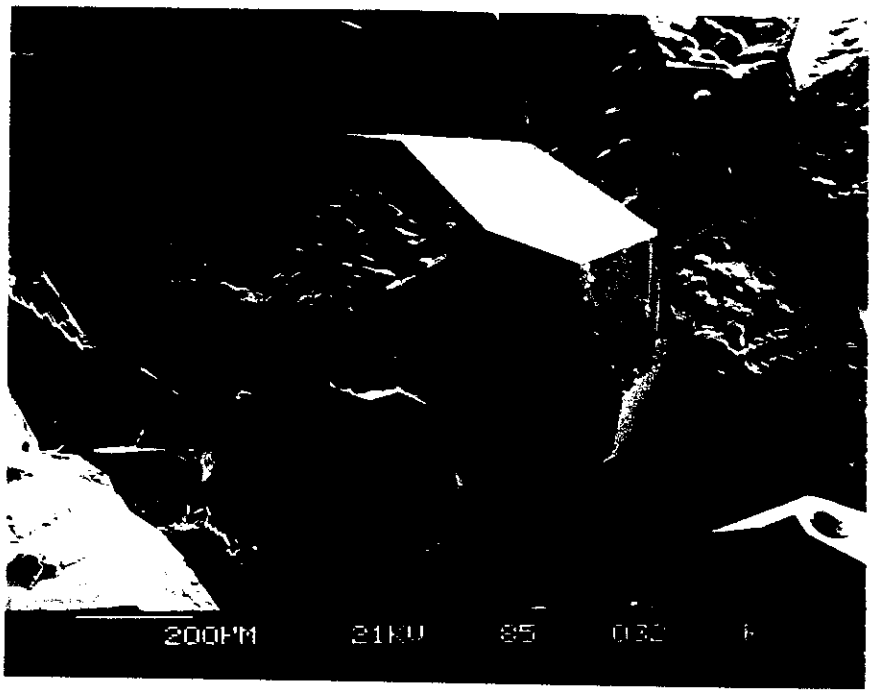

5. Ca+Mg—Na—K+Ba+Sr ternary diagram for electron microprobe analyses of analcime and wairakite (data from Table 2).

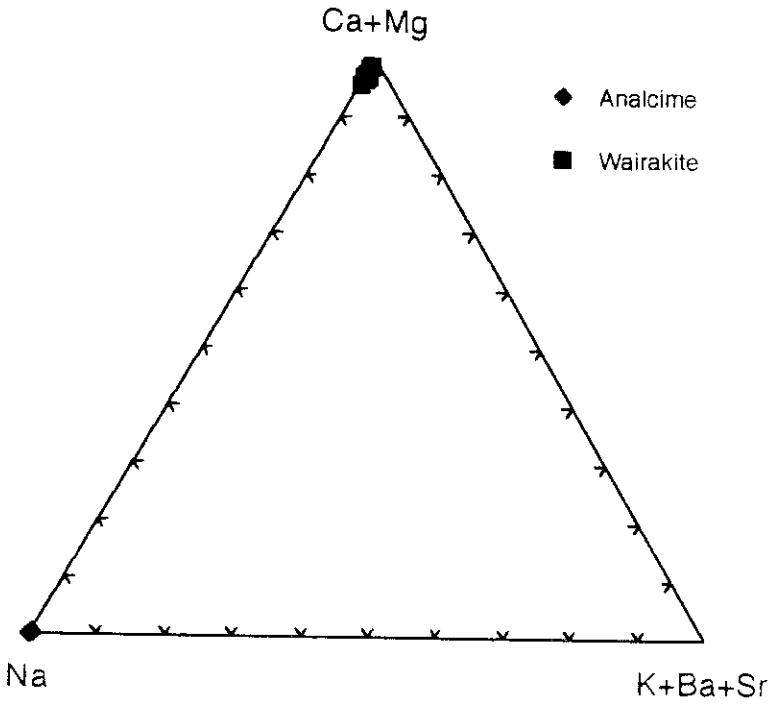

6. Scanning electron micrograph of subhedral, trapezohedral wairakite crystals that coat a fracture along with euhedral quartz prisms and smectite in core from 1,328.2 m depth in the ML 28-32 drill hole.

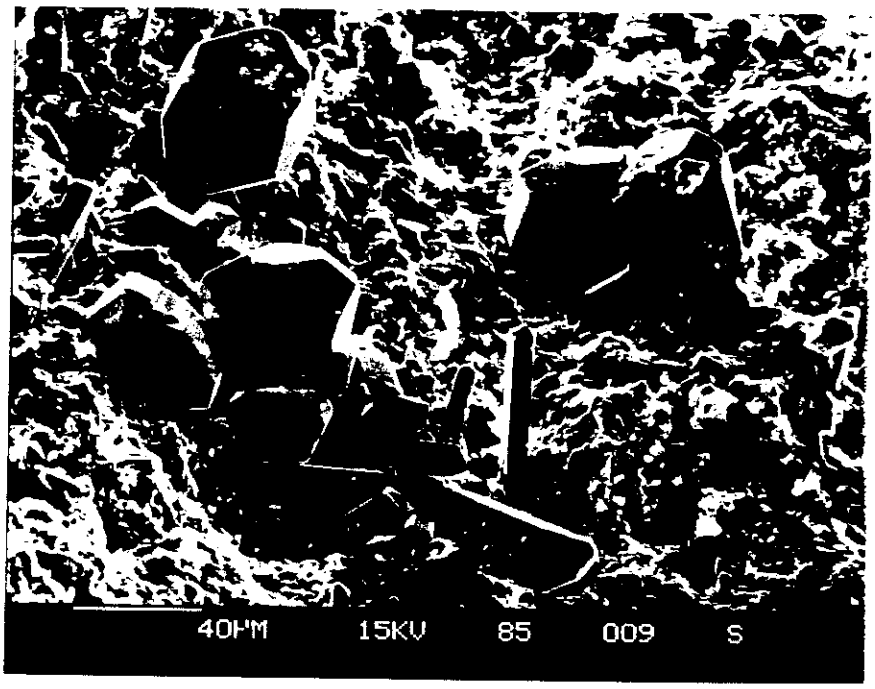

7. Scanning electron micrograph showing euhedral, twinned chabazite crystals that coat fractures at 791 m depth in the OWML5 drill hole. Smectite (lower left) and tiny, tabular stilbite/stellerite crystals (bottom) are earlier deposits.

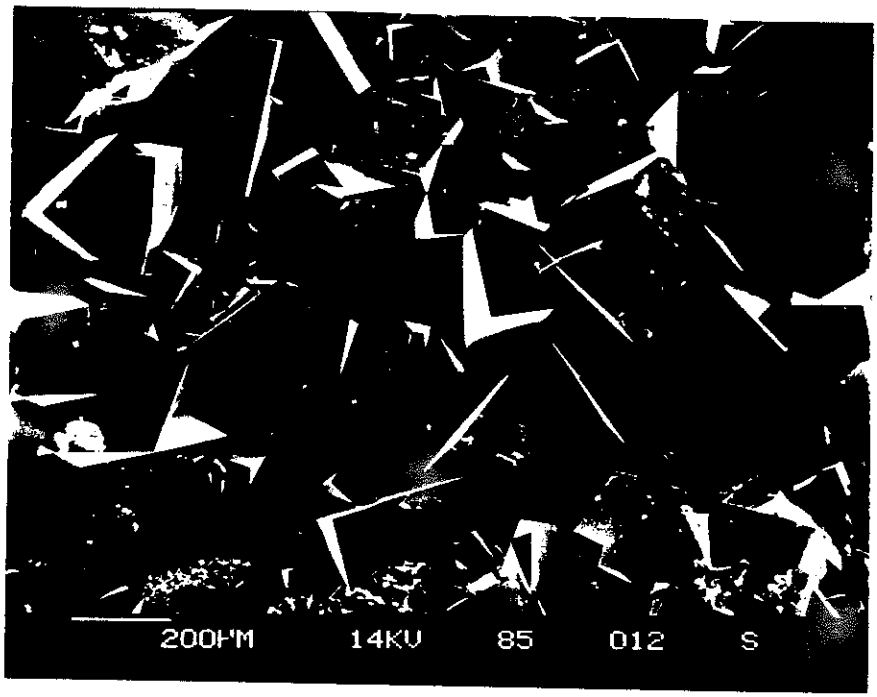

8. Scanning electron micrograph of euhedral to subhedral (many twinned) crystals of a heulandite group mineral from 634.2 m depth in the ML 28-32 drill hole. Lower right corner of micorgraph shows earlier, tiny, fuzzy patches of smectite coating pyrite; rounded crystal clusters (lower right and upper left corners of micrograph) are siderite that formed later than heulandite. Scattered patches of a second generation of smectite formed later than heulandite (upper right corner of micrograph).

9. Ca+Mg—Na—K+Ba+Sr ternary diagram showing chemical differences between heulandite group minerals clinoptilolite and heulandite (data from Table 3).

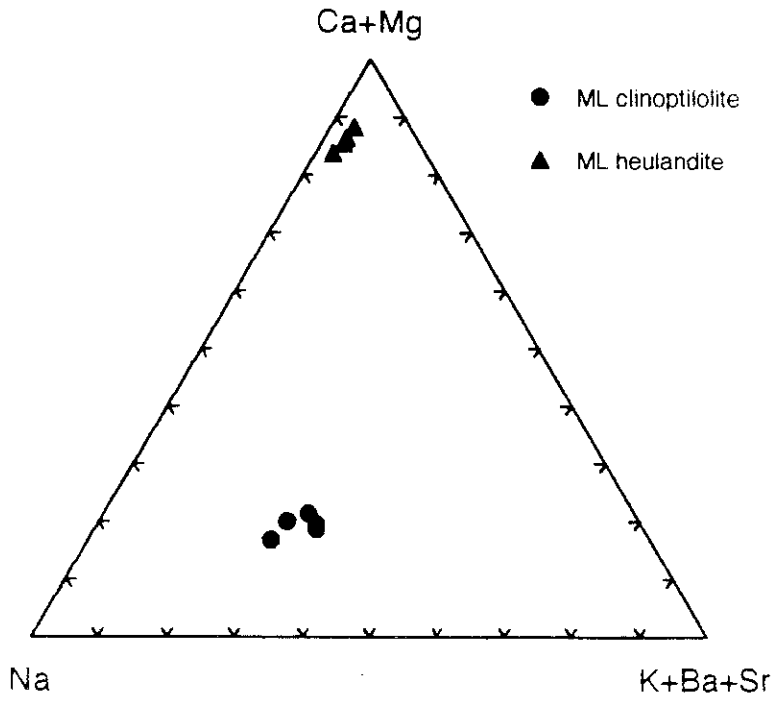

10. Scanning electron micrograph of euhedral, prismatic laumontite crystals from 1,068 m depth in the ML 88-12 drill hole.

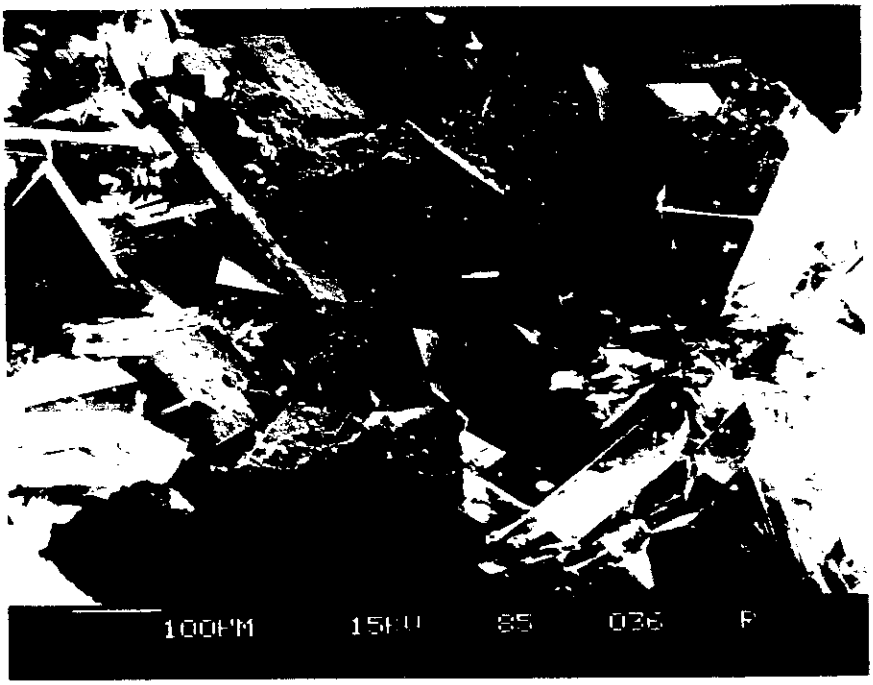

11. Ca+Mg—Na—K+Ba+Sr ternary diagram for electron microprobe analyses of laumontite from the two intracaldera drill holes (data from Table 4). Calcium is always the dominant exchangeable cation in laumontite.

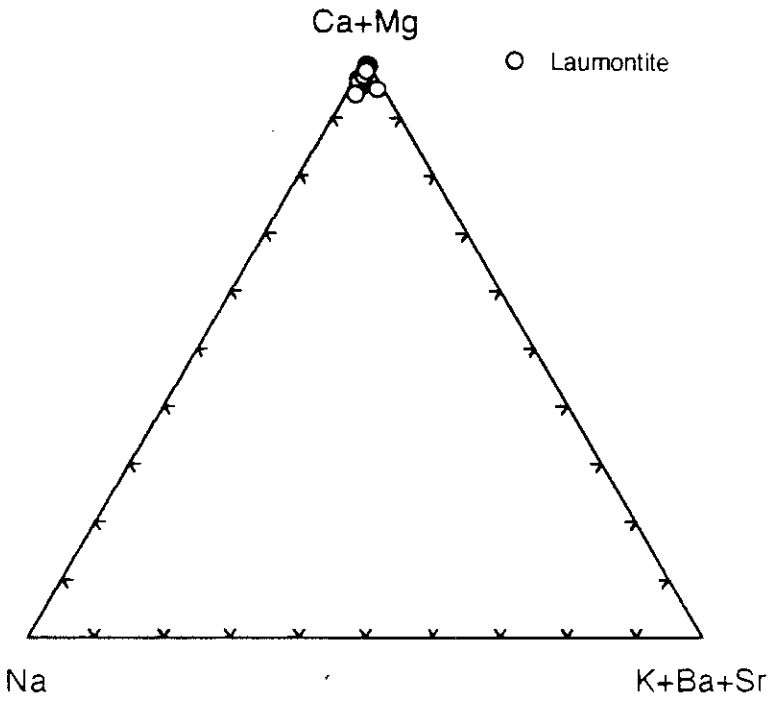

12. Ca+Mg—Na—K+Ba+Sr ternary diagram for electron microprobe analyses of levyne from the ML 86-23 drill hole (data from Table 5) compared with other analyses of levyne (Gottardi and Galli, 1985; Tschernich, 1992).

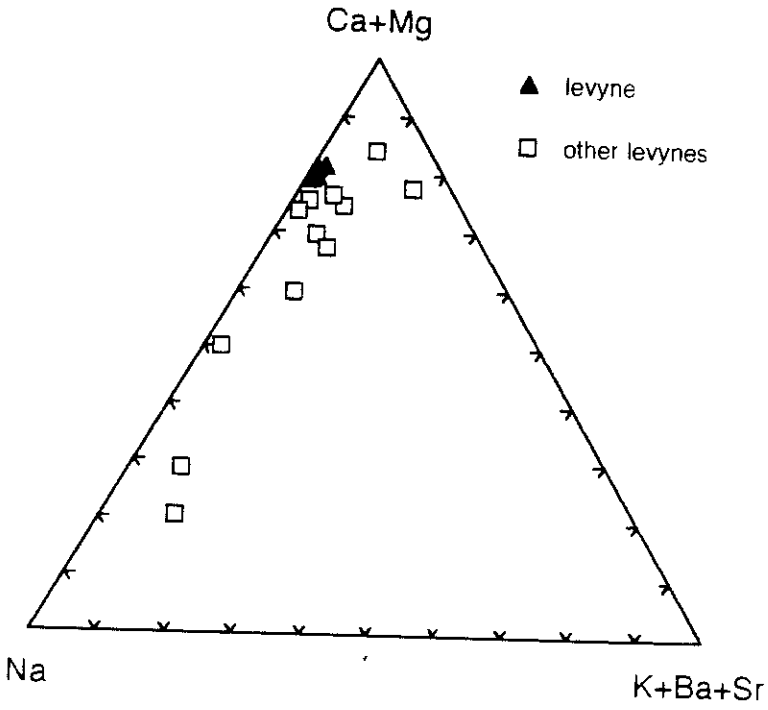

13. Scanning electron micrograph showing radiating, fibrous, mordenite crystals that fill vesicles at 428.2 m depth in the ML 45-36 drill hole.

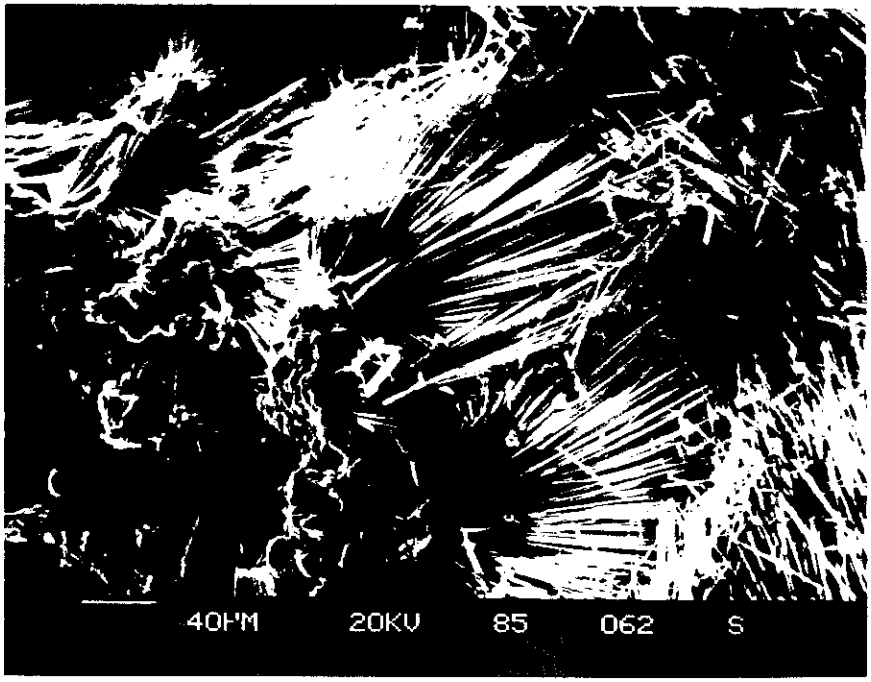

14. Scanning electron micrograph of euhedral, blocky phillipsite crystals that fill vesicles at 1,055.2 m depth in the ML 18-34 drill hole.

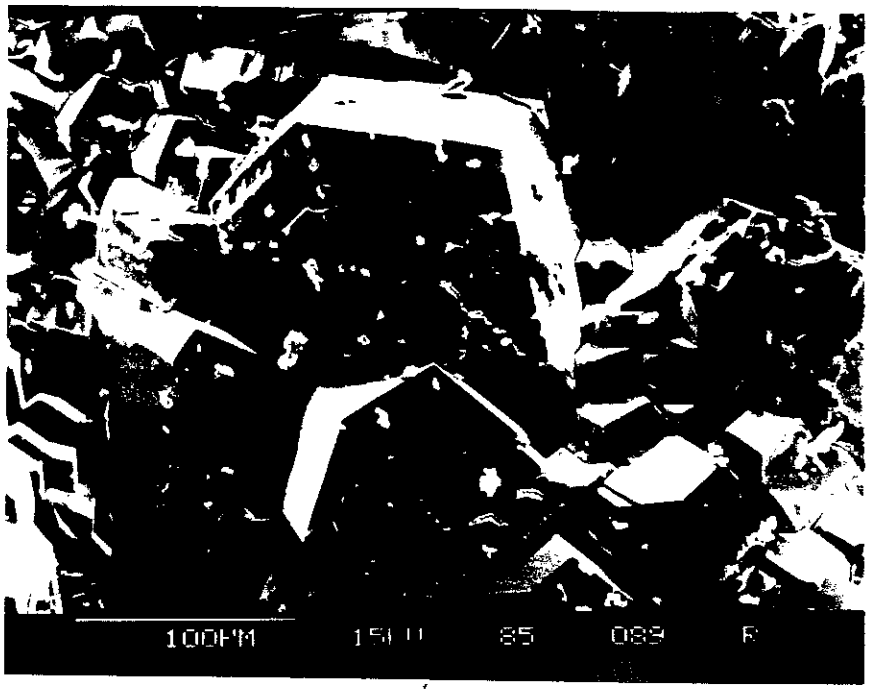

15 Ca+Mg—Na—K+Ba+Sr ternary diagram for electron microprobe analyses of phillipsite from the ML 18-34 drill hole (data from Table 6) compared with analyses of phillipsite from Oregon (OR phillipsite) (Oscarson and Bargar, 1996) and other phillipsites (Gottardi and Galli, 1985; Tschernich, 1992).

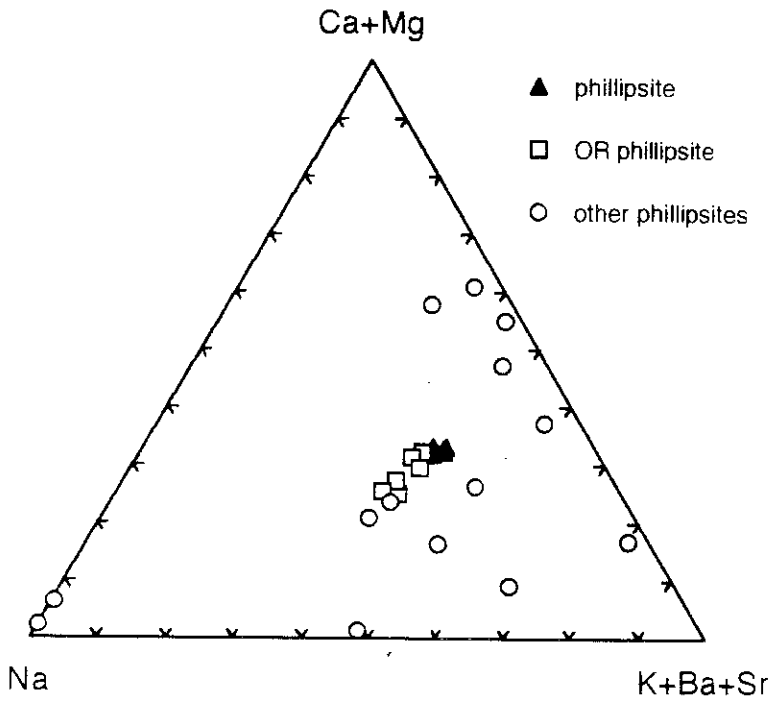

16. Scanning electron micrograph showing acicular to fibrous crystals of scolecite that fills vesicles at 1,039.4 m depth in the ML 86-23 drill hole.

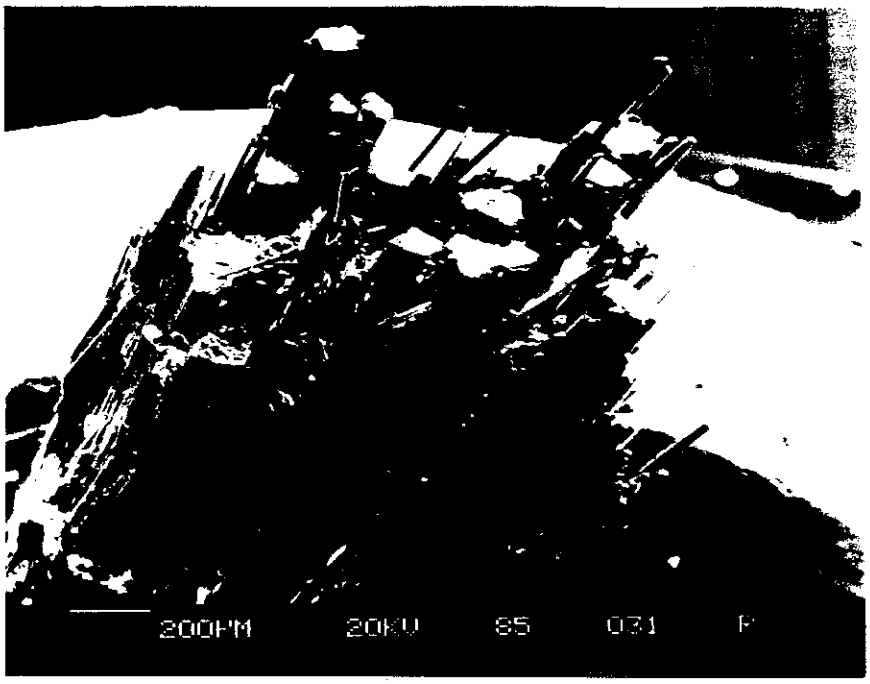

17. Ca+Mg—Na—K+Ba+Sr ternary diagram for electron microprobe analyses of scolecite (data from Table 7) compared with published analyses of other scolecites (Gottardi and Galli, 1985; Tschernich, 1992).

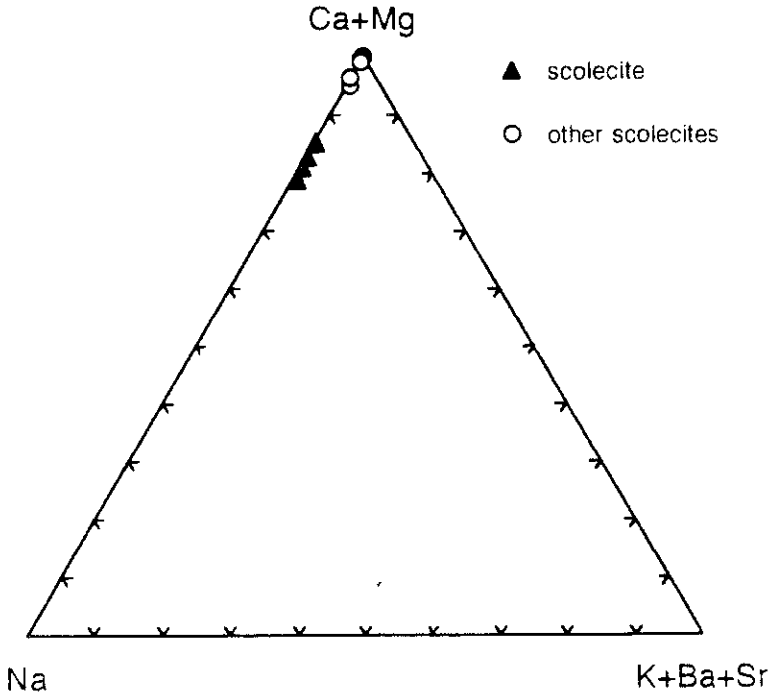

18. Scanning electron micrograph showing flat-topped rectangular crystals of stilbite/stellerite that line a fracture at 805.6 m depth in the OWML 5 drill hole. The specimen also contains earlier smectite (upper right corner of micrograph) and fibrous mordenite(?).

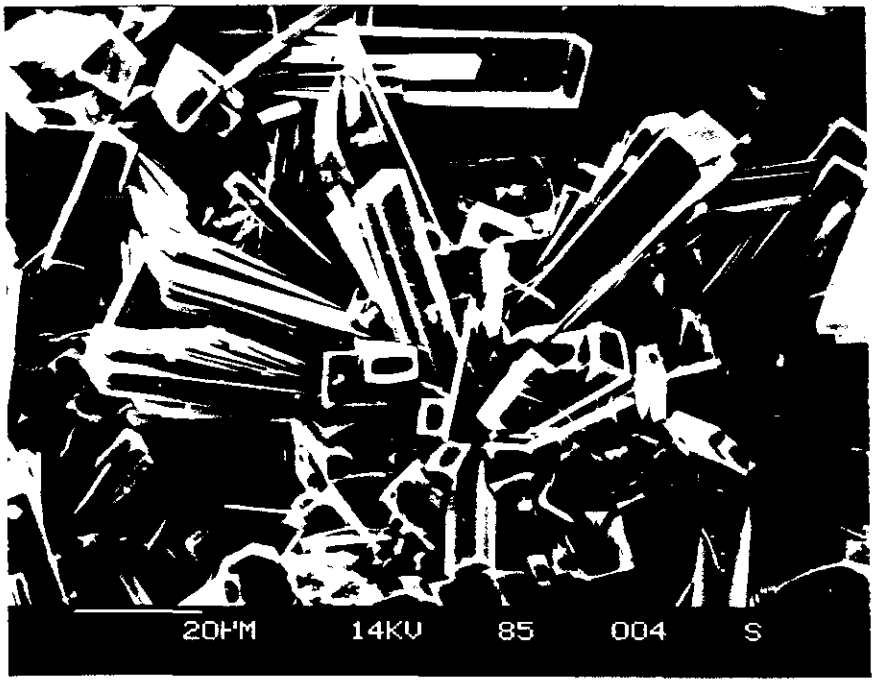

19. Ca+Mg—Na—K+Ba+Sr ternary diagram for electron microprobe analyses of thomsonite from the ML 86-23 drill hole (data from Table 8) compared with published analyses of other thomsonites (Gottardi and Galli, 1985; Tschernich, 1992).

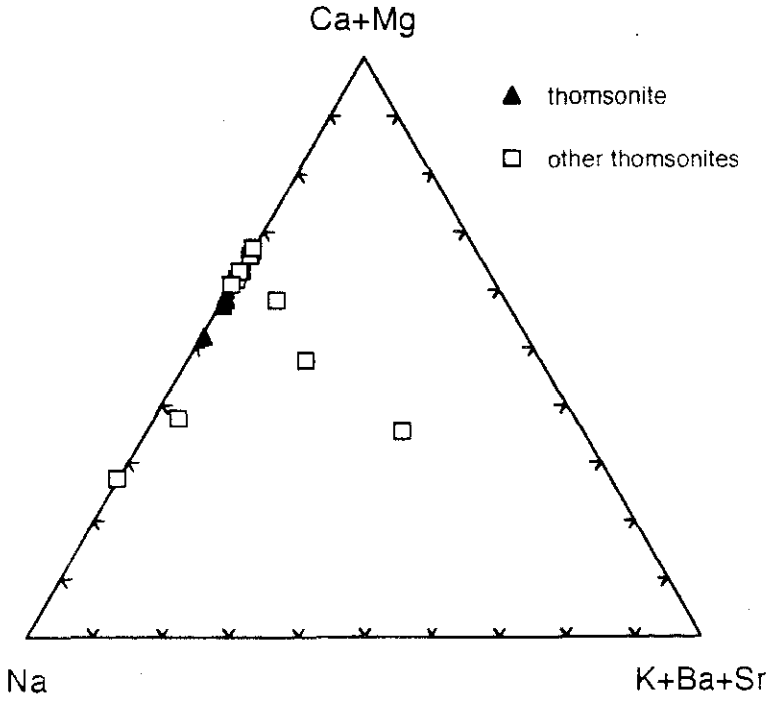

20. Scanning electron micrograph showing rhombic dolomite crystals that fill open spaces between breccia fragments at 748.6 m depth in the ML 28-32 drill hole.

21a. Scanning electron micrograph showing stacked clusters of rhombic siderite crystals that coat a fracture at 634.3 m depth in the ML 28-32 drill hole.

21b. Scanning electron micrograph of siderite crystal clusters filling a lithophysal cavity at 809.1 m depth in the ML 28-32 drill hole. Figure also shows traces of smectite (center of micrograph) and fibrous mordenite(?) (upper right corner of micrograph).

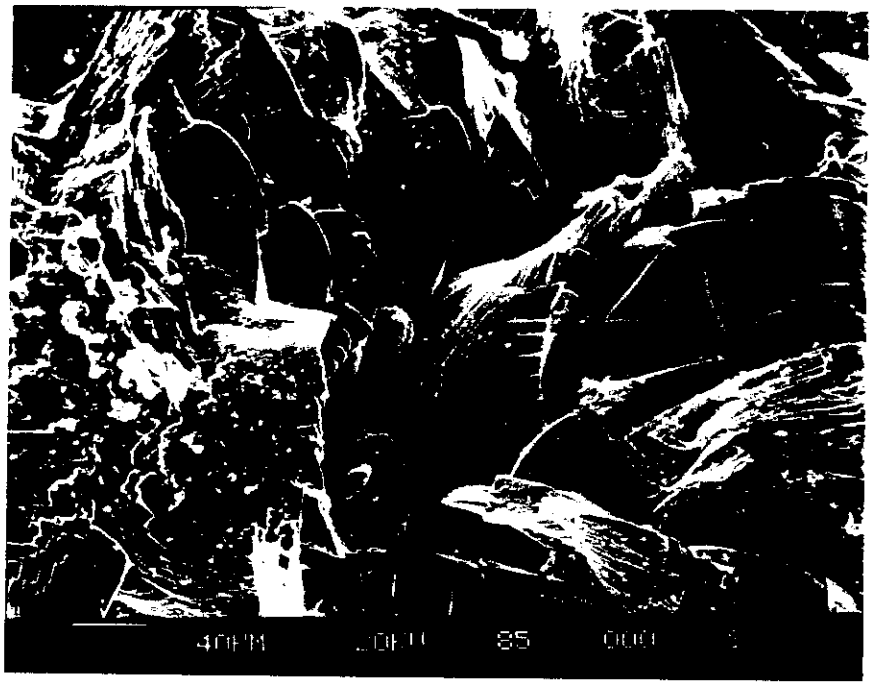

21c. Scanning electron micrograph of spherical and hemispherical clusters of rhombic siderite crystals lining a fracture surface at 585.8 m depth in the ML 28-32 drill hole.

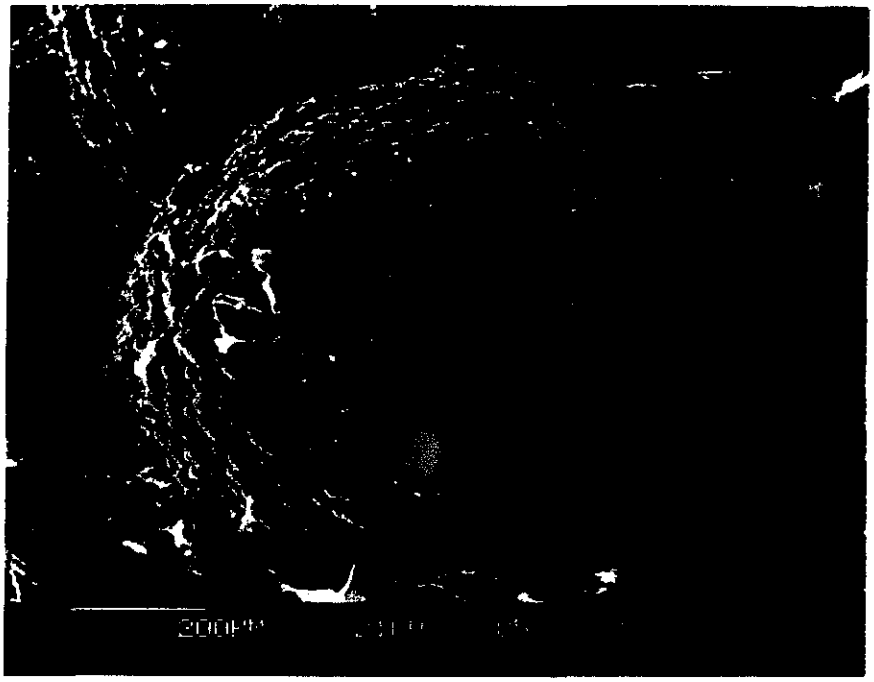

21d. Scanning electron micrograph showing the internal structure of broken spherical siderite crystal clusters that coat a fracture at 666.9 m depth in the ML 52-4 drill hole.

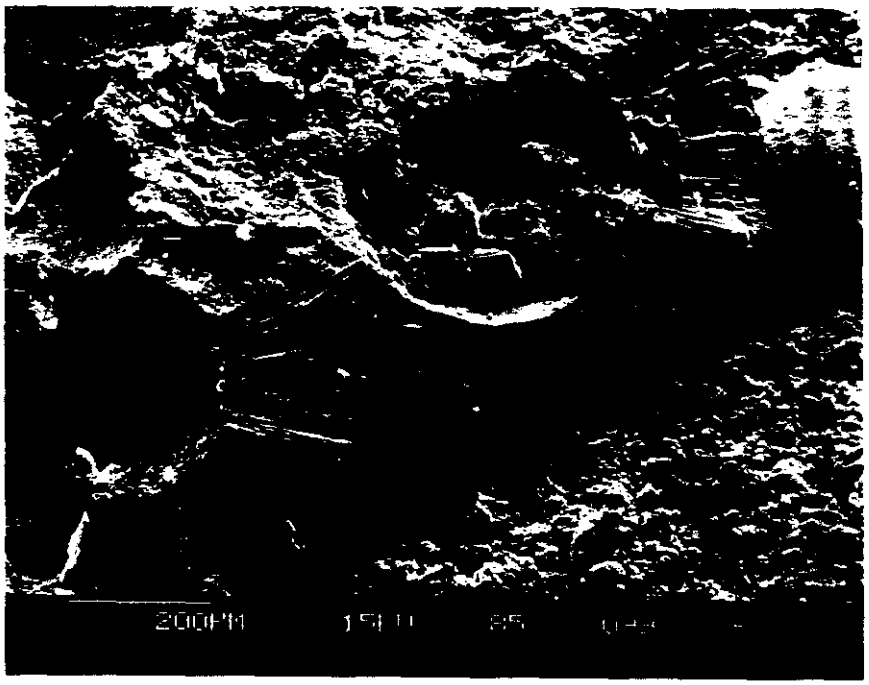

21e. Scanning electron micrograph of flattened disc-shaped cluster of siderite crystals from a fracture at 666.9 m depth in the ML 52-4 drill hole that had a narrow opening between top and bottom fracture surfaces.

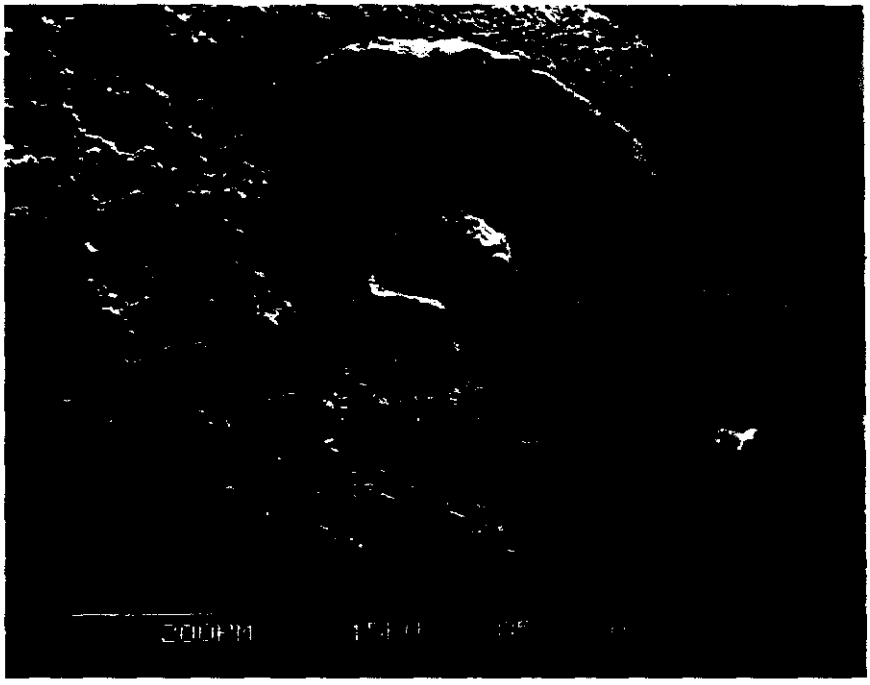

21f. Scanning electron micrograph showing a flattened disc-shaped cluster of siderite crystals from the same fracture surface as e; the siderite crystals formed in a series of concentric growth rings.

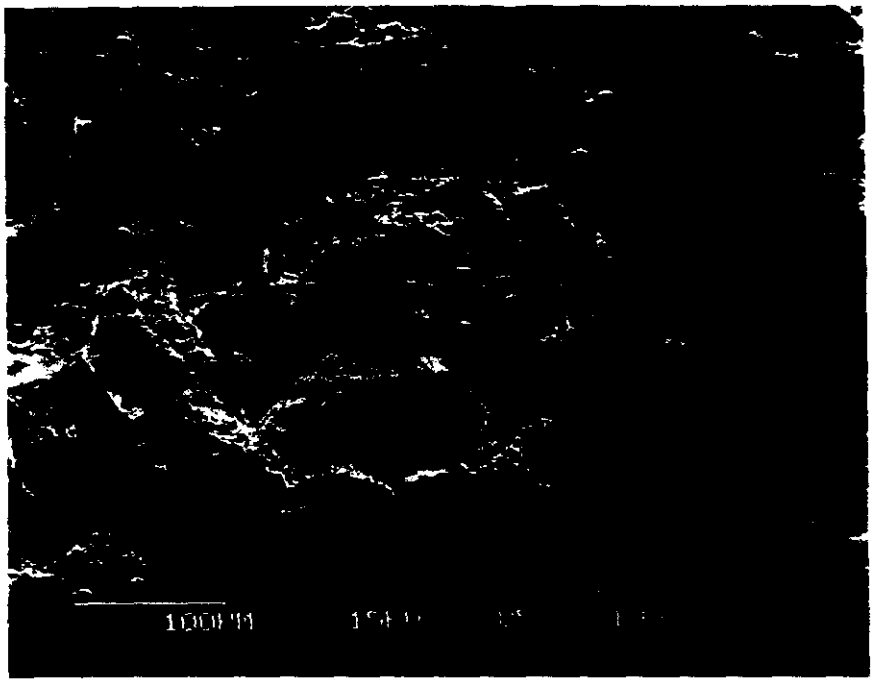

22. Photograph of different colored (pale yellow to dark caramel) concentric growth rings of siderite crystals that line cavities at 718.4 m depth in the ML 52-4 drill hole.

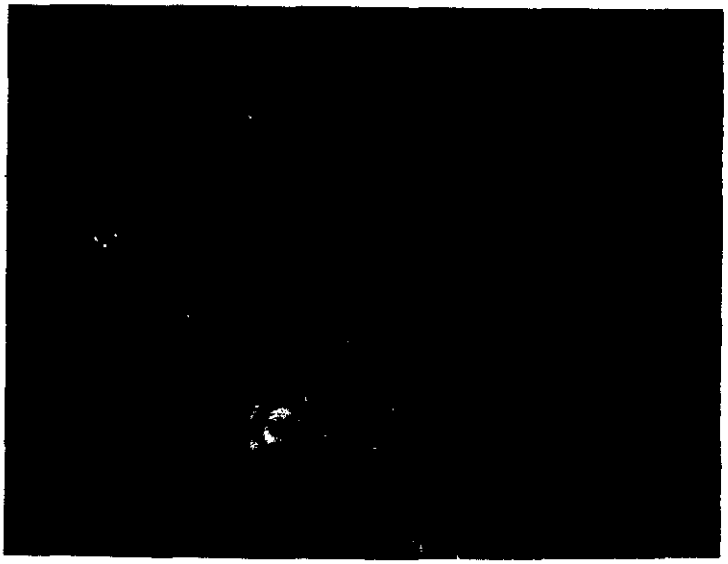

23a. Scanning electron micrograph showing rhombic calcite crystals coating a fracture at 1,022.9 m depth in the OWML5 drill hole.

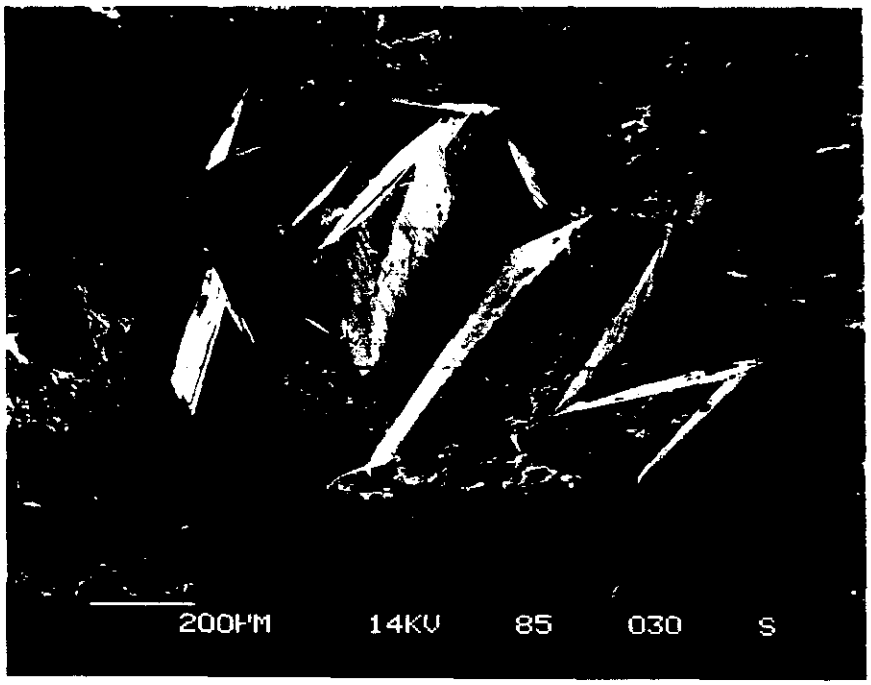

23b. Scanning electron micrograph of scalenohedral calcite crystals that line a fracture surface in core from 1,106.4 m depth in the ML 52-4 drill hole.

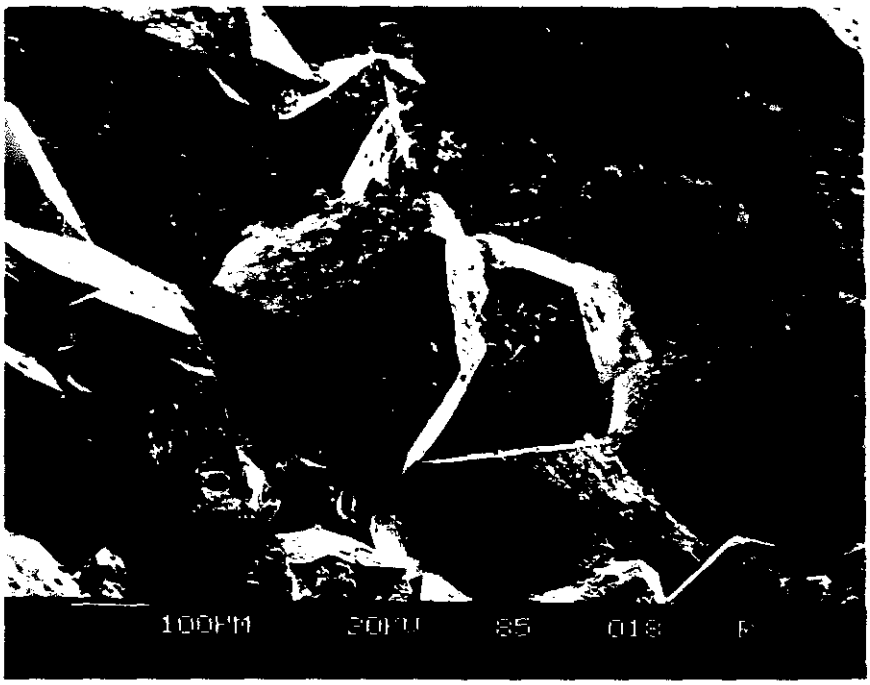

24a Scanning electron micrograph showing a vesicle filling of closely-packed, sheet-like, smectite crystals from 552.9 m depth in the ML 45-36 drill hole; blocky heulandite and fibrous to acicular mordenite are later deposits.

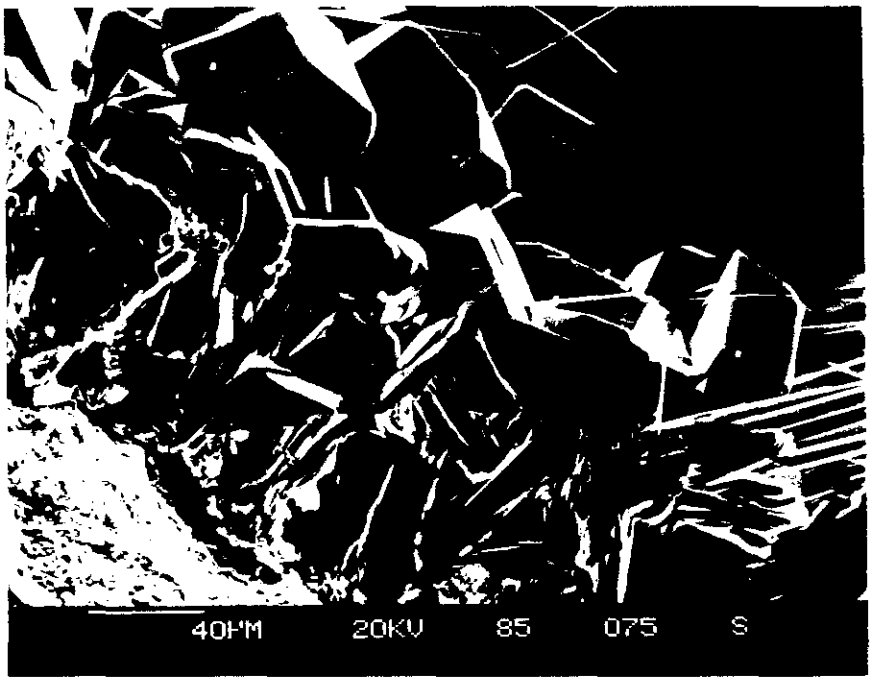

24b. Scanning electron micrograph of randomly-oriented (honeycomb), sheet-like, smectite crystals deposited in open spaces between fragments of a volcanic breccia at 1,117.7 m depth in the OWML5 drill hole.

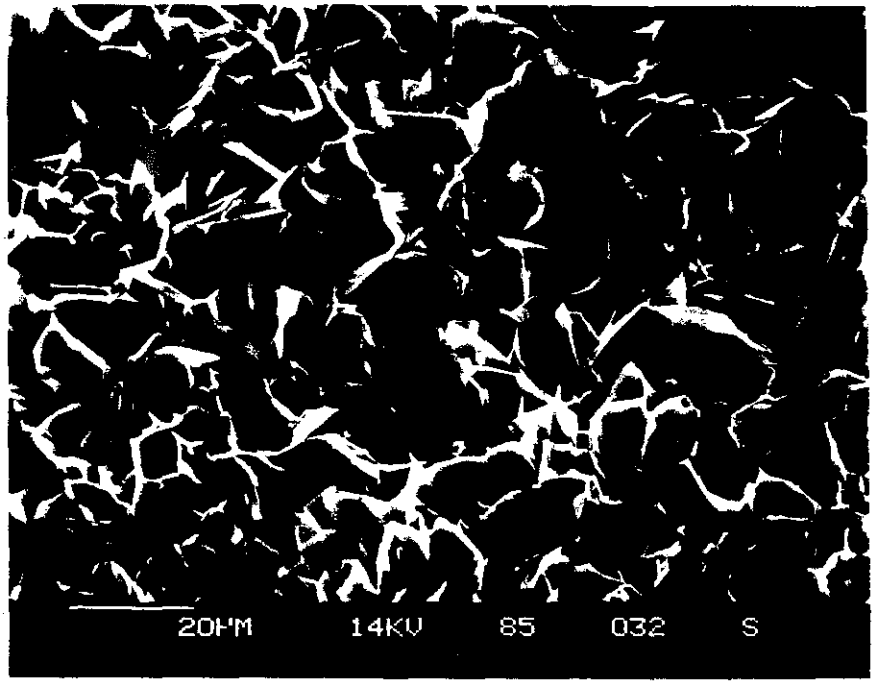

25. Scanning electron micrograph of drusy, euhedral, quartz crystals and later spherical clusters of randomly-oriented, sheet-like, illite crystals lining a cavity in drill core from 905.9 m depth in the ML 28-32 drill hole.

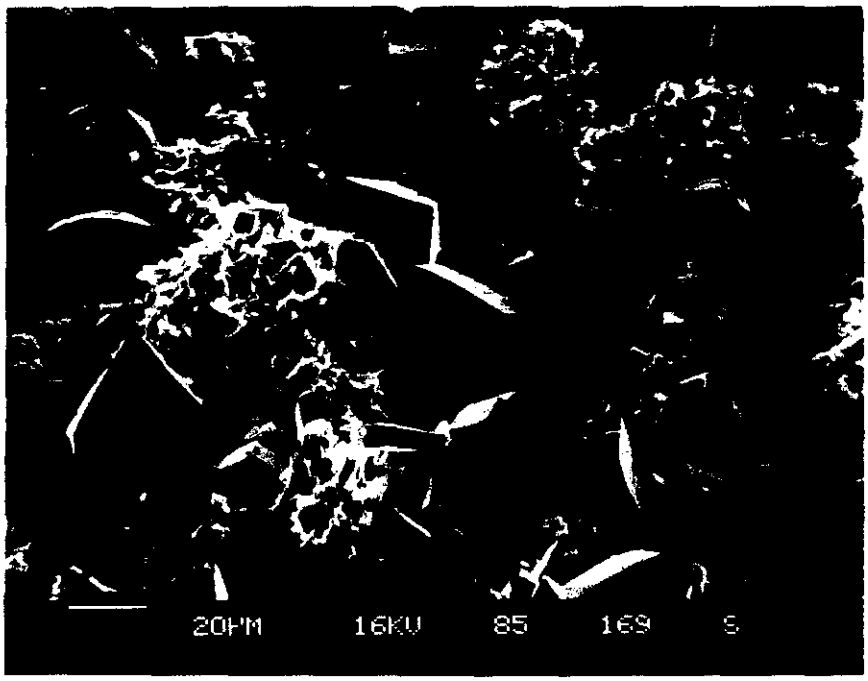

26a. Scanning electron micrographsshowing books of hexagonal, platy, chlorite crystals that partially coat quartz crystals lining fractures in a core specimen from 1,213.3 m depth in the ML 45-36 drill hole.

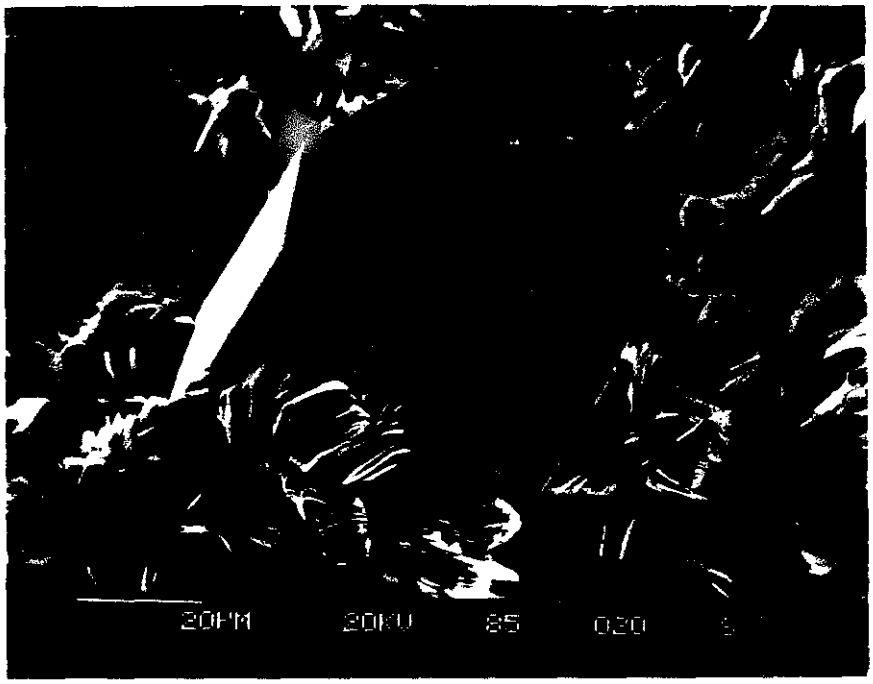

26b. Scanning electron micrograph of fracture filling in drill core from 1,179.6 m depth in the ML 28-32 drill hole containing euhedral quartz crystals that are coated by irregular, honeycomb-like masses of chlorite.

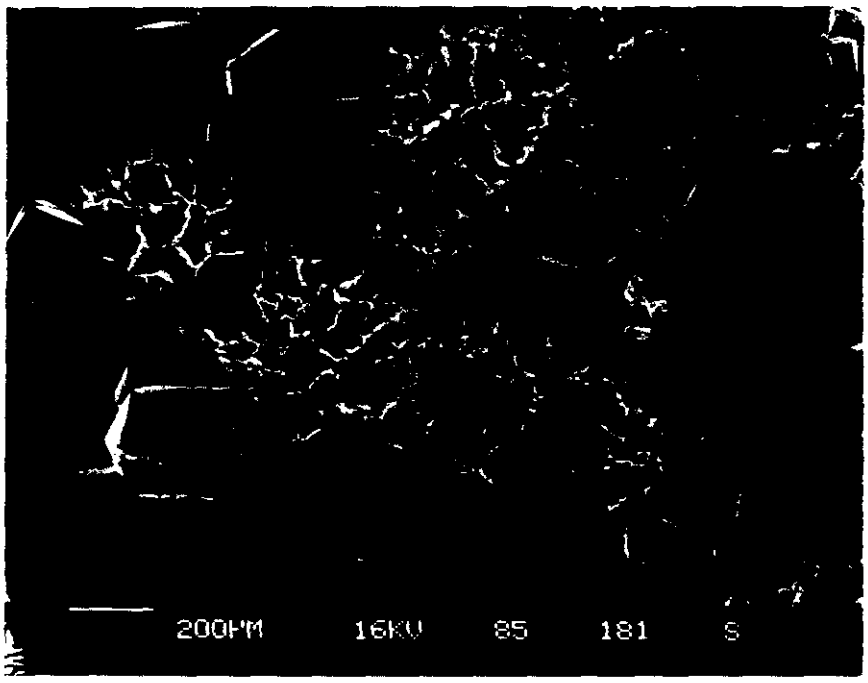

27. Scanning electron micrograph of radiating, fan-shaped aggregates of blocky, prehnite crystals filling vesicles in drill core from 1,156.7 m depth in the ML 45-36 hole.

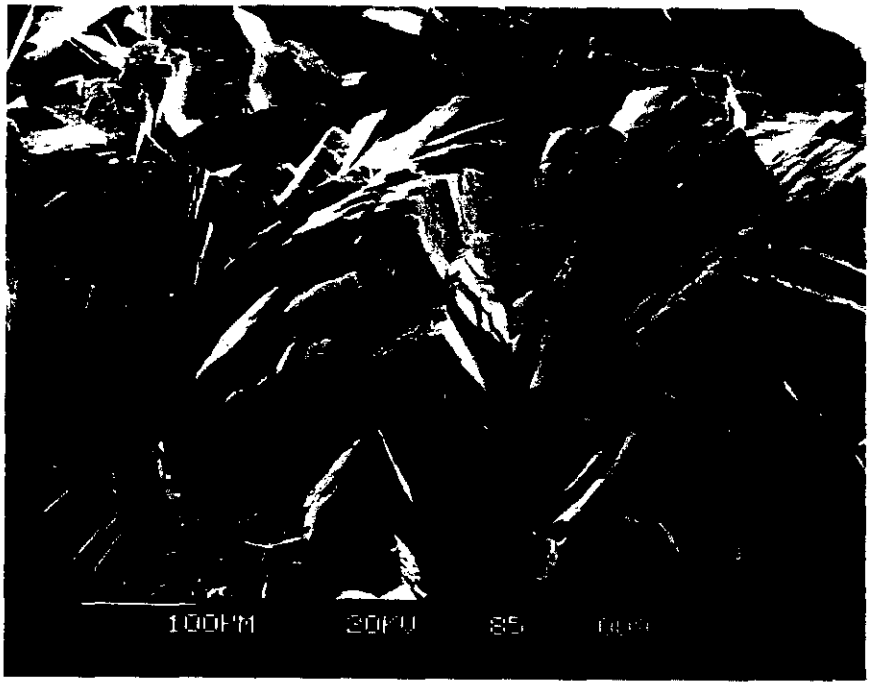

28. Scanning electron micrograph of tube-like opal deposits coating a fracture in core from 87.2 m depth in the ML 45-36 drill hole.

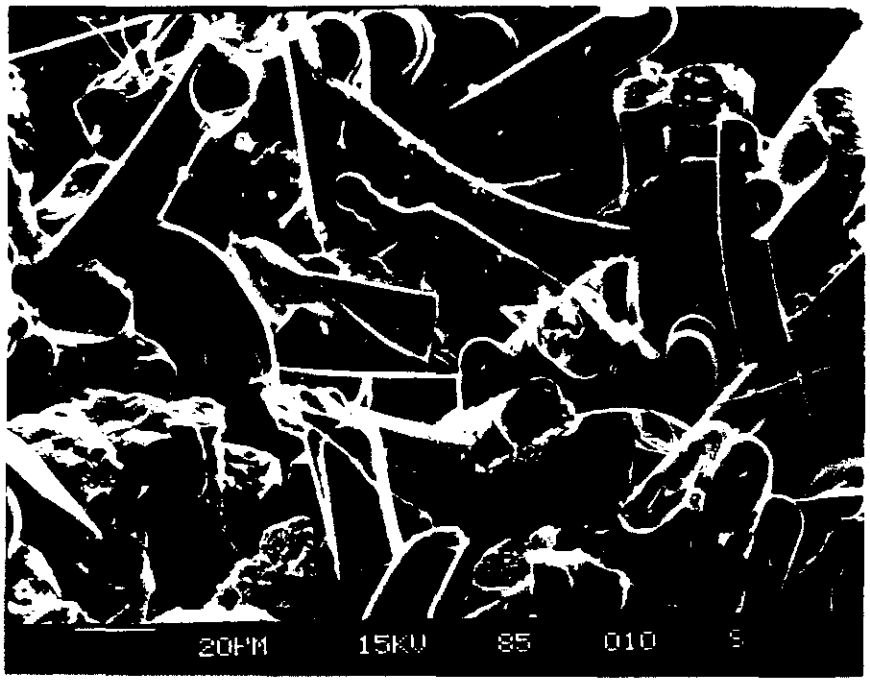

29. Scanning electron micrograph of botryoidal cristobalite/chalcedony deposited on heulandite at 1213.7 m in the ML 52-4 drill hole.

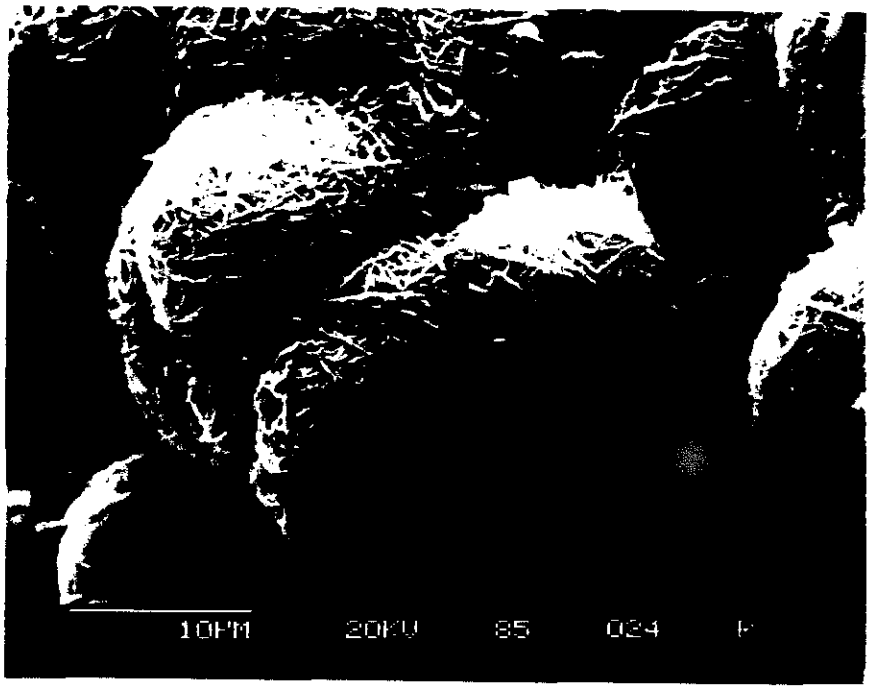

30. Scanning electron micrograph showing subhedral, diapyramidal, quartz crystals deposited on curved aggregates of siderite crystals that fill cavities at 804.1 m depth in the ML 28-32 drill hole; tiny, fibrous, mordenite crystals are a later deposit.

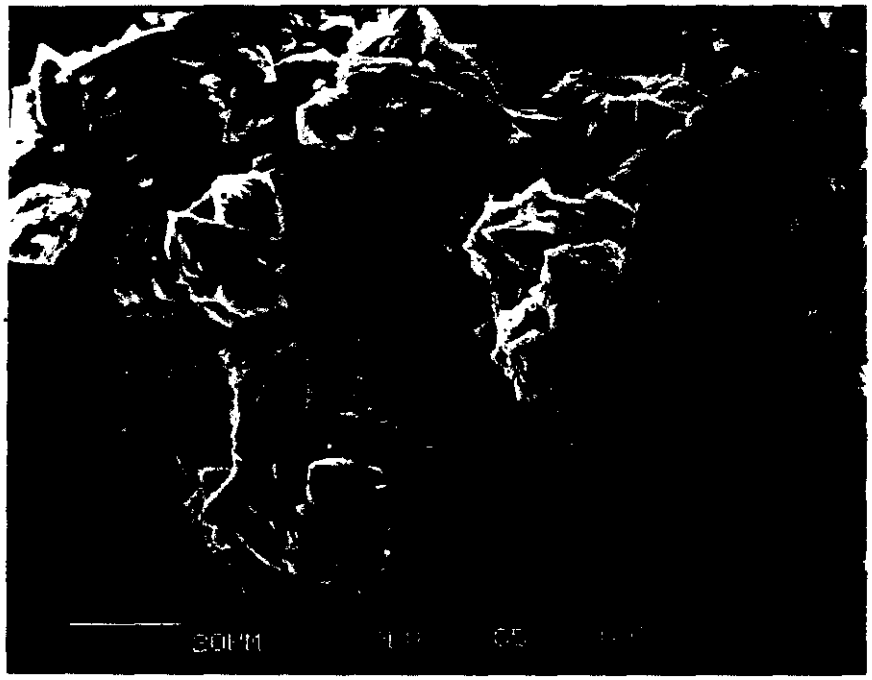

31. Scanning electron micrograph showing hexagonal, tabular, marcasite crystals and later rhombic siderite that line a fracture in core from 614.8 m depth in the ML 28-32 drill hole. Both minerals are partly coated by smectite.

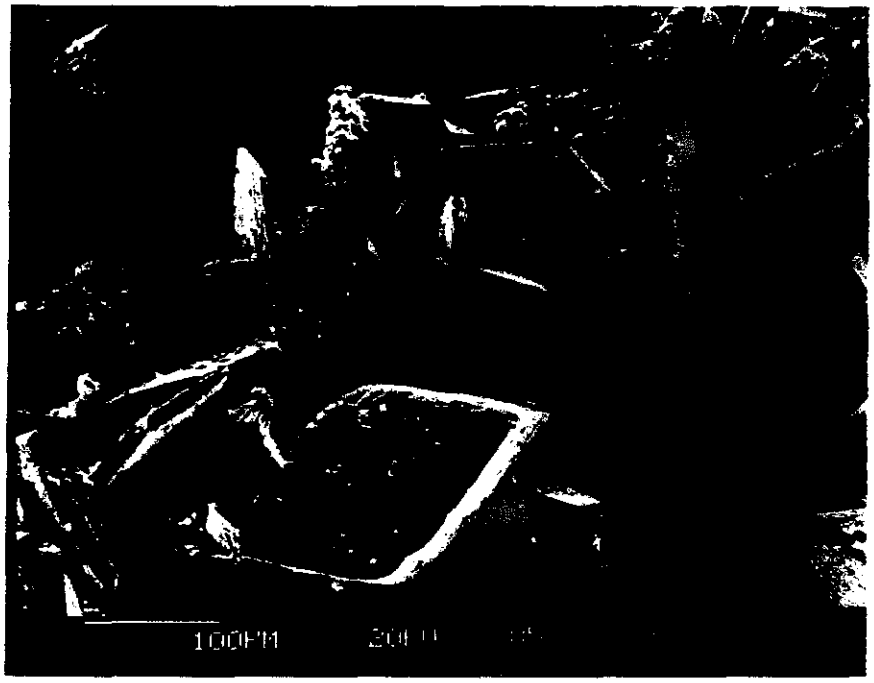

32. Scanning electron micrograph of aggregates of tabular, hexagonal, pyrrhotite crystals coating lithophysal cavities in core from 804.1 m depth in the ML 28-32 drill hole.

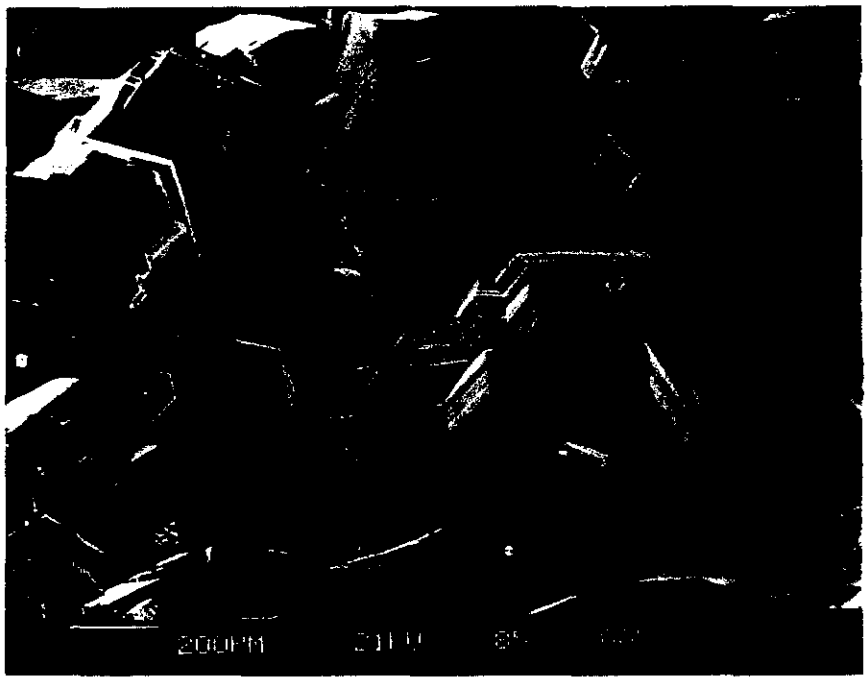

33a. Scanning electron micrograph showing an open-space filling of smectite, blocky heulandite, and tiny cubic pyrite crystals from 1,204 m depth in the ML 52-4 drill hole.

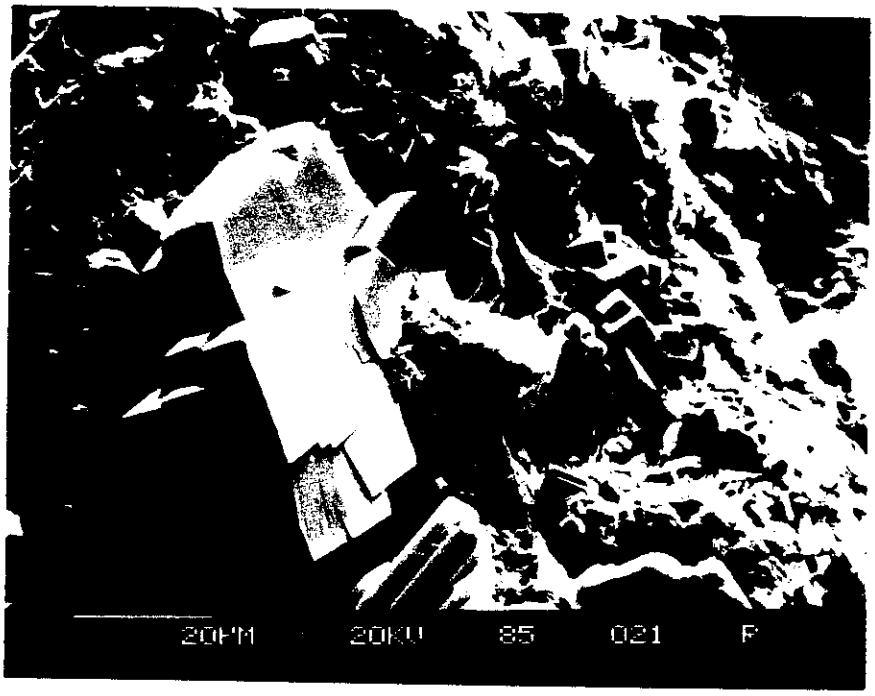

33b. Scanning electron micrograph of framboidal clusters of pyrite crystals and natrojarosite (right center of micrograph) in lithic tuff from 552.9 m depth in the ML 28-32 drill hole.

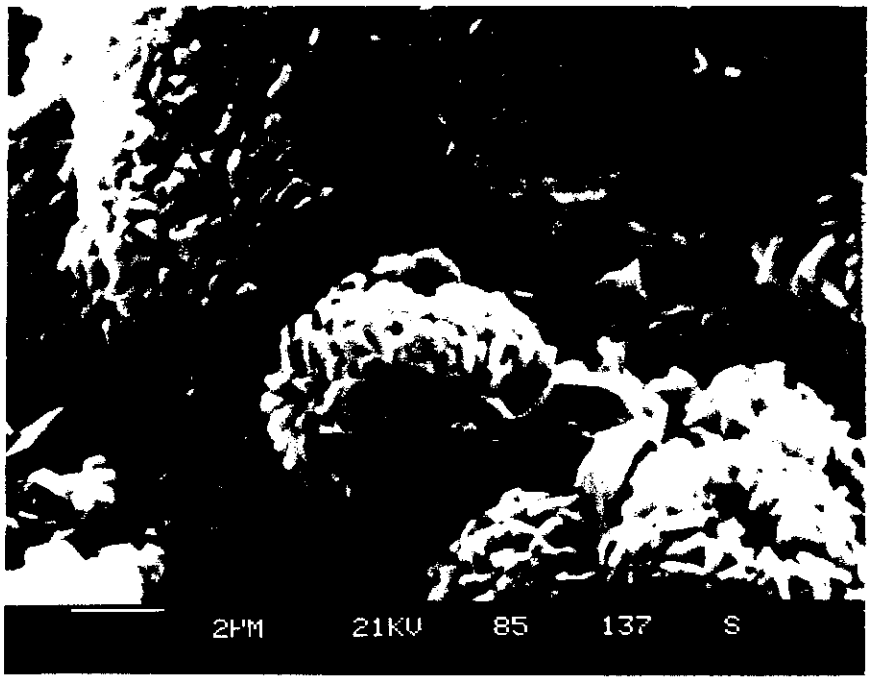

34. Scanning electron micrograph of a yellow, powdery, fracture filling from 565.4 m depth in the ML 28-32 drill hole. The powder grains consist of clusters of tiny hexagonal? natrojarosite crystals.

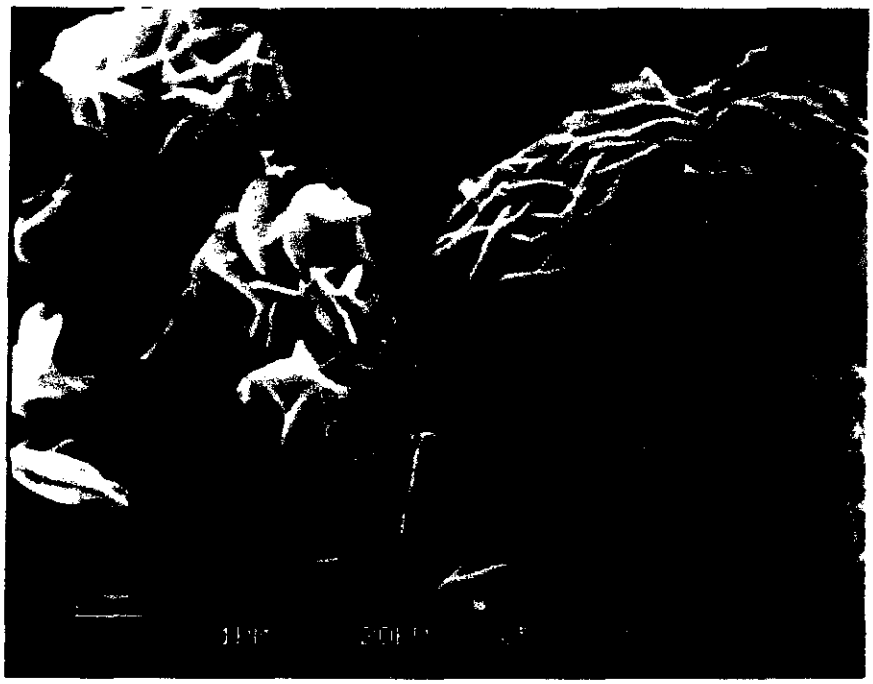

35. Scanning electron micrograph showing bladed hematite deposits coating open spaces along with later smectite in drill core from 616.3 m depth in the ML 18-34 drill hole.

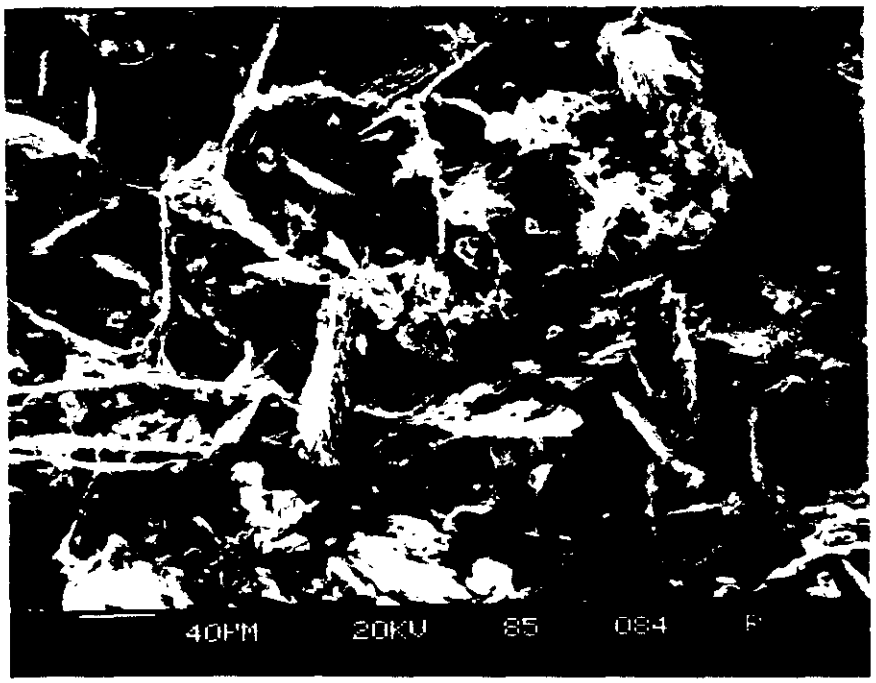

36. Scanning electron micrograph of euhedral adularia crystals that fill vesicles at 1,066.8 m depth in the ML 86-23 drill core.

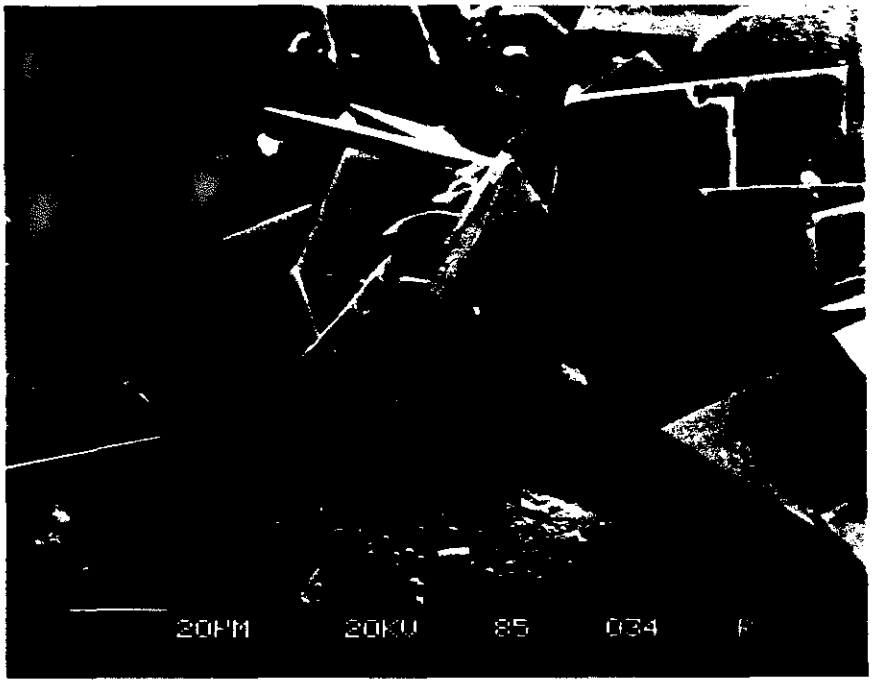

37a. Scanning electron micrograph of vesicle fillings in core specimens from 1,156.7 m depth in the ML 45-36 drill hole that show fibrous actinolite/tremolite crystals and later, blocky, prehnite crystals.

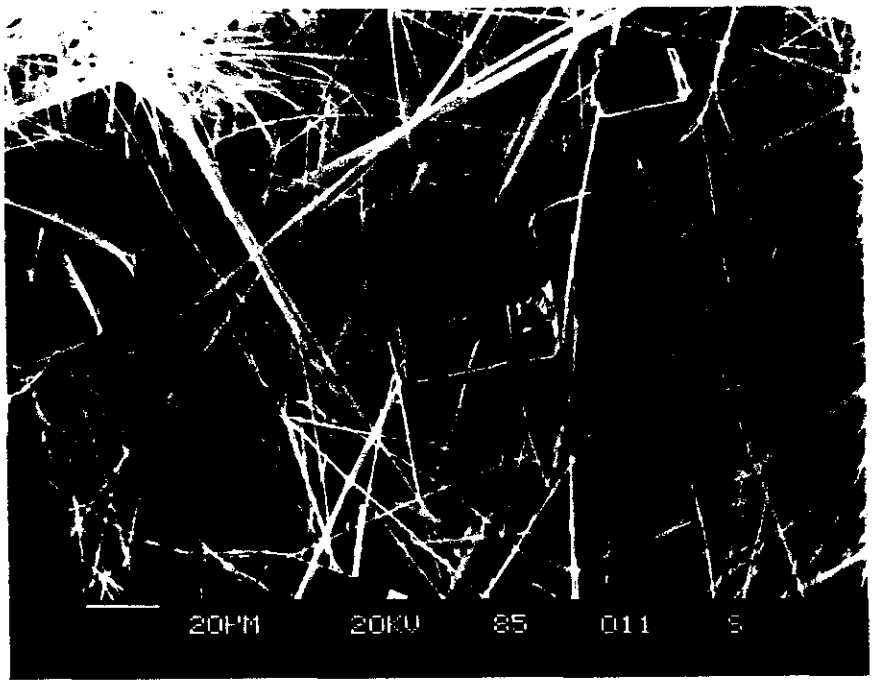

37b. Scanning electron micrograph showing fibrous to acicular actinolite/tremolite crystals with later prismatic epidote and blocky prehnite (lower left) crystals that fill vesicles in core from 1,156.7 m depth in the ML 45-36 drill hole.

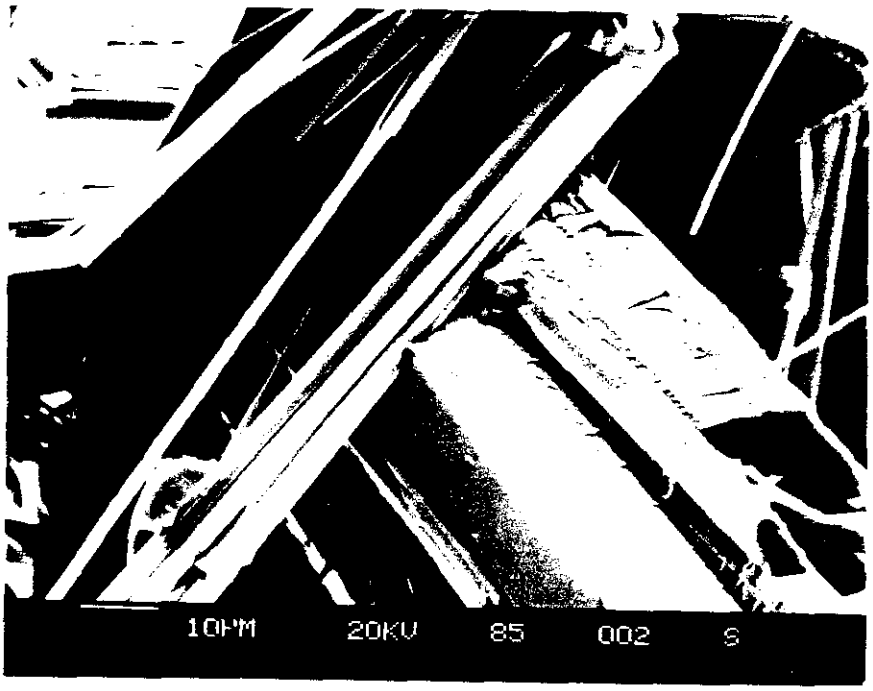

38. Scanning electron micrograph showing prismatic epidote crystal from 1,148.5 m depth in the ML 45-36 drill hole.

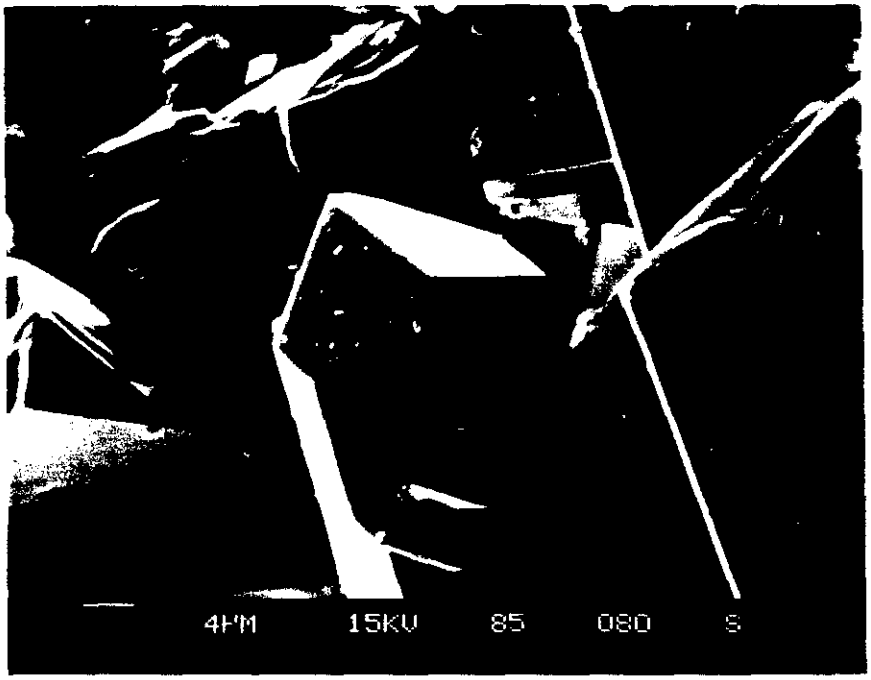

39. Scanning electron micrograph of andradite garnet crystals deposited on a fracture in drill core from 1,321.0 m depth in the ML 28-32 drill hole.

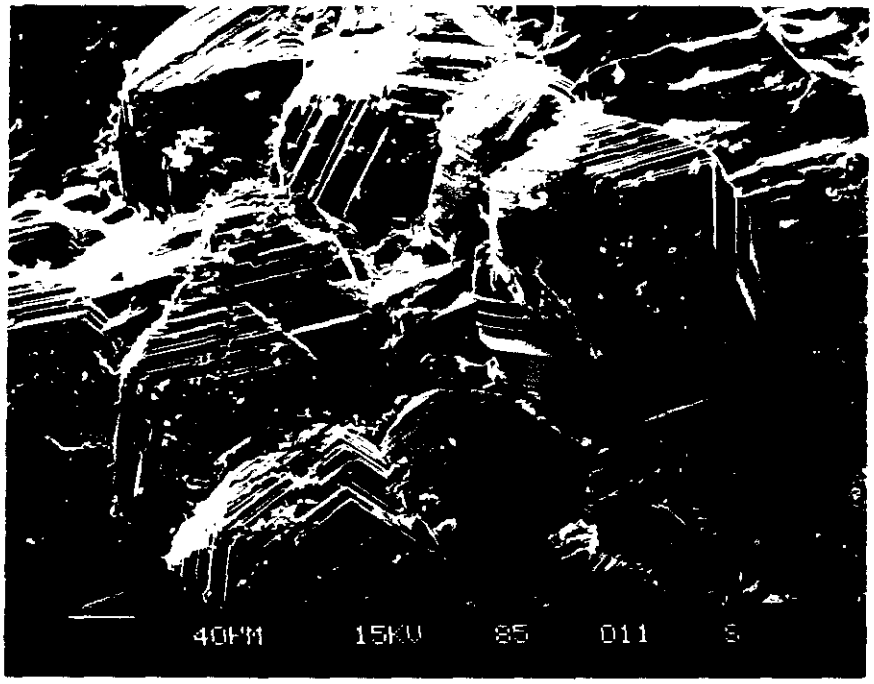

40. Plot of depth below ground surface vs. fluid-inclusion homogenization temperatures (T_h) for quartz and calcite fluid inclusions in core from the ML 28-32 drill hole (data from Table 15). Dashed curve is a theoretical reference boiling-point curve for pure water originating at the ground surface (after data in Elder, 1981, Table A5).

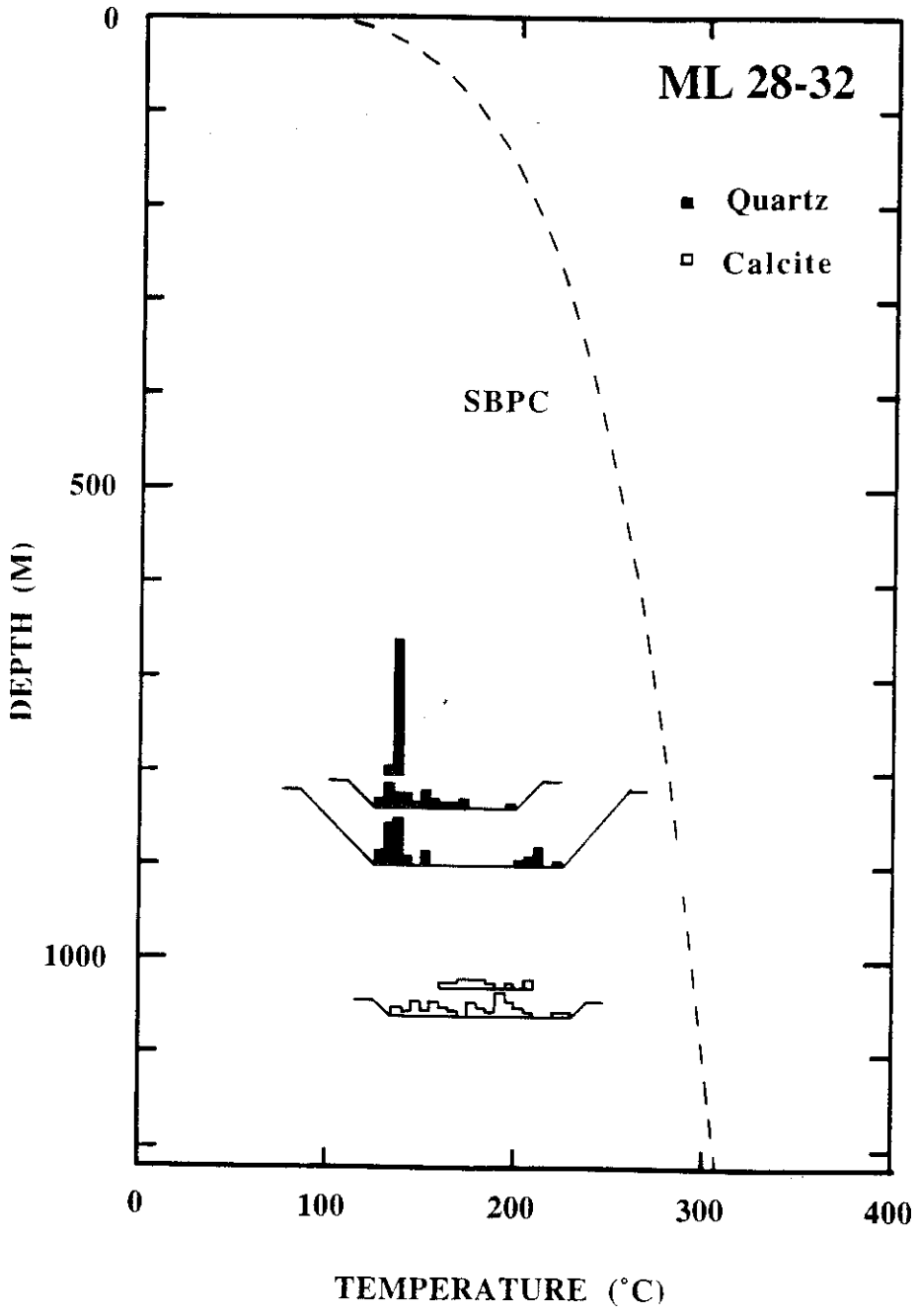

41. Plot of depth below ground surface vs. fluid-inclusion homogenization temperatures (T_h) for quartz, calcite, and wairakite fluid inclusions from the ML 45-36 drill hole (data from Table 15). Dashed curve is a theoretical reference boiling-point curve for pure water originating at the ground surface (after data in Elder, 1981, Table A5).

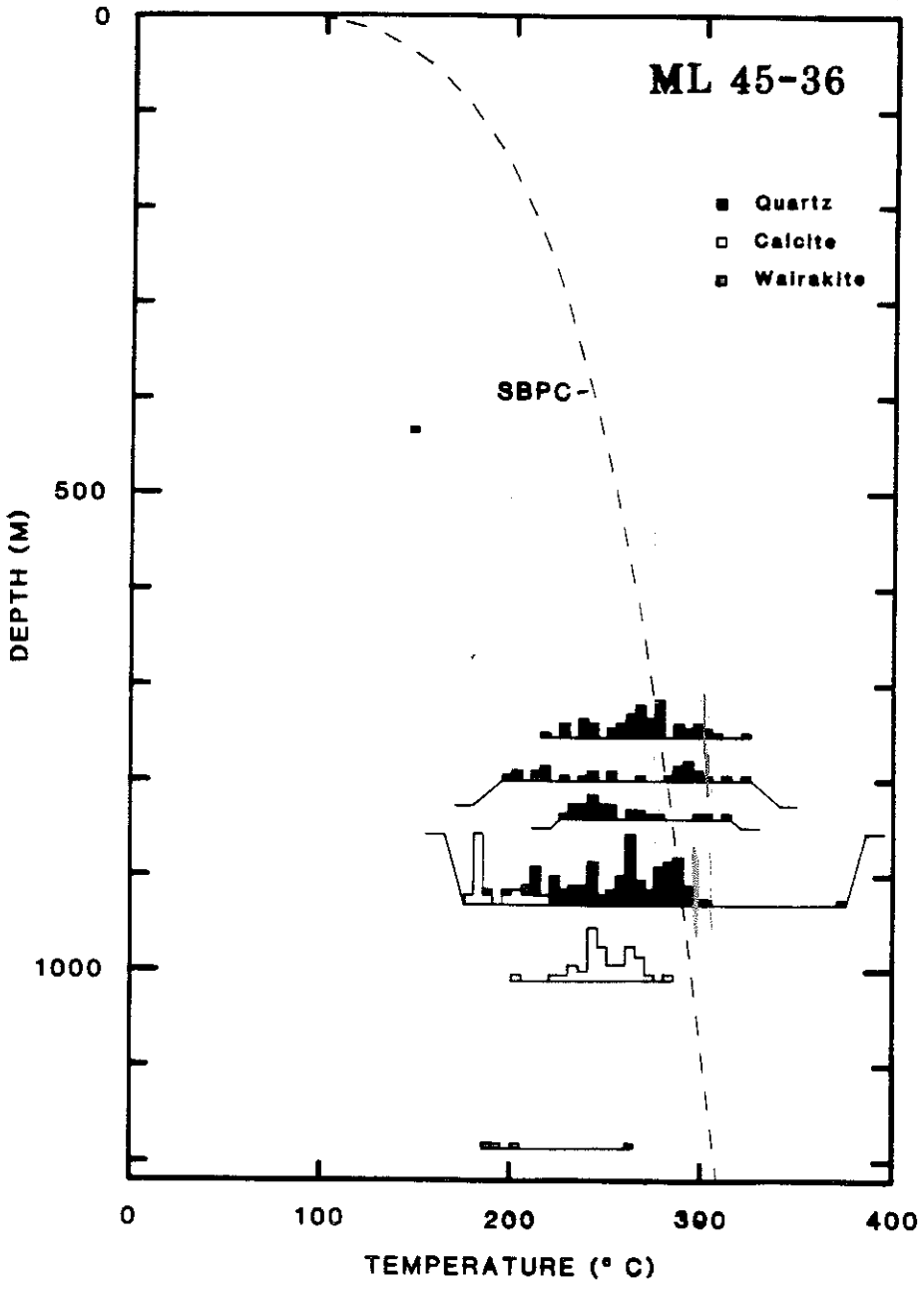

42a Scanning electron micrograph showing quartz crystals in drill core from 905.9 m depth in the ML 28-32 drill hole. Attached to many crystal surfaces are individual, clusters, and stringers of tiny bacteria-like particles.

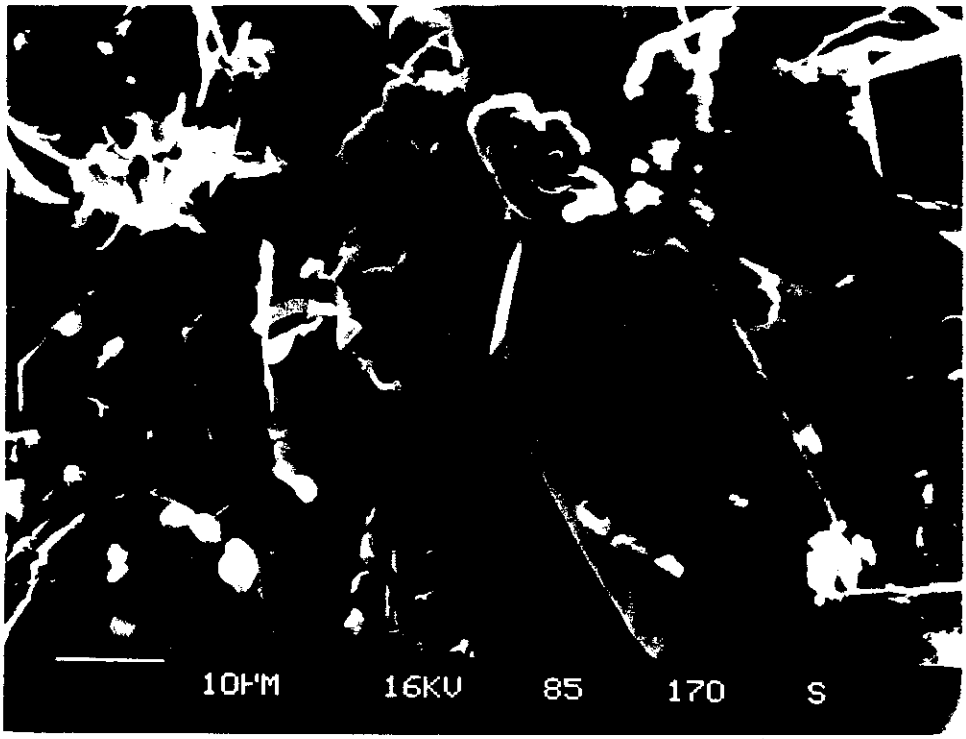

42b. Scanning electron micrograph from same specimen as Figure 42a showing a close-up view of one string and one cluster of spheroidal (cocus?) and dimpled bacteria-like particles.

43a. Scanning electron micrograph showing surfaces of a heulandite-group mineral from 488.9 m depth in the ML 45-36 drill hole that contain a string of spheroidal and dimpled bacteria-like particles.

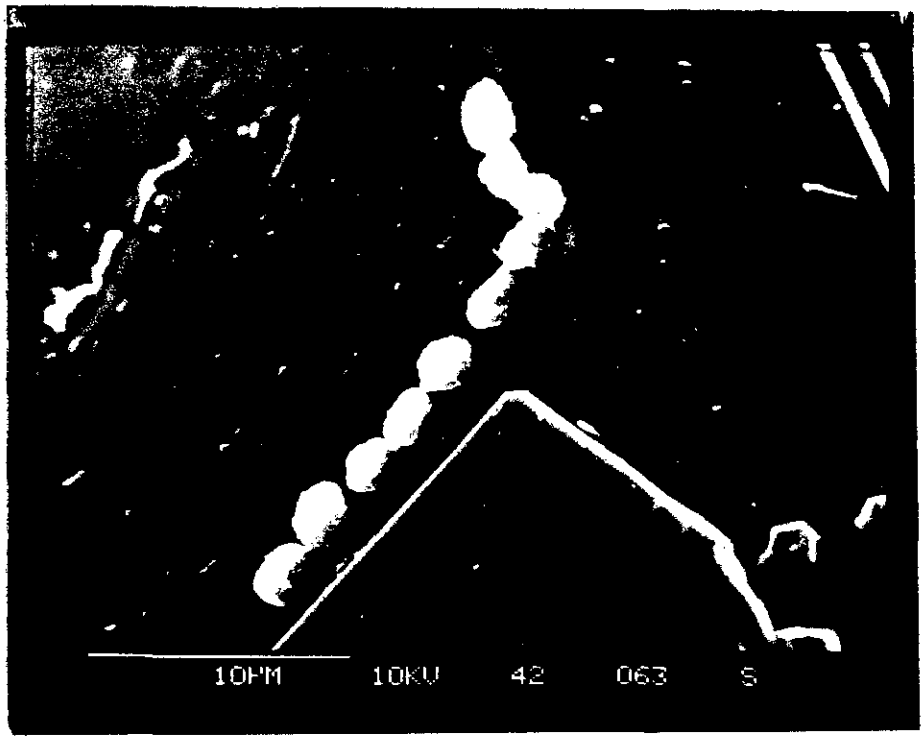

43b. Scanning electron micrograph of individual, clusters, and stringers of tiny bacteria-like particles, from 488.9 m depth in the ML 45-36 drill hole, some of which appear connected by a "trail" of viscous slime(?) (left by movement of particles across the crystal surface?).

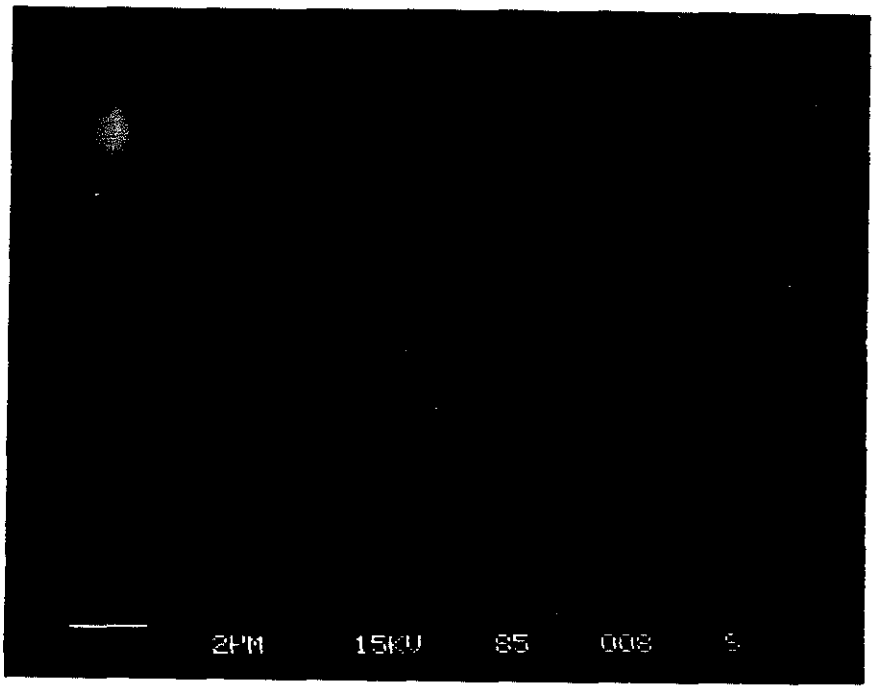

44. Photomicrograph of a 200 µm x 130 µm liquid-rich, primary fluid inclusion in a 2 mm long colorless quartz crystal from a fracture in a rhyolitic lava flow at 856 m depth in the ML 45-36 drill hole. The fluid inclusion contains dozens of tiny moving bacteria-like particles.

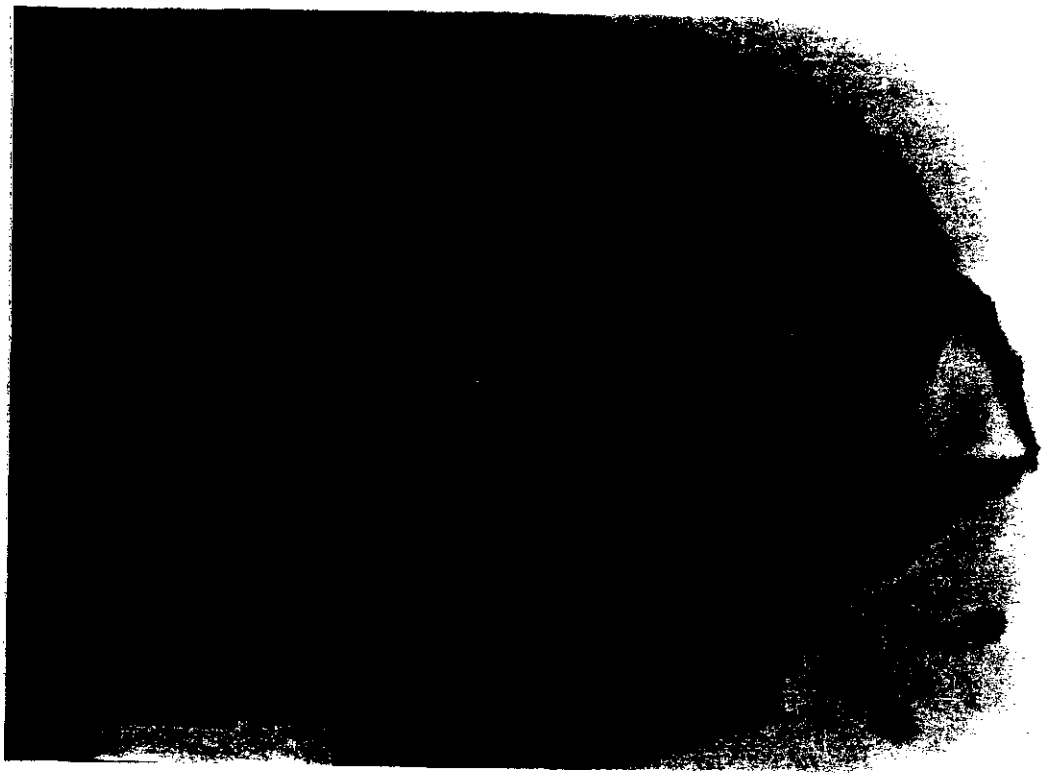

45. Photograph (using a laser scanning microscope) of tiny, rodlike particles trapped inside the fluid inclusion shown in Figure 44 (see Attachment 1 video tape).

ATTACHMENT 1

The video tape attached to this report shows moving particles that were trapped inside the fluid inclusion of Figure 44 (Bargar, 1992). These particles first were observed during initial heating of the inclusion to determine it's homogenization temperature. The ~3 to 4 μm-size, rodlike particles displayed only a very sluggish "Brownian" type of movement at ambient temperature, but submicron-size particles move rapidly throughout much of the fluid inclusion. As the temperature was increased (eventually to about 130°C), movement of the particles increased substantially defining a cylindrical-shaped thermally induced current near the lower part of the dark vapor bubble.

The first video tape segment was made using a television camera attached to a petrographic microscope modified for fluid-inclusion studies. This part of the video tape shows the ever increasing rate of motion of the particles caught up in the thermal current.

The second part of the videotape was made using a laser scanning microscope to obtain enlarged views of the mostly rodlike particles at room temperature. Submicron-size particles move rapidly in and out of the field of view while the larger, slower moving particles are clustered at one corner of the inclusion. Scale of the particles is shown by bringing two vertical lines together; the distance between the lines is printed in the lower right-hand part of the screen.

Table 1. Hydrothermal minerals identified from geothermal drill holes at Medicine Lake volcano and temperatures at which these minerals are found in studied modern geothermal areas.

Drill hole no.	OWML5	18-34	27-27	28-32	36-28	45-36	52-4	57-13	62-21	68-16	86-23	88-12	Temp.[2]
Zeolite minerals													
Analcime	--	--	--	--	--	--	--	--	--	--	X	--	70—300
Chabazite	X	--	--	--	--	--	X	--	--	--	--	--	<75
Heulandite	X	--	--	X	--	X	X	--	X	--	--	--	60—170
Laumontite	--	--	--	X	--	X	--	--	--	--	--	X	43—230
Levyne	--	--	--	--	--	--	--	--	--	--	X	--	<70
Mordenite	--	--	--	X	--	X	X	--	X	--	--	--	85—230
Phillipsite	--	X	--	--	--	--	--	--	--	--	X	--	37—85
Scolecite	--	--	--	--	--	--	--	--	--	--	X	--	65—100
Stellerite/Stilbite?	X	--	--	--	--	--	X	--	--	--	X	--	70—170
Thomsonite	--	--	--	--	--	--	--	--	--	--	X	--	60—110
Wairakite	--	--	--	X	--	X	--	--	--	--	--	--	180—300
Carbonate minerals													
Aragonite	--	--	--	X	--	--	--	--	--	--	--	--	<80
Calcite	X	X	X	X	X	X	X	X	X	--	X	X	<100—350
Dolomite	X	--	--	X	--	--	--	--	X	--	--	--	<10—250
Kutnohorite	--	--	X	X	--	--	--	--	--	--	--	--	<10—70
Rhodochrosite	--	--	--	--	--	X	--	--	--	--	--	--	30—130
Siderite	X	X	--	X	--	--	X	--	--	--	--	--	<10—160
Sheet-silicate minerals													
Kaolinite	--	--	--	X	--	--	--	--	--	--	--	--	<50—170
Halloysite	--	--	--	--	--	--	X	--	--	--	--	--	<50
Smectite	X	X	X	X	X	X	X	X	X	--	X	X	<200
Illite-Smectite	--	--	X	X	--	--	--	--	--	--	--	X	50—270
Illite	--	--	--	X	--	X	--	--	--	--	--	--	150—<300
Chlorite-Smectite	--	--	--	X	--	X	--	--	--	--	--	--	<100—240
Chlorite	--	--	--	X	--	X	--	--	--	--	--	X	<100—350
Apophylite	--	--	--	--	--	--	--	--	--	--	X	--	50—70
Prehnite	--	--	--	--	--	X	--	--	--	--	--	--	210—350
Talc	--	--	--	X	--	--	--	--	--	--	--	--	290—320
Silica minerals													
Opal	--	--	--	--	--	X	--	--	--	--	--	--	<100
Cristobalite	X	--	--	X	--	X	X	--	X	--	--	--	<100—210
Chalcedony	X	--	--	X	--	X	X	--	X	--	--	--	<100—240
Quartz	X	--	--	X	X	X	--	--	X		--	X	100—300+
Sulfide minerals													
Marcasite	--	--	--	X	X	--	--	--	--	--	--	--	80—170
Pyrite	--	--	--	X	X	X	X	--	--	--	--	X	<100—350+
Pyrrhotite	--	--	--	X	--	X	--	--	--	--	--	--	97—265
Sulfate minerals													
Anhydrite	--	--	--	X	--	X	--	--	--	--	--	--	60—300
Gypsum	--	--	--	X	X	--	--	--	--	--	--	--	<70
Natrojarosite	--	--	--	X	X	--	--	--	--	--	--	--	50
Other minerals													
Iron oxide[1]	X	X	--	X	--	X	X	--	X	X	--	X	<100—250
Magnetite	--	--	--	X	--	--	--	--	--	--	--	--	>200?
Gyrolite	--	--	--	--	--	--	--	--	--	--	X	--	<50—>200
Adularia	--	--	--	X	--	--	--	--	--	--	X	--	150—300+
Actinolite	--	--	--	X	--	X	--	--	--	--	--	--	260—400
Epidote	--	--	--	X	--	X	--	--	--	--	--	--	220—350
Garnet	--	--	--	X	--	--	--	--	--	--	--	--	250—300+

[1]Iron oxide includes both amorphous iron oxide and hematite in XRD analyses.

[2]Measured temperatures (in °C) at which minerals occur in modern geothermal areas. Data from Tómasson and Kristmannsdóttir (1972); Kristmannsdóttir (1975); Kristmannsdóttir and Tómasson (1978); Kristmannsdóttir (1979); Jakobsson and Moore (1986); Fridleifsson (1991); Honda and Muffler (1970); Keith, White, and Beeson (1978); Holland and Malinin (1979); Elders and others (1979); Cavarretta, Gianelli, and Puxeddu (1982); Leach, Wood, and Reyes (1983); Aumento and Liguori (1986); Hulen and Nielson (1986); White, Hutchinson, and Keith (1988); Horton (1985); Bargar and Keith (in press)) McDowell and Paces (1985).

Table 2. Electron microprobe analyses of analcime and wairakite.

Mineral	Analcime					Wairakite				
Sample no.	ML 86-23 3500					ML 28-32 4490				
Analysis no.	1	2	3	4	5	1	2	3	4	5
	Major-element chemical analyses (weight percent oxides)									
SiO_2	55.72	55.83	56.18	54.94	55.44	55.40	55.57	55.49	55.09	54.82
Al_2O_3	22.12	22.53	21.99	22.54	22.24	22.98	23.38	23.26	22.95	23.44
Fe_2O_3	0.00	0.03	0.01	0.04	0.00	0.00	0.00	0.07	0.01	0.00
MgO	0.00	0.00	0.00	0.00	0.00	0.00	0.00	0.00	0.00	0.00
CaO	0.02	0.05	0.02	0.05	0.08	12.37	12.67	12.01	12.39	12.27
Na_2O	13.83	13.53	13.35	13.68	13.34	0.14	0.14	0.08	0.13	0.15
K_2O	0.03	0.03	0.02	0.03	0.03	0.00	0.01	0.02	0.02	0.02
MnO	0.00	0.03	0.00	0.00	0.00	0.05	0.00	0.05	0.01	0.03
SrO	0.03	0.02	0.00	0.00	0.01	0.07	0.00	0.04	0.00	0.09
BaO	0.01	0.05	0.00	0.09	0.00	0.00	0.01	0.06	0.00	0.07
Total	91.76	92.10	91.57	91.37	91.14	91.01	91.78	91.08	90.60	90.89
	Number of atoms on the basis of 96 oxygens									
Si	32.61	32.53	32.84	32.33	32.60	32.25	32.10	32.25	32.21	32.00
Al	15.26	15.48	15.15	15.63	15.41	15.77	15.92	15.93	15.82	16.12
Fe	0.00	0.01	0.00	0.02	0.00	0.00	0.00	0.03	0.01	0.00
Mg	0.00	0.00	0.00	0.00	0.00	0.00	0.00	0.00	0.00	0.00
Ca	0.01	0.03	0.01	0.03	0.05	7.72	7.84	7.48	7.76	7.67
Na	15.69	15.28	15.13	15.61	15.21	0.15	0.16	0.09	0.14	0.17
K	0.02	0.02	0.01	0.03	0.02	0.00	0.01	0.01	0.02	0.02
Mn	0.00	0.02	0.00	0.00	0.00	0.03	0.00	0.02	0.00	0.01
Sr	0.01	0.01	0.00	0.00	0.00	0.02	0.00	0.01	0.00	0.03
Ba	0.00	0.01	0.00	0.02	0.00	0.00	0.00	0.01	0.00	0.02
Si+Al	47.87	48.01	47.99	47.96	48.01	48.02	48.02	48.18	48.03	48.12
Si/(Al+Fe)	2.14	2.10	2.17	2.07	2.12	2.04	2.02	2.02	2.04	1.98
Si/(Si+Al+Fe)	0.68	0.68	0.68	0.67	0.68	0.67	0.67	0.67	0.67	0.67
Balance Error	-3.21	0.41	-0.05	0.53	0.38	0.48	0.40	5.37	0.80	3.06

Table 2. Continued.

Mineral	Wairakite									
Sample no.	ML 45-36 3820					ML 45-36 3887				
Analysis no.	1	2	3	4	5	1	2	3	4	5
	Major-element chemical analyses (weight percent oxides)									
SiO_2	54.25	53.08	53.47	54.27	54.16	54.73	53.87	55.24	54.82	55.14
Al_2O_3	22.50	22.76	22.59	22.69	22.32	22.85	22.84	22.70	22.93	22.97
Fe_2O_3	0.02	0.00	0.03	0.05	0.00	0.03	0.00	0.03	0.00	0.02
MgO	0.00	0.00	0.00	0.00	0.02	0.00	0.01	0.00	0.01	0.01
CaO	12.37	12.10	12.40	12.33	11.92	12.34	12.54	12.09	12.45	12.35
Na_2O	0.24	0.20	0.18	0.23	0.29	0.23	0.19	0.23	0.23	0.19
K_2O	0.05	0.02	0.03	0.00	0.03	0.02	0.01	0.03	0.04	0.02
MnO	0.00	0.00	0.04	0.02	0.07	0.00	0.05	0.00	0.00	0.00
SrO	0.00	0.08	0.10	0.00	0.03	0.00	0.01	0.07	0.00	0.06
BaO	0.01	0.00	0.00	0.00	0.00	0.00	0.04	0.06	0.00	0.11
Total	89.44	88.24	88.84	89.59	88.84	90.20	89.56	90.45	90.48	90.87
	Number of atoms on the basis of 96 oxygens									
Si	32.19	31.93	31.99	32.13	32.30	32.17	31.95	32.36	32.13	32.19
Al	15.74	16.14	15.93	15.83	15.69	15.83	15.97	15.67	15.84	15.81
Fe	0.01	0.00	0.01	0.02	0.00	0.01	0.00	0.02	0.00	0.01
Mg	0.00	0.00	0.00	0.00	0.02	0.00	0.01	0.00	0.01	0.01
Ca	7.86	7.80	7.95	7.82	7.62	7.77	7.97	7.59	7.82	7.73
Na	0.27	0.23	0.21	0.26	0.34	0.26	0.22	0.26	0.26	0.22
K	0.04	0.01	0.02	0.00	0.02	0.01	0.01	0.02	0.03	0.02
Mn	0.00	0.00	0.02	0.01	0.04	0.00	0.03	0.00	0.00	0.00
Sr	0.00	0.03	0.03	0.00	0.01	0.00	0.00	0.02	0.00	0.02
Ba	0.00	0.00	0.00	0.00	0.00	0.00	0.01	0.01	0.00	0.02
Si+Al	47.92	48.06	47.91	47.97	47.99	48.00	47.92	48.03	47.97	48.00
Si/(Al+Fe)	2.04	1.98	2.01	2.03	2.06	2.03	2.00	2.06	2.03	2.04
Si/(Si+Al+Fe)	0.67	0.66	0.67	0.67	0.67	0.67	0.67	0.67	0.67	0.67
Balance Error	-1.83	1.54	-1.88	-0.42	-0.23	0.22	-1.88	1.04	-0.65	0.18

Table 3. Electron microprobe analyses of heulandite group minerals.

Mineral	Heulandite					Clinoptilolite				
Sample no.	ML 45-36 1604					ML 52-4 3982				
Analysis no.	1	2	3	4	5	1	2	3	4	5
	Major-element chemical analyses (weight percent oxides)									
SiO_2	64.97	64.43	64.13	64.01	64.14	69.61	71.84	69.72	69.75	70.20
Al_2O_3	15.20	15.31	14.91	15.23	14.72	12.30	12.51	12.81	12.98	12.49
Fe_2O_3	0.05	0.03	0.02	0.01	0.00	0.00	0.02	0.03	0.00	0.05
MgO	0.07	0.08	0.07	0.04	0.07	0.26	0.49	0.55	0.48	0.28
CaO	6.78	7.13	6.81	7.00	6.84	1.46	1.33	1.54	1.44	1.61
Na_2O	0.61	0.47	0.49	0.37	0.36	3.33	2.85	2.88	2.84	3.12
K_2O	0.20	0.18	0.18	0.22	0.19	2.05	2.57	2.31	2.40	2.24
MnO	0.01	0.00	0.00	0.02	0.00	0.01	0.02	0.02	0.03	0.00
SrO	0.02	0.10	0.12	0.05	0.10	0.11	0.16	0.25	0.19	0.25
BaO	0.00	0.00	0.00	0.00	0.07	1.05	0.76	0.91	1.21	1.00
Total	87.91	87.73	86.73	86.95	86.49	90.18	92.55	91.02	91.32	91.24
	Number of atoms on the basis of 72 oxygens									
Si	28.36	28.23	28.38	28.26	28.45	29.84	29.94	29.64	29.61	29.79
Al	7.82	7.91	7.77	7.93	7.70	6.21	6.14	6.42	6.50	6.25
Fe	0.02	0.01	0.01	0.00	0.00	0.00	0.01	0.01	0.00	0.02
Mg	0.05	0.05	0.05	0.03	0.05	0.17	0.30	0.35	0.30	0.17
Ca	3.17	3.34	3.23	3.31	3.25	0.67	0.59	0.70	0.65	0.73
Na	0.52	0.40	0.42	0.31	0.31	2.77	2.30	2.37	2.33	2.57
K	0.11	0.10	0.10	0.12	0.11	1.12	1.37	1.25	1.30	1.21
Mn	0.00	0.00	0.00	0.01	0.00	0.00	0.01	0.01	0.01	0.00
Sr	0.00	0.03	0.03	0.01	0.02	0.03	0.04	0.06	0.05	0.06
Ba	0.00	0.00	0.00	0.00	0.01	0.18	0.12	0.15	0.20	0.17
Si+Al	36.18	36.14	36.16	36.19	36.15	36.06	36.08	36.06	36.11	36.04
Si/(Al+Fe)	3.62	3.57	3.65	3.56	3.70	4.80	4.87	4.61	4.56	4.75
Si/(Si+Al+Fe)	0.78	0.78	0.79	0.78	0.79	0.83	0.83	0.82	0.82	0.83
Balance Error	10.69	7.79	9.02	10.99	8.50	3.89	6.05	4.34	7.07	3.43

Table 4. Electron microprobe analyses of laumontite.

Sample no.	ML 28-32 3637					ML 45-36 3458					
Analysis no.	1	2	3	4	5	1	2	3	4	5	6
	Major-element chemical analyses (weight percent oxides)										
SiO_2	48.66	49.55	50.01	50.01	50.55	49.35	50.06	49.93	52.28	51.31	51.82
Al_2O_3	19.95	20.77	20.64	20.32	20.95	18.24	19.82	20.09	20.86	19.86	20.22
Fe_2O_3	0.03	0.00	0.00	0.00	0.04	0.01	0.02	0.00	0.02	0.02	0.00
MgO	0.00	0.00	0.00	0.00	0.00	0.00	0.00	0.01	0.00	0.00	0.00
CaO	11.02	11.52	11.34	11.15	11.63	10.55	11.20	11.22	11.15	11.22	10.69
Na_2O	0.05	0.02	0.11	0.05	0.04	0.18	0.19	0.11	0.21	0.19	0.30
K_2O	0.04	0.02	0.04	0.04	0.03	0.06	0.09	0.06	0.08	0.08	0.09
MnO	0.04	0.00	0.01	0.00	0.00	0.00	0.00	0.00	0.05	0.04	0.00
SrO	0.05	0.06	0.07	0.03	0.03	0.00	0.05	0.07	0.04	0.00	0.05
BaO	0.08	0.08	0.07	0.00	0.00	0.03	0.10	0.00	0.01	0.00	0.03
Total	79.92	82.02	82.29	81.60	83.27	78.42	81.53	81.49	84.70	82.72	83.20
	Number of atoms on the basis of 48 oxygens										
Si	16.15	16.04	16.13	16.22	16.10	16.63	16.29	16.24	16.32	16.41	16.45
Al	7.81	7.92	7.84	7.77	7.87	7.24	7.60	7.70	7.68	7.49	7.57
Fe	0.01	0.00	0.00	0.00	0.01	0.00	0.01	0.00	0.00	0.01	0.00
Mg	0.00	0.00	0.00	0.00	0.00	0.00	0.00	0.00	0.00	0.00	0.00
Ca	3.92	4.00	3.92	3.87	3.97	3.81	3.91	3.91	3.73	3.85	3.64
Na	0.03	0.01	0.07	0.03	0.02	0.11	0.12	0.07	0.12	0.11	0.18
K	0.01	0.01	0.01	0.02	0.01	0.02	0.04	0.02	0.03	0.03	0.04
Mn	0.01	0.00	0.00	0.00	0.00	0.00	0.00	0.00	0.01	0.01	0.00
Sr	0.01	0.01	0.01	0.01	0.01	0.00	0.01	0.01	0.01	0.00	0.01
Ba	0.01	0.01	0.01	0.00	0.00	0.00	0.01	0.00	0.00	0.00	0.00
Si+Al	23.96	23.97	23.97	23.99	23.96	23.87	23.89	23.94	24.00	23.90	24.01
Si/(Al+Fe)	2.07	2.02	2.06	2.09	2.04	2.30	2.14	2.11	2.13	2.19	2.17
Si/(Si+Al+Fe)	0.67	0.67	0.67	0.67	0.67	0.70	0.67	0.68	0.68	0.69	0.69
Balance Error	-1.69	-1.68	-1.50	-0.44	-1.38	-6.79	-5.07	-3.08	0.31	-4.65	0.60

Table 4. Continued.

Sample no.	ML 45-36 3908					
Analysis no.	1	2	3	4	5	6
	Major-element chemical analyses (weight percent oxides)					
SiO_2	49.91	50.25	51.00	50.58	50.50	51.76
Al_2O_3	20.48	20.68	20.91	20.46	20.59	21.11
Fe_2O_3	0.06	0.03	0.01	0.20	0.14	0.05
MgO	0.12	0.00	0.00	0.17	0.13	0.05
CaO	11.41	11.12	11.55	11.42	11.70	11.65
Na_2O	0.05	0.11	0.06	0.07	0.12	0.06
K_2O	0.03	0.05	0.06	0.04	0.08	0.05
MnO	0.03	0.00	0.05	0.00	0.05	0.00
SrO	0.00	0.08	0.02	0.00	0.10	0.11
BaO	0.00	0.04	0.05	0.00	0.00	0.00
Total	82.09	82.36	83.71	82.94	83.41	84.84
	Number of atoms on the basis of 48 oxygens					
Si	16.12	16.17	16.16	16.18	16.11	16.18
Al	7.80	7.84	7.81	7.71	7.74	7.78
Fe	0.02	0.01	0.03	0.05	0.04	0.01
Mg	0.06	0.00	0.00	0.08	0.06	0.02
Ca	3.95	3.83	3.92	3.91	4.00	3.90
Na	0.03	0.07	0.03	0.04	0.07	0.03
K	0.03	0.02	0.02	0.18	0.03	0.02
Mn	0.03	0.00	0.01	0.00	0.01	0.00
Sr	0.00	0.01	0.00	0.00	0.02	0.02
Ba	0.00	0.01	0.01	0.00	0.00	0.00
Si+Al	23.92	24.01	23.97	23.89	23.85	23.96
Si/(Al+Fe)	2.06	2.06	2.06	2.09	2.07	2.08
Si/(Si+Al+Fe)	0.67	0.67	0.67	0.68	0.67	0.68
Balance Error						

Table 5. Electron microprobe analyses of levyne.

Sample no.	ML 86-23 3410				
Analysis no.	1	2	3	4	5
Major-element chemical analyses (weight percent oxides)					
SiO_2	51.67	52.24	51.81	50.85	51.30
Al_2O_3	23.92	22.98	23.41	23.80	24.22
Fe_2O_3	0.02	0.04	0.04	0.04	0.00
MgO	0.01	0.00	0.01	0.00	0.00
CaO	10.50	10.62	10.50	11.17	11.02
Na_2O	1.31	1.51	1.40	1.26	1.40
K_2O	0.11	0.09	0.12	0.09	0.08
MnO	0.01	0.05	0.01	0.03	0.00
SrO	0.01	0.02	0.06	0.22	0.06
BaO	0.00	0.02	0.03	0.00	0.00
Total	87.56	87.57	87.39	87.46	88.08
Number of atoms on the basis of 36 oxygens					
Si	11.75	11.90	11.82	11.64	11.64
Al	6.41	6.17	6.29	6.42	6.48
Fe	0.00	0.00	0.01	0.01	0.00
Mg	0.00	0.00	0.00	0.00	0.00
Ca	2.56	2.59	2.57	2.74	2.68
Na	0.58	0.66	0.62	0.56	0.61
K	0.03	0.03	0.04	0.03	0.02
Mn	0.00	0.01	0.00	0.01	0.00
Sr	0.00	0.00	0.01	0.03	0.01
Ba	0.00	0.00	0.00	0.00	0.00
Si+Al	18.16	18.07	18.11	18.06	18.12
Si/(Al+Fe)	1.83	1.93	1.88	1.81	1.80
Si/(Si+Al+Fe)	0.64	0.66	0.65	0.64	0.64
Balance Error	11.87	5.11	8.25	4.89	7.82

Table 6. Electron microprobe analyses of phillipsite.

Sample no.	ML 18-34 3462				
Analysis no.	1	2	3	4	5
Major-element chemical analyses (weight percent oxides)					
SiO_2	50.83	51.93	50.15	51.53	52.04
Al_2O_3	24.24	24.72	24.25	24.51	24.54
Fe_2O_3	0.00	0.04	0.04	0.01	0.01
MgO	0.00	0.00	0.01	0.00	0.00
CaO	6.16	6.40	6.23	6.49	6.13
Na_2O	2.39	2.50	2.27	2.60	2.64
K_2O	7.06	7.38	7.03	7.11	6.99
MnO	0.02	0.02	0.00	0.00	0.00
SrO	0.05	0.06	0.13	0.02	0.05
BaO	0.02	0.03	0.14	0.00	0.15
Total	90.77	93.08	90.25	92.27	92.55
Number of atoms on the basis of 32 oxygens					
Si	10.30	10.28	10.24	10.28	10.33
Al	5.79	5.77	5.84	5.76	5.74
Fe	0.00	0.01	0.01	0.00	0.00
Mg	0.00	0.00	0.00	0.00	0.00
Ca	1.34	1.36	1.36	1.39	1.31
Na	0.94	0.96	0.90	1.01	1.02
K	1.82	1.86	1.83	1.81	1.77
Mn	0.00	0.00	0.00	0.00	0.00
Sr	0.01	0.01	0.01	0.00	0.01
Ba	0.00	0.00	0.01	0.00	0.01
Si+Al	16.08	16.05	16.08	16.04	16.08
Si/(Al+Fe)	1.78	1.78	1.75	1.78	1.80
Si/(Si+Al+Fe)	0.64	0.64	0.64	0.64	0.64
Balance Error	6.04	3.82	6.02	3.06	5.69

Table 7. Electron microprobe analyses of scolecite.

Sample no.	ML 86-23 3410				
Analysis no.	1	2	3	4	5
Major-element chemical analyses (weight percent oxides)					
SiO_2	45.47	43.44	44.74	45.62	45.23
Al_2O_3	24.22	23.34	24.32	24.63	23.89
Fe_2O_3	0.00	0.00	0.00	0.02	0.03
MgO	0.00	0.00	0.00	0.00	0.01
CaO	12.43	11.09	12.44	12.53	11.54
Na_2O	1.38	1.40	1.17	1.21	1.66
K_2O	0.01	0.02	0.02	0.01	0.03
MnO	0.00	0.02	0.00	0.00	0.00
SrO	0.06	0.06	0.00	0.03	0.08
BaO	0.04	0.00	0.00	0.08	0.00
Total	83.61	79.37	82.69	84.13	82.47
Number of atoms on the basis of 80 oxygens					
Si	24.50	24.57	24.36	24.42	24.65
Al	15.38	15.56	15.61	15.54	15.35
Fe	0.00	0.00	0.00	0.01	0.01
Mg	0.00	0.00	0.00	0.00	0.01
Ca	7.18	6.72	7.26	7.19	6.74
Na	1.44	1.53	1.23	1.25	1.76
K	0.01	0.02	0.01	0.01	0.02
Mn	0.00	0.01	0.00	0.00	0.00
Sr	0.02	0.02	0.00	0.01	0.03
Ba	0.01	0.00	0.00	0.02	0.00
Si+Al	39.88	40.13	39.96	39.96	40.00
Si/(Al+Fe)	1.59	1.58	1.56	1.57	1.61
Si/(Si+Al+Fe)	0.61	0.61	0.61	0.61	0.61
Balance Error	-2.90	3.57	-0.92	-0.88	0.18

Table 8. Electron microprobe analyses of thomsonite.

Sample no.	ML 86-23 3420					
Analysis no.	1	2	3	4	5	6
	Major-element chemical analyses (weight percent oxides)					
SiO_2	40.91	41.60	41.13	41.33	41.44	41.35
Al_2O_3	28.32	27.89	28.38	27.76	27.53	28.08
Fe_2O_3	0.12	0.08	0.11	0.06	0.09	0.11
MgO	0.00	0.00	0.01	0.00	0.00	0.01
CaO	10.80	10.82	10.78	10.65	10.93	10.66
Na_2O	5.51	4.42	4.37	4.36	4.26	4.17
K_2O	0.02	0.02	0.02	0.02	0.04	0.02
MnO	0.05	0.01	0.00	0.01	0.00	0.05
SrO	0.08	0.12	0.13	0.08	0.07	0.06
BaO	0.00	0.00	0.07	0.11	0.00	0.01
Total	85.81	84.96	85.00	84.38	84.36	84.52
	Number of atoms on the basis of 80 oxygens					
Si	21.96	22.40	22.17	22.41	22.47	22.35
Al	17.92	17.70	18.03	17.74	17.60	17.89
Fe	0.05	0.03	0.05	0.03	0.04	0.05
Mg	0.00	0.00	0.01	0.00	0.00	0.01
Ca	6.22	6.24	6.23	6.19	6.35	6.18
Na	5.74	4.61	4.56	4.58	4.47	4.37
K	0.01	0.02	0.01	0.02	0.03	0.02
Mn	0.02	0.01	0.00	0.01	0.00	0.02
Sr	0.02	0.04	0.04	0.03	0.02	0.02
Ba	0.00	0.00	0.01	0.02	0.00	0.00
Si+Al	39.89	40.11	40.19	40.15	40.07	40.24
Si/(Al+Fe)	1.22	1.26	1.23	1.26	1.27	1.25
Si/(Si+Al+Fe)	0.55	0.56	0.55	0.56	0.56	0.55
Balance error	-1.40	3.19	5.36	4.09	2.31	6.79

Table 9. Electron microprobe analyses of smectite.

Sample no.	ML 86-23 3500					ML 18-34 3462				
Analysis no.	1	2	3	4	5	1	2	3	4	5
	Major-element chemical analyses (weight percent oxides)									
SiO_2	44.03	40.62	42.39	43.05	44.01	47.35	45.67	47.54	46.12	46.21
Al_2O_3	12.76	11.65	11.18	9.21	13.04	6.50	6.96	6.51	6.61	6.67
Fe_2O_3	7.43	7.12	7.57	11.85	8.49	13.42	13.51	14.05	12.76	12.76
MgO	19.91	18.04	18.96	18.20	19.40	17.90	16.59	17.98	17.37	17.10
CaO	3.43	3.41	3.18	3.07	3.66	3.34	3.76	3.17	1.94	1.57
Na_2O	0.21	0.24	0.24	0.18	0.16	1.14	0.77	0.74	0.36	0.57
K_2O	0.04	0.03	0.03	0.04	0.03	1.03	1.05	0.95	0.59	0.76
MnO	0.12	0.11	0.17	0.15	0.16	0.11	0.11	0.06	0.10	0.14
SrO	0.01	0.08	0.03	0.01	0.04	0.00	0.07	0.10	0.01	0.01
BaO	0.00	0.00	0.03	0.18	0.05	0.00	0.00	0.00	0.01	0.02
Total	87.94	81.30	83.78	85.94	89.04	90.79	88.49	91.10	85.87	85.81
	Number of atoms on the basis of 22 oxygens									
Si	6.46	6.47	6.55	6.66	6.43	7.02	6.97	7.03	7.13	7.15
Al	2.21	2.19	2.04	1.68	2.24	1.14	1.25	1.13	1.21	1.22
Fe	0.82	0.85	0.88	1.38	0.93	1.50	1.55	1.56	1.48	1.49
Mg	4.36	4.28	4.37	4.20	4.22	3.95	3.78	3.96	4.00	3.95
Ca	0.54	0.58	0.53	0.51	0.57	0.53	0.61	0.50	0.32	0.26
Na	0.06	0.07	0.07	0.06	0.04	0.33	0.23	0.21	0.11	0.17
K	0.01	0.01	0.01	0.01	0.01	0.19	0.20	0.18	0.12	0.15
Mn	0.02	0.01	0.02	0.02	0.02	0.01	0.01	0.01	0.01	0.02
Sr	0.00	0.01	0.00	0.00	0.00	0.00	0.01	0.01	0.00	0.00
Ba	0.00	0.00	0.00	0.01	0.00	0.00	0.00	0.00	0.00	0.00

Table 10. Electron microprobe analyses of illite and chlorite.

Mineral	Illite					Chlorite	
Sample no.	ML 28-32 4460					ML 45-36 3795	
Analysis no.	1	2	3	4	5	1	2
	Major-element chemical analyses (weight percent oxides)						
SiO_2	49.00	48.56	47.39	48.83	48.16	26.65	27.53
Al_2O_3	32.30	31.85	31.23	32.20	32.00	15.65	15.80
Fe_2O_3	0.87	0.69	0.65	0.72	0.82	—	—
FeO	—	—	—	—	—	16.28	17.23
MgO	1.29	1.28	1.22	1.26	1.37	18.09	19.26
CaO	0.08	0.09	0.07	0.16	0.05	0.34	0.28
Na_2O	0.09	0.12	0.15	0.13	0.12	0.04	0.06
K_2O	9.50	9.69	9.41	9.57	9.44	0.08	0.05
MnO	0.02	0.00	0.06	0.03	0.05	0.30	0.16
SrO	0.01	0.06	0.00	0.00	0.02	0.00	0.00
BaO	0.13	0.07	0.22	0.00	0.09	0.09	0.00
Total	93.29	92.41	90.30	92.90	92.12	77.51	80.37
	Number of atoms on the basis of 24 oxygens (illite) and 28 oxygens (chlorite)						
Si	7.17	7.18	7.17	7.17	7.14	6.10	6.09
Al	5.57	5.55	5.57	5.57	5.59	4.22	4.12
Fe	0.10	0.08	0.07	0.08	0.09	3.11	3.19
Mg	0.28	0.28	0.28	0.28	0.30	6.18	6.35
Ca	0.01	0.01	0.01	0.02	0.01	0.08	0.07
Na	0.02	0.03	0.04	0.04	0.04	0.02	0.02
K	1.77	1.83	1.82	1.79	1.79	0.02	0.0
Mn	0.00	0.00	0.01	0.00	0.01	0.06	0.03
Sr	0.00	0.01	0.00	0.00	0.00	0.00	0.00
Ba	0.01	0.00	0.01	0.00	0.01	0.01	0.00

Table 11. Electron microprobe analyses of apophyllite.

Sample no.	ML 86-23 3420							
Analysis no.	1	2	3	4	5	6	7	8
	Major-element chemical analyses (weight percent oxides)							
SiO_2	45.72	47.06	50.17	50.97	50.81	50.75	50.11	50.44
Al_2O_3	1.98	2.27	0.10	0.07	0.14	0.21	0.20	0.14
FeO	0.00	0.00	0.00	0.01	0.01	0.00	0.00	0.00
MgO	0.00	0.00	0.00	0.00	0.00	0.00	0.00	0.00
CaO	29.79	30.34	22.99	24.28	23.49	23.56	23.44	24.22
Na_2O	0.22	0.19	0.09	0.04	0.09	0.10	0.12	0.09
K_2O	0.16	0.04	4.72	4.91	4.76	4.97	4.29	4.80
MnO	0.02	0.00	0.00	0.00	0.03	0.00	0.01	0.00
SrO	0.00	0.00	0.00	0.02	0.01	0.03	0.03	0.04
BaO	0.11	0.00	0.00	0.05	0.12	0.00	0.00	0.05
Total	78.00	79.90	78.07	80.35	79.46	79.62	78.20	79.78
	Number of atoms on the basis of 29 oxygens							
Si	10.42	10.43	11.34	11.26	11.31	11.29	11.30	11.23
Al	0.53	0.59	0.03	0.02	0.04	0.06	0.05	0.04
Fe	0.00	0.00	0.00	0.00	0.00	0.00	0.00	0.00
Mg	0.00	0.00	0.00	0.00	0.00	0.00	0.00	0.00
Ca	7.28	7.21	5.57	5.74	5.60	5.61	5.67	5.78
Na	0.10	0.08	0.04	0.02	0.04	0.04	0.05	0.04
K	0.05	0.01	1.36	1.38	1.35	1.41	1.23	1.36
Mn	0.00	0.00	0.00	0.00	0.01	0.00	0.00	0.00
Sr	0.00	0.00	0.00	0.00	0.00	0.00	0.00	0.00
Ba	0.01	0.00	0.00	0.00	0.01	0.00	0.00	0.00

Table 12. Electron microprobe analyses of prehnite.

Sample no.	ML 45-36 3795					ML 45-36 3820				
Analysis no.	1	2	3	4	5	1	2	3	4	5
	Major-element chemical analyses (weight percent oxides)									
SiO_2	43.89	43.49	43.28	43.59	43.33	44.21	43.31	42.05	43.08	43.62
Al_2O_3	22.97	21.99	22.84	22.36	21.95	19.39	23.34	23.58	23.15	21.94
FeO	1.93	2.57	1.84	2.49	3.07	1.82	0.86	0.83	1.40	2.77
MgO	0.01	0.00	0.00	0.02	0.01	1.22	0.02	0.02	0.01	0.02
CaO	27.05	27.10	27.17	26.81	27.30	25.87	26.92	26.56	26.71	26.32
Na_2O	0.02	0.01	0.00	0.02	0.04	0.03	0.03	0.01	0.03	0.02
K_2O	0.01	0.02	0.04	0.03	0.02	0.02	0.01	0.02	0.03	0.00
MnO	0.01	0.03	0.02	0.07	0.06	0.62	0.20	0.18	0.20	0.11
SrO	0.01	0.00	0.05	0.00	0.00	0.02	0.00	0.01	0.00	0.01
BaO	0.03	0.00	0.05	0.05	0.00	0.00	0.08	0.00	0.00	0.05
Total	95.93	95.21	95.29	95.44	95.78	93.20	94.77	93.26	94.61	94.86
	Number of atoms on the basis of 24 oxygens									
Si	6.62	6.65	6.59	6.64	6.61	6.87	6.59	6.50	6.58	6.68
Al	4.09	3.96	4.10	4.01	3.94	3.55	4.19	4.30	4.17	3.96
Fe	0.24	0.33	0.23	0.32	0.39	0.24	0.11	0.11	0.18	0.35
Mg	0.00	0.00	0.00	0.00	0.00	0.28	0.00	0.00	0.00	0.00
Ca	4.37	4.44	4.43	4.37	4.46	4.31	4.39	4.40	4.37	4.32
Na	0.00	0.00	0.00	0.00	0.01	0.01	0.01	0.00	0.01	0.01
K	0.02	0.00	0.01	0.01	0.00	0.00	0.00	0.00	0.01	0.00
Mn	0.00	0.00	0.00	0.01	0.01	0.08	0.03	0.02	0.03	0.01
Sr	0.00	0.00	0.00	0.00	0.00	0.00	0.00	0.00	0.00	0.00
Ba	0.00	0.00	0.00	0.00	0.00	0.00	0.00	0.00	0.00	0.00

Table 13. Electron microprobe analyses of epidote. [Pistacite (PS) component was determined by the calculation Fe/Fe+Al].

Sample no.	ML 28-32 4467					ML 45-36 3458					
Analysis no.	1	2	3	4	5	1	2	3	4	5	6
	Major-element chemical analyses (weight percent oxides)										
SiO_2	37.64	37.79	37.76	37.96	37.80	39.84	42.42	40.42	42.69	44.12	44.17
Al_2O_3	19.95	20.92	20.85	21.91	20.45	21.81	20.66	21.11	20.58	20.66	20.59
TiO_2	0.19	0.27	0.36	0.15	0.43	—	—	—	—	—	—
Fe_2O_3	17.25	16.05	16.22	14.94	16.49	12.65	10.05	13.81	12.50	12.28	12.00
MgO	0.01	0.02	0.01	0.01	0.02	0.11	0.19	0.11	0.11	0.15	0.09
CaO	22.50	22.98	23.20	23.38	23.31	21.44	19.61	21.83	21.21	20.78	20.95
Na_2O	—	—	—	—	—	0.03	0.07	0.00	0.02	0.01	0.01
K_2O	—	—	—	—	—	0.02	0.06	0.04	0.03	0.03	0.02
MnO	0.13	0.17	0.16	0.26	0.14	0.15	0.06	0.13	0.12	0.15	0.16
SrO	—	—	—	—	—	0.14	0.19	0.29	0.10	0.24	0.24
BaO	—	—	—	—	—	0.00	0.03	0.11	0.00	0.06	0.06
Total	97.67	98.20	98.56	98.61	98.64	96.19	93.34	97.85	97.36	98.48	98.23
	Number of atoms on the basis of 13 oxygens										
Si	3.17	3.15	3.14	3.14	3.15	3.43	3.66	3.45	3.60	3.66	3.66
Al	1.98	2.06	2.04	2.13	2.01	2.21	2.10	2.12	2.04	2.02	2.01
Ti	0.01	0.02	0.02	0.01	0.03	—	—	—	—	—	—
Fe	1.09	1.01	1.02	0.93	1.03	0.82	0.65	0.89	0.79	0.77	0.75
Mg	0.00	0.00	0.00	0.00	0.00	0.01	0.02	0.01	0.01	0.02	0.01
Ca	2.03	2.05	2.07	2.07	2.08	1.98	1.81	1.99	1.91	1.85	1.86
Na	—	—	—	—	—	0.01	0.01	0.00	0.00	0.00	0.00
K	—	—	—	—	—	0.00	0.01	0.00	0.00	0.00	0.00
Mn	0.01	0.00	0.01	0.02	0.01	0.01	0.00	0.01	0.01	0.01	0.01
Sr	—	—	—	—	—	0.01	0.01	0.01	0.01	0.01	0.01
Ba	—	—	—	—	—	0.00	0.00	0.00	0.00	0.00	0.00
Ps (mol %)	35.6	32.9	33.2	30.3	34.0	27.0	23.7	29.5	27.9	27.5	27.1

Table 13. Continued.

Sample no.	ML 45-36 3795					ML 45-36 3820				
Analysis no.	1	2	3	4	5	1	2	3	4	5
Major-element chemical analyses (weight percent oxides)										
SiO_2	38.75	38.13	38.70	38.41	38.53	37.36	38.25	38.17	38.08	37.49
Al_2O_3	24.80	22.42	25.40	23.62	24.06	23.50	23.63	24.57	23.02	22.71
TiO_2	0.02	0.17	0.08	0.09	0.13	—	—	—	—	—
Fe_2O_3	12.04	14.86	11.18	13.38	12.72	12.19	10.54	11.83	13.19	12.73
MgO	0.01	0.01	0.02	0.04	0.02	0.08	0.33	0.03	0.00	0.11
CaO	23.55	23.06	23.32	23.48	23.49	23.19	23.38	22.29	23.40	23.44
Na_2O	—	—	—	—	—	0.02	0.01	0.01	0.02	0.01
K_2O	—	—	—	—	—	0.01	0.03	0.00	0.04	0.04
MnO	0.05	0.07	0.07	0.05	0.04	0.30	0.24	0.24	0.19	0.16
SrO	—	—	—	—	—	0.14	0.26	0.22	0.12	0.00
BaO	—	—	—	—	—	0.03	0.01	0.03	0.03	0.03
Total	99.22	98.72	98.77	99.07	98.99	96.79	96.68	97.39	98.09	96.72
Number of atoms on the basis of 13 oxygens										
Si	3.14	3.14	3.14	3.14	3.14	3.22	3.27	3.24	3.25	3.25
Al	2.37	2.17	2.43	2.27	2.31	2.39	2.38	2.46	2.32	2.32
Ti	0.00	0.01	0.00	0.01	0.01	—	—	—	—	—
Fe	0.74	0.92	0.68	0.82	0.78	0.79	0.68	0.76	0.85	0.83
Mg	0.00	0.00	0.00	0.00	0.00	0.01	0.04	0.00	0.00	0.01
Ca	2.05	2.04	2.03	2.06	2.05	2.14	2.14	2.03	2.14	2.17
Na	—	—	—	—	—	0.00	0.00	0.00	0.00	0.00
K	—	—	—	—	—	0.00	0.00	0.00	0.00	0.00
Mn	0.00	0.00	0.00	0.00	0.00	0.02	0.02	0.02	0.01	0.01
Sr	—	—	—	—	—	0.01	0.01	0.01	0.01	0.00
Ba	—	—	—	—	—	0.00	0.00	0.00	0.00	0.00
Ps (mole %)	23.7	29.7	21.9	26.6	25.2	24.9	22.2	23.5	26.8	26.4

Table 13. Continued.

Sample no.	ML 45-36 3887					ML 45-36 3908			
Analysis no.	1	2	3	4	5	1	2	3	4
Major-element chemical analyses (weight percent oxides)									
SiO_2	37.87	37.86	38.23	40.45	38.11	38.29	38.18	37.39	37.84
Al_2O_3	23.23	24.25	23.57	23.00	22.93	24.35	23.50	24.12	22.96
TiO_2	—	—	—	—	—	—	—	—	—
Fe_2O_3	13.13	11.68	12.72	11.66	13.04	12.25	12.50	11.22	13.79
MgO	0.05	0.03	0.01	0.04	0.07	0.01	0.05	0.03	0.02
CaO	23.80	23.05	23.15	22.10	23.32	22.50	23.26	23.66	23.35
Na_2O	0.00	0.01	0.00	0.00	0.00	0.03	0.00	0.01	0.03
K_2O	0.00	0.03	0.00	0.00	0.00	0.04	0.00	0.00	0.02
MnO	0.03	0.18	0.09	0.21	0.12	0.26	0.14	0.21	0.16
SrO	0.16	0.53	0.34	0.81	0.41	0.22	0.30	0.39	0.23
BaO	0.26	0.09	0.04	0.02	0.58	0.02	0.02	0.13	0.09
Total	98.53	97.71	98.15	98.29	98.58	97.97	97.95	97.17	98.49
Number of atoms on the basis of 13 oxygens									
Si	3.23	3.22	3.25	3.40	3.26	3.25	3.25	3.20	3.24
Al	2.33	2.43	2.36	2.28	2.31	2.43	2.36	2.44	2.31
Ti	—	—	—	—	—	—	—	—	—
Fe	0.84	0.75	0.81	0.74	0.84	0.78	0.80	0.72	0.89
Mg	0.01	0.00	0.00	0.01	0.01	0.00	0.01	0.00	0.00
Ca	2.17	2.10	2.11	1.99	2.14	2.04	2.12	2.17	2.14
Na	0.00	0.00	0.00	0.00	0.00	0.01	0.00	0.00	0.01
K	0.00	0.00	0.00	0.00	0.00	0.00	0.00	0.00	0.00
Mn	0.00	0.01	0.01	0.01	0.01	0.02	0.01	0.02	0.01
Sr	0.01	0.03	0.02	0.04	0.02	0.01	0.01	0.02	0.01
Ba	0.01	0.00	0.00	0.00	0.00	0.00	0.00	0.00	0.00
Ps (mol %)	26.5	23.5	25.6	24.4	26.6	24.3	25.3	22.9	27.7

Table 14. Electron microprobe analyses of garnet.

Sample no.	ML 28-32 4334				
Analysis no.	1	2	3	4	5
Major-element chemical analyses (weight percent oxides)					
SiO_2	36.78	36.51	36.70	36.50	36.71
Al_2O_3	0.01	0.00	0.03	0.01	0.02
FeO	27.32	27.07	27.34	27.33	27.99
MgO	0.35	0.39	0.45	0.37	0.02
CaO	34.59	34.62	34.68	34.27	34.23
Na_2O	0.00	0.00	0.01	0.01	0.00
K_2O	0.03	0.02	0.03	0.02	0.02
MnO	0.12	0.17	0.20	0.21	0.17
SrO	0.01	0.00	0.00	0.01	0.00
BaO	0.00	0.00	0.00	0.00	0.00
Total	99.21	98.78	99.44	98.73	99.16
Number of atoms on the basis of 24 oxygens					
Si	6.58	6.56	6.56	6.57	6.59
Al	0.00	0.00	0.01	0.00	0.00
Fe	4.09	4.07	4.08	4.11	4.20
Mg	0.09	0.11	0.12	0.10	0.01
Ca	6.63	6.67	6.64	6.61	6.58
Na	0.00	0.00	0.00	0.00	0.00
K	0.01	0.01	0.01	0.01	0.00
Mn	0.02	0.03	0.03	0.03	0.03
Sr	0.00	0.00	0.00	0.00	0.00
Ba	0.00	0.00	0.00	0.00	0.00

Table 15. Fluid-inclusion heating/freezing data for hydrothermal minerals in geothermal drill core from Medicine Lake volcano

Sample depth (m)	Host mineral	Number of melting-point temperature measurements	Melting-point temperatures T_m (°C)	Salinity (wt percent NaCl equivalent)	Number of homogenization temperature measurements	Range of homogenization temperatures T_h (°C)	Mean homogenization temperature T_h (°C)
Drill hole ML 45-36							
432.5	quartz	1	0.0	0.0	1	145	145
753.8	"	33	0.0, -0.1	0.0, 0.2	51	211 – 324	268
827.2	"	15	0.0, -0.1	0.0, 0.2	28	198 – 324	259
841.6	"	19	0.0, -1.7	0.0, 2.9	27	227 – 312	254
854.4	calcite	0	—	—	25	178 – 213	188
855.5	quartz	29	0.0, -0.1	0.0, 0.2	53	189 – 304	268
856.2	"	33	0.0, -0.1	0.0, 0.2	56	197 – 373	244
1011.0	calcite	30	0.0, -1.1	0.0, 1.9	46	202 – 285	249
1184.8	wairakite	0	—	—	4	186 – 263	211
Drill hole ML 28-32							
804.1	quartz	0	—	—	31	130 – 138	136
811.2	"	8	-0.5, -0.6, +4.1		26	125 – 196	147
819.8	"	16	-0.2, -0.4, -0.5 -0.9, -1.2, +2.6 +3.1, +3.2		37	127 – 223	154
1030.2	calcite	0	—	—	12	163 – 207	183
1043.9	"	0	—	—	32	139 – 225	177